Re-engineering Bacterial Two-Component Signalling Systems

Gareth Blades

A thesis submitted in partial fulfilment of
the requirements for the degree of
Doctor of Philosophy at the University of Oxford

Jesus College
University of Oxford
Hilary Term 2014

Abstract

Re-engineering Bacterial Two-Component Signalling Systems

Gareth Blades

Thesis submitted for the degree of Doctor of Philosophy,
University of Oxford, Hilary Term 2014

Bacteria use Two Component Systems (TCS) to sense and respond to changes in their external environment. TCS are used to navigate to nutrients or away from toxins (chemotaxis) and to adapt to changes in osmolarity (osomosensing). TCS are composed of a histidine protein kinase (HPK) which trans-autophosphorylates in response to environmental change, transferring the phosphoryl group to a cognate response regulator (RR). Phosphorylated RRs modulate an output response such as protein-protein interaction for chemotaxis, and transcription for osmosensing. RRs are composed of a conserved amino terminal REC domain, and where present a variable effector domain. CheY, the chemotaxis RR, contains only a REC domain, whilst OmpR, the osmosensing RR, also contains a DNA binding effector domain. Recently, TCS have been used in synthetic biology applications due to their modularity and conserved signalling mechanism.

This thesis aimed to investigate whether it was possible to design a synthetic TCS composed of fused chemotaxis and osmosensing components. Synthetic RRs were designed, fusing the highly conserved REC domains of CheY and OmpR upstream of the OmpR effector domain. REC domains were fused across the α_4-β_5-α_5 region, a region which transmits REC domain phosphorylation into effector domain activation. Synthetic RRs were designed to undergo phosphotransfer to their fused REC domains from the chemotaxis HPK, CheA, activate the attached OmpR effector domain and bind promoter DNA.

Four chimeric RRs were created, although only three were structurally viable; F2, F3 and F4. Each fusion bound CheA, and F3 and F4 bound CheA with a significantly higher affinity than CheY. The chimeric RRs could all be phosphorylated by CheA-P; F4 and F3 were phosphorylated to wild-type levels. DNA binding affinity was investigated with fluorescence anisotropy, phosphorylated and unphosphorylated F3 could not bind promoter DNA. F2 bound promoter DNA regardless of phosphorylation state. These data indicate that phosphorylation of the F2 REC domain does not lead to activation of the effector domain. F2 is likely to be constitutively active suggesting a previously unknown role for OmpR α_5 as a mediator of effector domain activation. Furthermore, using a simple fusion approach to design RRs is not a viable method to create a synthetic TCS with a controllable output.

The work in this thesis was undertaken at the University of Oxford, in the Department of Biochemistry. Work was perormed from October 2009 to September 2013 under the supervision of Dr. G Wadhams. All the work in this thesis is my own unless stated and has not been submitted for a degree at this or any other university.

I'd like to thank George Wadhams for the opportunity to work with such freedom and find my own way to investigate my own ideas.

Huge thanks to Kathryn Scott for her invaluable support in the lab, her willingness to listen and help and her wonderful store of knowledge on practically everything protein related.

The members of the Armitage and Wadhams labs have made doing this DPhil such an enjoyable experience. I'd like to thank them all for making the lab such a fun and interesting place to work.

Many thanks to John Sinfield for allowing me access to the SPR facilities in Leeds, which let me complete my sensogram analysis without having to travel to Oxford.

A special thanks must go to my wife, Jen, who has supported me through this endeavour despite me trying her patience on many many many occasions. Thanks to Eli for making my life so much more fun and fulfilled.

Note to self; think of something pithy to put here

Abbreviations

Amp^r	Ampicillin resistant
ATP	Adenosine triphosphate
BeF_3^-	Beryllium Fluoride
BSA	Bovine serum albumin
CA	Catalytic and ATP binding domain
Cm^r	Chloramphenicol resistant
CTD	Carboxyl terminal domain
DHp	Dimerisation and histidine phosphotransfer domain
DMSO	Dimethylsulphoxide
dNTP	Deoxynucleoside 5'-triphosphate
DTT	Dithiothreitol
EDTA	Ethylenediamine-tetraacetic acid
Fl-DNA	Fluorescein tagged DNA
HEPES	Sodium N-2-hydroxyethylpiperazine-N'-2-ethanesulphonic acid
HPK	Histidine protein kinase
HPt	Histidine containing phosphotransfer domain
IPTG	Isopropyl-β-D-thiogalactopyranoside
Kan^r	Kanamycin resistant
LB	Luria-Bertani
MCP	Methyl-accepting chemoreceptor protein
MOPES	3-morpholinopropane-1-sulfonic acid
NTD	Amino terminal domain
PIPES	1,4-piperazinediethanesulfonic acid
Protein-P	Phosphorylated protein
RR	Response Regulator
SDR	Specificity determining residue
SDS	Sodium Dodecyl Sulfate
TCEP	Tris 2-carboxyethyl-phosphine
TCS	Two component system
TE	Tris-EDTA buffer
TEMED	Tetramethylethylenediamine
Tet^r	Tetracycline resistant
Tricine	N-2-Hydroxy-1,1-bis-hydroxymethyl-ethyl-glycine

Contents

List of Figures

List of Tables

Chapter 1

Introduction

1.1 Chapter Summary

This introduction will firstly address what a two-component system (TCS) is and why they are important to study, there will be a focus on the general features of response regulators (RRs) in particular. Moving on from this foundation, the two systems of interest to this study, chemotaxis and osmosensing, will be explored. These sections will briefly cover the roles these systems play in *Escherichia coli*, while the interactions of their histidine protein kinase (HPK) and response regulator (RR) and the outputs they modulate will be covered in more detail.

1.2 Two Component Systems

Bacteria use TCS to sense and respond to many different changes in their external environment. TCS are used to respond to diverse environmental challenges, such as; navigating to nutrients and away from toxins (Chemotaxis), adaptive responses to nitrogen starvation, nutrient starvation (Sporulation), uptake of foreign DNA (Competence), anti-biotic resistance and changes in osmolarity (81) (38) (65) (25). Chemotaxis has been shown to be essential for virulence in *Helicobacter pylori*, a human pathogen that can colonise the gastric mucus layer causing gastric ulcers and increasing the risk of gastric cancer. However, non-chemotactic and non-motile *H. pylori* mutants cannot colonise the gut of hosts (66). Furthermore, motility aids virulence in other pathogens, including *Vibrio cholerae*, *Salomella enterica* and *Legionella pneumophila* (39). Consequently, understanding the general mechanisms of protein interaction and regulation of TCS could aid drug discovery, understanding less well investigated TCS and in the design of synthetic biology applications utilising TCS.

1.2.1 Types of TCS and HPKs

The information flow in a schematic TCS is represented in Figure 1.1. The Sensor domain detects a change in an environmental stimulus causing the HPK dimer to trans-autophosphorylate, transferring a phosphoryl group from ATP bound to the ATP Kinase domain to the phosphorylatable His of the H box on the other monomer. The RR binds to the HPK, catalysing transfer of the phosphoryl group to a conserved aspartate in the RR active site. This event activates the RR, allowing it to modu-

late an output response such as gene expression. The transfer of phosphoryl groups from can be summarised in three equations, where Eq 1.1 represents HPK trans-autophosphorylation, Eq 1.2 is HPK:P phosphotransfer to RR and Eq 1.3 is RR:P dephosphorylation;

$$ATP + HPK - His \leftrightarrow ADP + HPK - His : P \tag{1.1}$$

$$HPK - His : P + RR - Asp \leftrightarrow HPK + RR - Asp : P \tag{1.2}$$

$$H_2O + RR - Asp : P \leftrightarrow RR - Asp + Pi \tag{1.3}$$

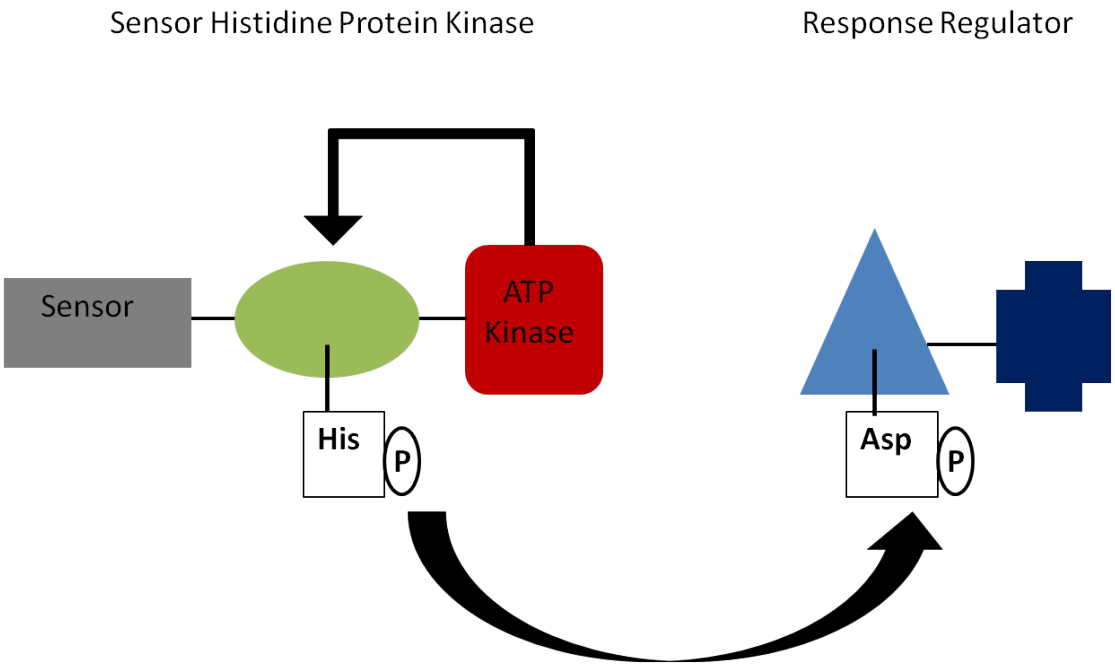

Figure 1.1: Information flow in TCS. Schematic of components of a TCS; Sensor domain, conserved phosphorylatable His containing H box of HPK, ATP Kinase domain of HPK, REC domain of RR containing a conserved phosphorylatable Asp. See text for details.

There are two different classes of TCS, defined by the relative orientation of the sub-domains of the HPK, specifically the location of the phosphorylatable His containing H box with respect to the ATPase domain, Figure 1.2. Class I TCS have the phosphorylatable His proximal to the ATP kinase domain, while Class II TCS

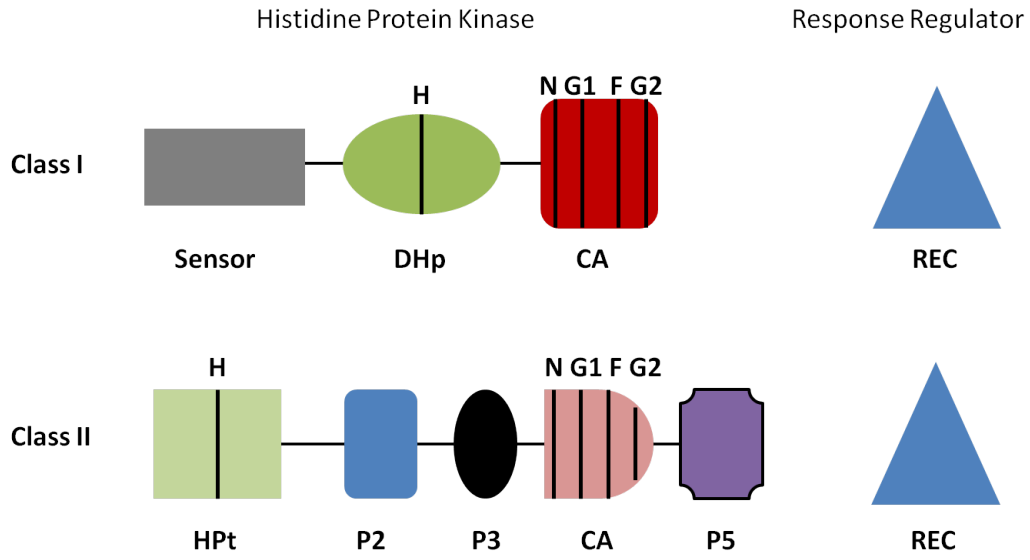

Figure 1.2: Schematic of Class I and Class II TCS. The different domains of Class I and II TCS are depicted, of particular importance is the orientation of the HPK domains. Class I TCS contain a periplasmic Sensor domain, a Dimerisation and Histidine phosphotransfer (DHp) domain containing the H box, proximal to the DHp is a Catalytic and ATP binding (CA) domain containing the conserved boxes which coordinate ATP and Mg^{2+} for trans-autophosphorylation. Class II TCS are composed of 5 domains, P1-5. A Histidine containing Phosphotransfer (HPt) domain contains the His box (P1), which is distal from the CA domain (P4).

have the His distal to this domain, Figure 1.2. Class I HPKs, which in this study are represented by EnvZ from the osmosensing system, are the more abundant type of HPK and contain a Dimerisation and Histidine phosphotransfer (DHp) domain in which the H box resides (20). This central domain is flanked by the ATP kinase domain, specifically referred to as the Catalytic and ATP binding (CA) domain. The CA domain contains conserved N, G1, F and G2 boxes responsible for ATP binding and Mg^{2+} coordination (68) (10) (20) (61) (15). Class II HPKs, comprising only CheA containing TCS and represented by *E. coli* CheA in this study, are composed of 5 different domains, P1-5 (62) (10) (63) (59). The His containing H box resides in the P1 domain of CheA, which resembles a Histidine containing Phosphotransfer (HPt) domain (20) (62). P2 is specific to CheA type HPKs and provides a high affinity binding site for CheY, P3 is a dimerisation domain, P4 is the ATP kinase domain containing the conserved N, G1, F and G2 boxes and P5 a regulatory domain that connects to receptors (10) (63) (59).

1.2.2 Response Regulators

Classification of RRs is dependent on the presence of an amino-terminal receiver (REC) domain. CheY is a single domain RR and is the archetype of the REC domain (80), (95) (74). The REC domain is a 5 stranded parallel β sheet surrounded by five α helices, Figure 1.3. The REC domain is responsible for HPK binding, catalysing phosphotransfer from the cognate HPK, autodephosphorylation and also acts to activate an attached carboxyl-terminal domain (CTD), the effector domain, if present (82) (43). 66% of RR effector domains are DNA-binding, the OmpR/PhoB family comprises the largest single grouping of this type; 33.1% of DNA binding RRs belong to the OmpR/PhoB family (27). The single domain RR grouping are composed of a stand-alone REC domain, the CheY family are the largest constituent member of this type, accounting for 14.3%. Enzymatic output domains, such as the methylesterase CheB, constitute 12% of the RR population.

RRs can be identified based on the presence of a REC domain, specifically based on the presence of conserved residues, Figures 1.3 and 1.4. The primary amino acids that contribute to the active site; Asp12, Asp13, Asp57, Thr87 and Lys109 (CheY numbering), Figure 1.3 (95) (94) (80) (95) (74), along with the essential divalent metal cation co-factor Mg^{2+}, are responsible for catalysing the transfer of the phosphoryl group from the histidine on a HPK to the phosphorylatable aspartate in the REC domain of the RR (93). The auto-dephosphorylation rate of a RR is dependent on residues at position 59 and 89 (CheY numbering). A positively charged residue at position 89 results in a relatively slower auto-dephosphorylation, while the opposite is true of a negatively charged residue at this position (86). It is worth noting that CheY has a K_{dephos} of 3 min^{-1} and contains glutamate at 89, while OmpR has a K_{dephos} of 0.002 min^{-1} and has positive lysine at 89. The movement of residues at position 59 and 89 upon RR phosphorylation has also been demonstrated to be important for the auto-dephosphorylation rate (69). Where residues 59 and 89 move to block access to the phosphate group to an incoming nucleophile, such as water, the auto-dephosphorylation rate is slowed.

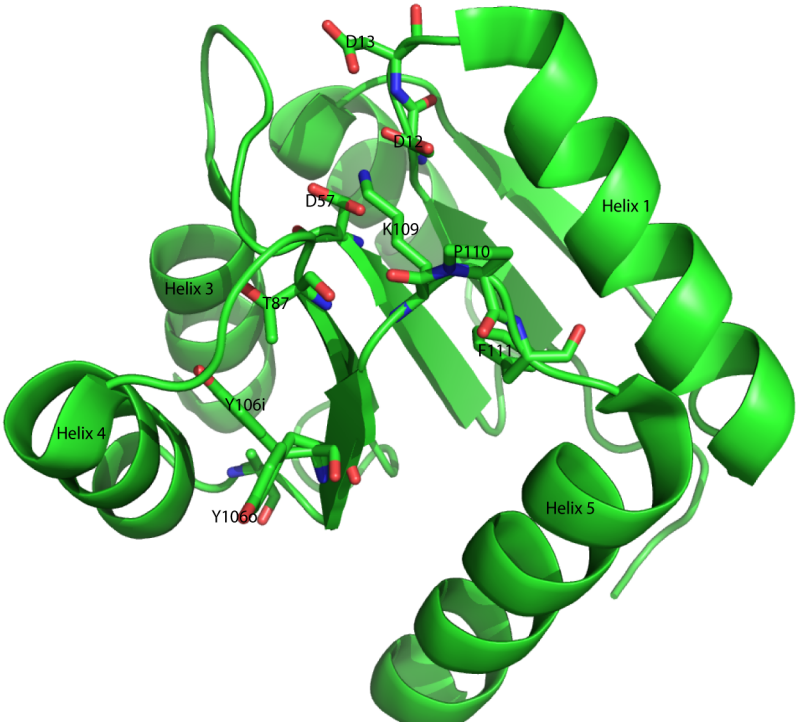

Figure 1.3: Active site and highly conserved RR residues. Active site residues Asp12, Asp13, Asp57, Thr87 and Lys109 are shown as sticks and coloured by element; C=green, O=red and N=blue. Highly conserved residues, Ala103, Tyr106, Pro110 and Phe111 are shown as sticks and coloured by element also. The two rotomers of Tyr106 are labelled Y106i (inward) and Y106o (outward), discussed further in Section 1.4.1.

Figure 1.4: *E. coli* RR REC Domain Alignment. Only CheY and OmpR sequences are shown from an alignment of all *E. coli* RR REC domains, REC domain sequences as defined by the MiSTdb Agfam classification (92). Active site residues Asp12, Asp13, Asp57, Thr87 and Lys109 and highly conserved residues Ala103, Tyr106, Pro110 and Phe111 are highlighted. A sequence logo shows the most highly occurring residues at each position. Alignment generated in Clustal W (46).

1.2.3 TCS Specificity

Most bacteria encode 10s-100s of TCS (91), and much research has been directed at determining how phosphotransfer specificity is maintained between cognate pairs of these TCS proteins (76) (14) (13). The REC domain contains specificity determining residues (SDRs), that are used by the RR to recognise only its cognate HPK. Similarly, a HPK has SDRs that allow it to bind preferentially with its cognate RR. SDRs were identified for Class I TCS using coevolution; looking for correlated changes between RR residues and HPK residues (76) (14) (13). The authors looked at the probability of finding residue X at position 1 in a HPK, and residue Y at position 1 in a RR. Comparing this to the number of sequences with those residues at position 1 (76) (14) (13), produces a list of residues in certain positions that preferentially co-occur and therefore coevolve. This approach was greatly helped by mapping putative SDRs on the solved HPK-RR complex structure of RR468:HPK853 from *Thermotoga maritima*.

This approach found 9 HPK and 7 RR residues, forming 12 coevolving pairs. These SDRs have been mapped on to RR468 and HPK853, in Figures 1.5, 1.6 and 1.7. The SDRs on the HPK reside below the conserved histidine on helix 1 and 2 of the DHp stem. To change the specificity of EnvZ from OmpR to a non-cognate RR, RstA, required only three amino acid changes on α_1, resulting in no phosphotransfer between OmpR and the mutant EnvZ (76). EnvZ and RstB are closely related and the number of changes is strikingly small, although changing the phosphotransfer profile of EnvZ to that of more distantly related HPKs, such as CpxA, PhoR, AtoS and PhoQ, required changes to all 7 SDRs plus the entire loop between helix 1 and 2 (76). This indicates that areas not identified in the initial coevolution analysis are likely required to switch specificity in the majority of class I HPKs.

The co-evolution approach identified that SDRs on class I TCS RR are clustered in helix α_1 and there is an additional residue in loop 5. To change the specificity of OmpR from EnvZ to RstB required three changes to the SDRs and the whole of loop 5 (14). It should be noted that OmpR and RstA, the RR OmpR was changed to mimic, already share four SDRs in common out of the 7 identified. Similarly to the HPK data presented above, further changes may need to be made to change the specificity of more distantly related class I TCS RRs. Nevertheless, the mutant OmpR demonstrated a change in specificity, undergoing phosphotransfer only from RstB and not EnvZ (14).

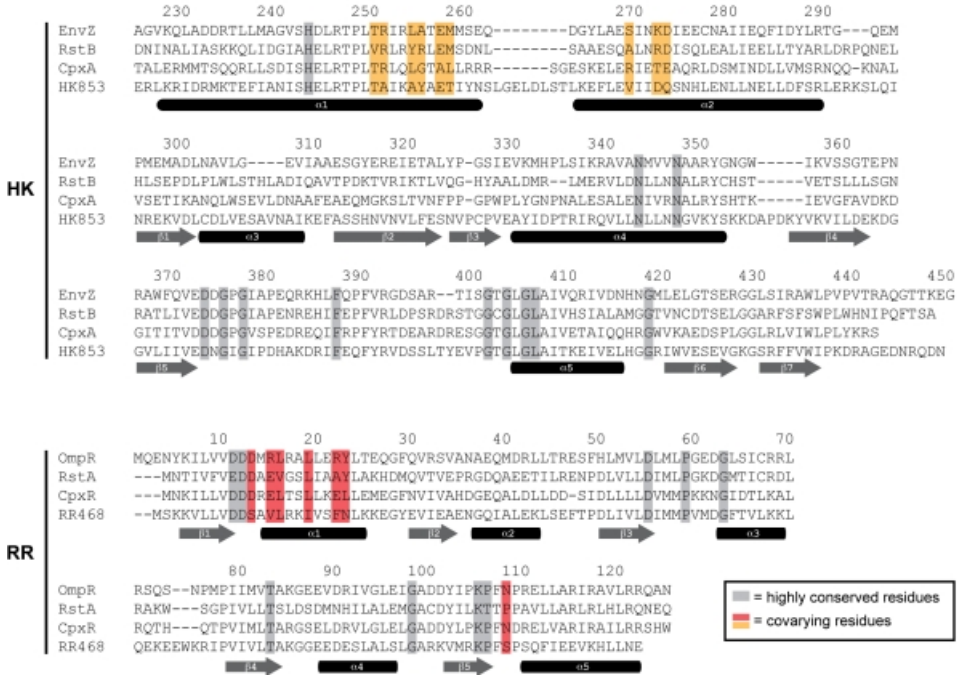

Figure 1.5: SDRs of Class I TCS. Alignment of class I HPKs and RRs, highly conserved and covarying residues are highlighted, the secondary structure of each domain is also shown. Adapted from (14).

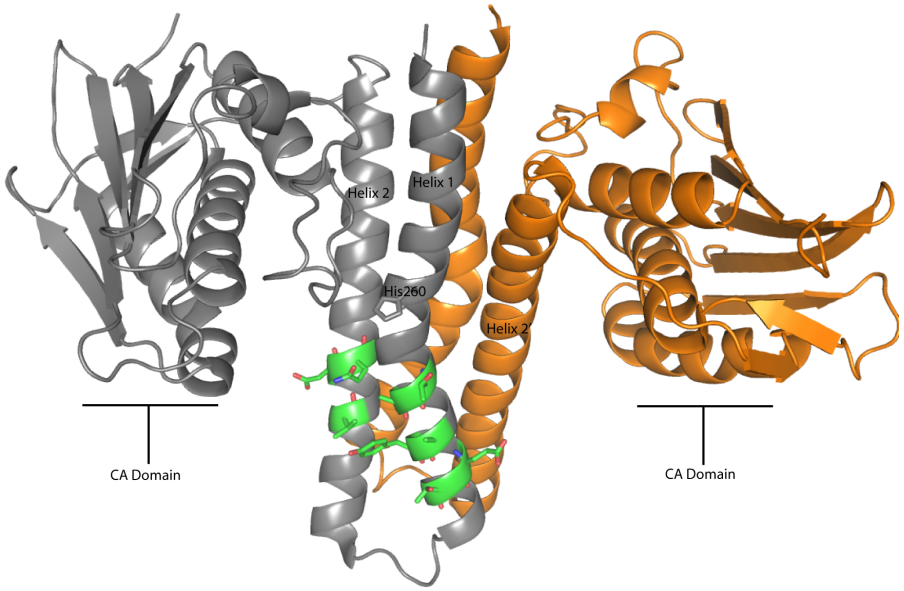

Figure 1.6: SDRs mapped on HPK853 (pdb:3DGE). The first protomer of HPK853 is coloured grey, the second orange. SDRs are shown as sticks and coloured by element; C=green, N=blue, O=red. The phosphorylatable histidine is depicted as sticks and labelled. Image created with Pymol.

SDRs have been probed in class II TCS, however only one class II TCS has been investigated, the $CheY_6$ SDRs for the $CheA_3$ HPt P1 domain of *Rhodobacter sphaeroides* (8). The $CheA_3$ HPt P1 domain is composed of a continuous central 5 helix bundle α A-E, the phosphorylatable histidine is located on αB. $CheA_3$ P1 interacts with its cognate RR, $CheY_6$, via αA, αB and a loop that connects αB and αC, Figure 1.8.

$CheY_6$ forms its part of the interface with contacts from α_1 and the amino terminus of its elongated loop connecting β_5 to α_5, Figure 1.8. Clearly, there are similarities here with the class I RR binding residues presented above. The contributions to the buried surface area of $CheY_6$ are dominated by one residue, methionine 13 on the first helix. It accounts for 156Å^2 of the buried surface area, almost a third of the total. Below this, the rest of the binding residues of α_1 account for another third. The dominance of the α_1 residues, M13 in particular, provided clues as to which residues drove specificity (8). The specificity of *R. sphaeroides* CheY's, $_1$, $_3$, $_4$ and $_5$ as well as *E. coli* CheY, could be rewired for phosphotransfer from $CheA_3$ P1 by changing only two residues corresponding to Met13 and the preceding residue, Ala12. Ala12 does not play a part in specificity but accommodates the full insertion of Met13 into

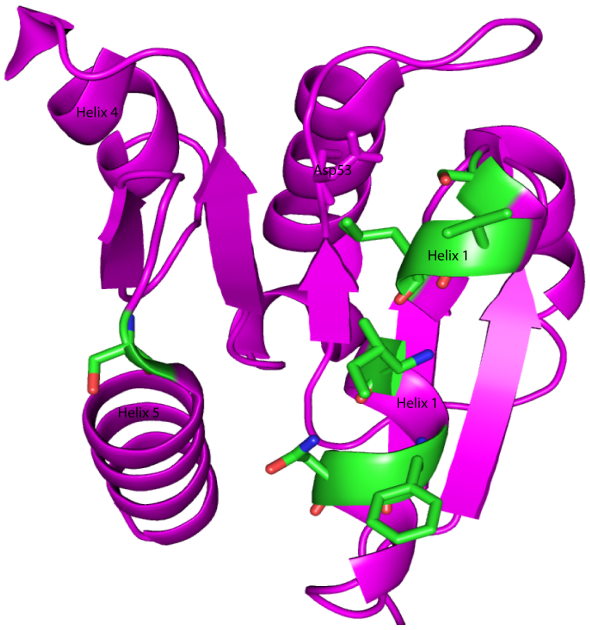

Figure 1.7: SDRs mapped on RR468 (pdb:3DGE). The RR is coloured magenta. SDRs identified are shown as sticks and coloured by element; C=green, N=blue, O=red. The phosphorylatable aspartate is depicted as sticks and labelled. Helix 1 is labelled twice due to a break in its structure. Image created with Pymol.

a hydrophobic pocket on $CheA_3$ P1 (8). Although, this study is useful in elucidating potential SDRs in class II TCS, no further studies have been undertaken to verify whether the observations are generalisable to other class II TCS.

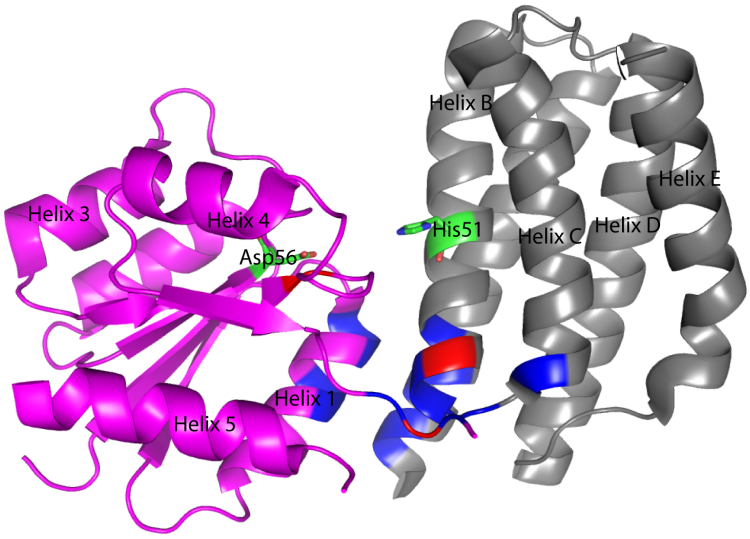

Figure 1.8: Complex of $CheA_3$ Hpt P1 domain and $CheY_6$ (pdb:3KYJ). $CheA_3$ P1 is a single domain, coloured grey, composed of five α helices A-E. The response regulator $CheY_6$ is magenta. The bond type formed by residues is indicated by colour, blue for hydrohobic and red for a hydrogen bond. The phosphorylatable histidine and aspartate are depicted as sticks and coloured by element; C=green, N=blue, O=red. Image created with Pymol.

1.3 Synthetic Biology

The term synthetic biology is generally used for the engineering of biology. The field of synthetic biology aims to create a suite of synthetic biological parts that have specific functions. Initially, synthetic biology research primarily focused on elucidating the functional principles behind naturally occurring gene circuits (30) (22) (23). This early work highlighted the importance of intrinsic and extrinsic noise in gene expression (23), and how complex behaviours such as bistability (30) and oscillations (22) can be produced by non-specialised and minimal components. This work has been built upon and advanced to create proof-of-principle devices, usually in bacteria, such as; molecular computers used to diagnose and treat cancer (9), bacterial 3-D printing (49), electron transfer from bacteria to man made devices (37) and synchronised behaviour across a bacterial population (19). Bacteria have also been used in whole-cell biosensor applications. As whole cell devices they have proved more robust than enzymatic technology while remaining highly specific, sensitive and portable (99).

The chemotaxis and osmosensing systems have previously been fused to create a

chimeric receptor-HPK (103). The periplasmic domain of the aspartate sensor Tar, a receptor of the chemotaxis system, was fused to the cytoplasmic domain of EnvZ, the HPK of the osmosensing system (103). The chimeric synthetic Taz receptor responded to aspartate and autophosphorylated EnvZ leading to OmpR phosphorylation. The synthetic biology field has grown rapidly and supports a annual global competition, iGEM, and a registry of standardised parts available to use to create biological devices. Recently attempts have been made to use TCS as novel parts for synthetic biology, engineering different types of regulatable behaviour into the EnvZ/OmpR TCS (16).

1.4 Chemotaxis

Chemotactic behaviour is a biased movement towards a chemical attractant or away from a chemical repellent (81). Movement is driven by a transmembrane molecular motor powering a long helical flagellum, which moves the bacteria through liquid media. A host of other proteins are involved upstream of this motor, together constituting a coordinated network that senses the concentration of chemicals in the environment, processes this information and results in a change in motor rotation and hence swimming behaviour in response to the signal, Figure 1.9 .

In *E. coli* chemical signals are detected by chemoreceptors; Methyl-Accepting Chemotaxis Proteins (MCPs), embedded in the membrane with a cytoplasmic C-terminal domain. An adaptor protein CheW links the MCPs to the HPK, CheA. Two RRs compete to bind to CheA, one RR is CheY, which can bind to the flagellar motor, the other is CheB a methylesterase which controls adaptation of the MCPs (33) (1). If CheY is phosphorylated (CheY-P) by CheA it can bind to the switch protein FliM on the flagellar motor leading to a reversal of motor rotation and a change in swimming direction (98) (87). This modulation is attenuated by CheZ, a phosphatase specific for CheY-P, Figure 1.9 (57).

The structures and interaction of CheY and CheA will be explored in the forthcoming sections.

1.4.1 CheY and CheY-P

CheY is a single domain RR, composed of an isolated REC domain (80) (95) (74). In structures determined by X-ray crystallography and NMR spectroscopy, helix 4

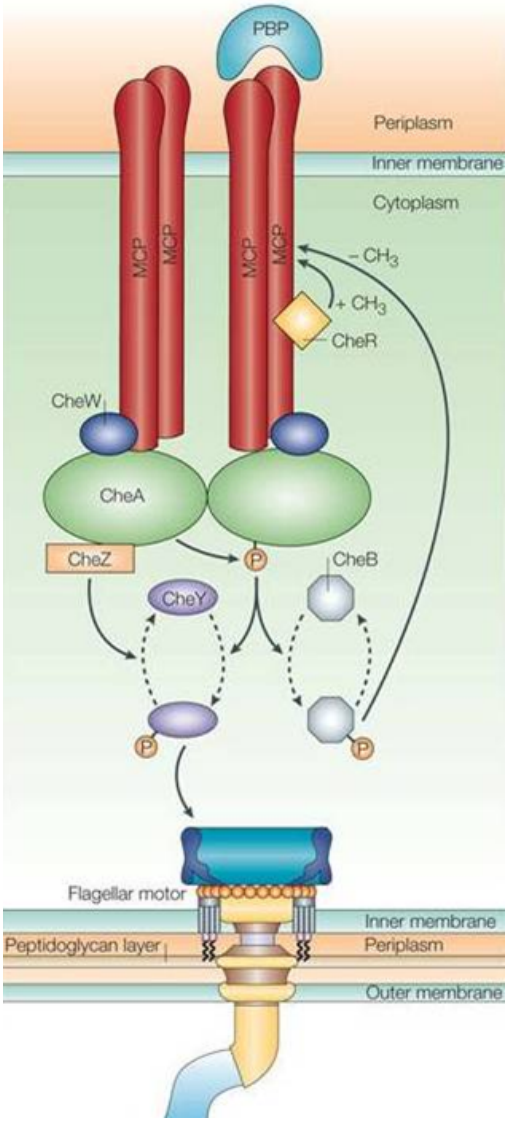

Figure 1.9: Schematic of the *E. coli* chemotaxis system . In response to a reduction is chemoattractant, CheA autophosphorylates leading to an increase in CheY-P concentration. CheY-P binds to the flagellar motor protein FliM causing a change in the direction of rotation from anti-clockwise to clockwise and the cell to change direction. The CheY-P signal is terminated by CheZ. CheR and CheB form an adaptation loop allowing the system to adapt to the current background level of chemoattractant. Image adapted from (96).

protrudes away from CheY and the hydrophobic core, taking no part in the core structure (80) (95) (74). As explored later, the distal location of helix 4, essentially its freedom from tethering interactions with the core of CheY, is exploited to propagate conformational changes on activation.

CheY structures have been determined for apo-CheY, without cation or phosphate, CheY.Mg^{2+} and CheY-P_{mimic}, where CheY is stably activated with a non-hydrolysable phosphomimic. Given its relevance to this study, and its position as a model for REC domain activation, the conformation of the activated CheY structure will be explored in some detail.

The activated form of CheY is dependent on phosphorylation at D57 (73). The autodephophorylation rate of CheY-P has been measured variously, with a $t_{\frac{1}{2}} \approx 6$s, $\approx$ 22.8s, $\approx$ 15.5 and $\approx$ 20s (11) (28) (106) (107) (52). Autodephosphorylation of CheY is therefore too fast to successfully crystallise CheY-P. Consequently, a phopshomimic that forms a stable covalent bond with D57 has been used instead. BeF_3^- binds to Asp57 but is unhydrolysable allowing crystallisation of the activated CheY structure (47) (17). As an overview, changes upon BeF_3^- activation include;

- a hydrogen bond between the hydroxyl of Thr87 and the phosphomimic bound to Asp57
- stabilisation of the internal rotomer of Tyr106 through hydrogen bonds to the backbone carbonyl of Glu89
- stabilisation of the internal rotomer of Tyr106 through hydrophobic interactions
- a salt bridge between Lys109 and the active site

A detailed examination of these changes will be presented, which will help illustrate the precise molecular movements required to activate a RR. Figure 1.10 shows the structure of activated CheY, using BeF_3^- complexed with CheY.Mn^{2+} (pdb:1FQW) (47). Mangenese has the same octahedral coordination geometry as Mg^{2+}, the usual cation found in the active site, and CheY.Mn^{2+} demonstrates similiar rates of phosphotransfer and dephosphorylation as CheY.Mg^{2+} (53). Consequently, using Mn^{2+} in place of Mg^{2+} should not have deleterious effects on the activated CheY structure.

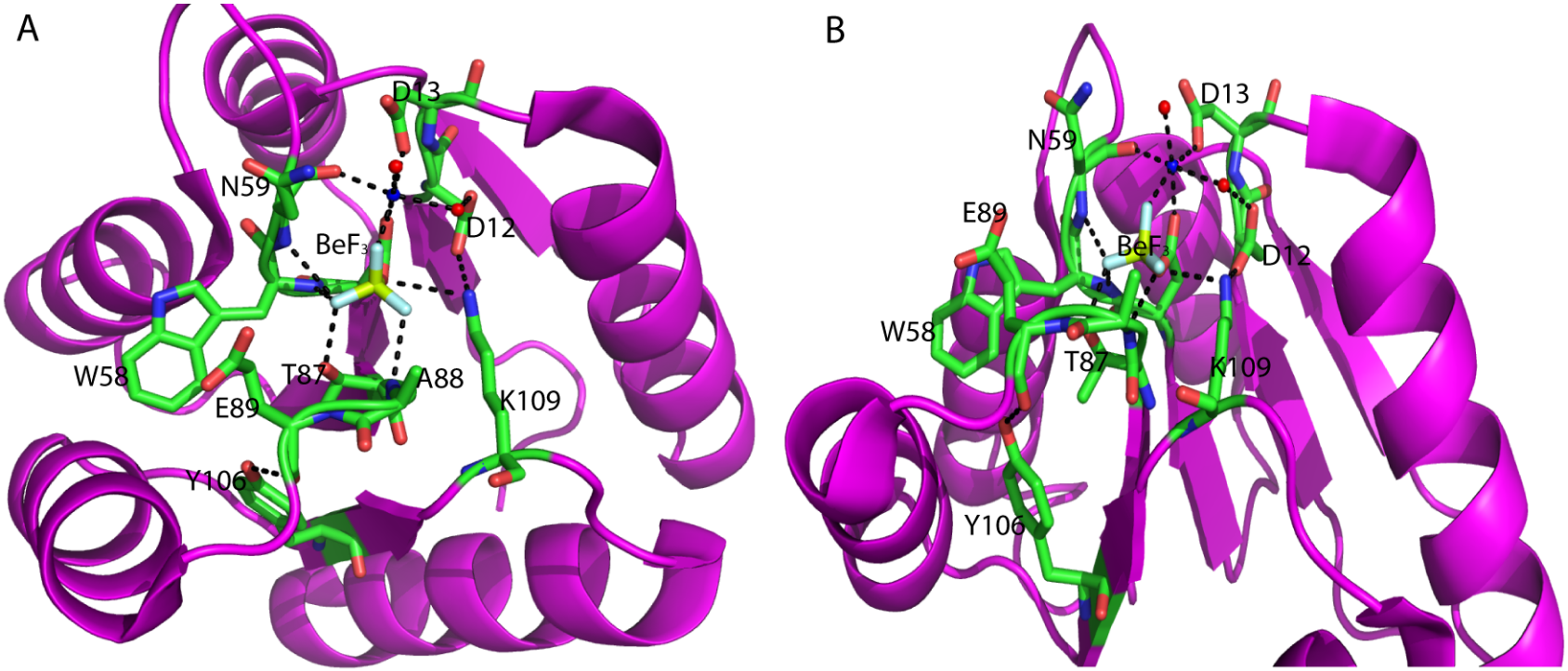

Figure 1.10: Active site of CheY-BeF_3^- (pdb:1FQW). Panel A and B represent different orientations of activated CheY. In Panel A, residue sidechains of Asp12, Asp13, Asp57, Asn59, Trp58, Thr87, Ala88, Glu89, Tyr106 and Lys109 are shown. Panel B omits the Ala88 label for clarity. Mn^{2+} (blue), BeF_3^- (yellow and white), and water (red). Side chain atoms are coloured, green=carbon, blue=nitrogen and red=oxygen. Hydrogen bonds are shown as black dotted lines. Images generated using PyMOL (Delano scientific).

As shown in Figure Figure 1.10, BeF_3^- covalently bonds with Asp57-Oγ. Hydrogen bonds are formed from fluorines to Thr87-Oγ, the backbone amide of Ala88, Lys109-Nζ, the Mn^{2+} ion, the backbone amide of Asn59 and the backbone amide of Trp58. These are extensive interactions, effectively, making BeF_3^- a second organising centre in the active site next to Mn^{2+}. BeF_3^- bridges the active site solvent between the divalent cation and the carboxyl terminal end of CheY. The interactions eminating from BeF_3^- help to stabilise the CTD in the active conformation. Thr87, the first residue in loop 4, moves out of a hydrophobic pocket between helix 4 and strand 5, stabilised in this out position by the bond to BeF_3^-. The second residue of loop 4, Ala88, is also stabilised by the bond with BeF_3^-. The movement of Thr87 and stabilisation of Ala88 moves the amino terminal of loop 4 towards the active site, which in turn repositions the rest of loop 4. The movement of loop 4 causes the side chain of Glu89 to rotate towards Trp58 and the repulsion between the negatively charged Glu89 and hydrophobic Trp58 causes Trp58 to rotate. The Nϵ of Trp58 moves closer to helix 3, while the Cη orients closer to helix 4.

Overall, the movement of loop 4 away and up from strand 5, caused by the movement of Thr87 and stabilisation of Ala88, helps reposition helix 4, Figure 1.11 demonstrates this movement. Compared to an inactive Mg^{2+} bound structure (pdb:2CHE), the amino terminus of helix 4 of CheY-BeF_3^- moves up and away from strand 5, as such helix 4 avoids a steric clash with the position of the Cη groups of Trp58. As a result of the movement of the amino-terminus of helix 4 in CheY-BeF_3^- the carboxyl terminus of helix 4 moves towards strand 5. The movement of activated helix 4 allows Tyr106 to access its internal rotameric conformation. The movement of the carboxyl terminal end of helix 4 towards strand 5, causes Tyr106 to face in and up. This position is vital in establishing a hydrogen bond between the backbone carbonyl of Glu89 and the η hydroxyl of the tyrosine. Ultimately, the movement initiated by the amino end of loop 4, transmitted via helix 4, which is free of core interactions, allows the rotameric Tyr106 side chain access to the hydrophobic pocket between helix 4 and strand 5. The hydrophobic interactions between Tyr106 and the pocket, composed of Trp58, Thr87, Asn94, Iso95 and Ala98, along with the hydrogen bond, stabilise Tyr106 in the internal position (Figure 1.12). The coupled movement of T87 out of the hydrophobic pocket and the insertion of Tyr106 is a general mechanism of RR activation and is referred to as Y/T coupling.

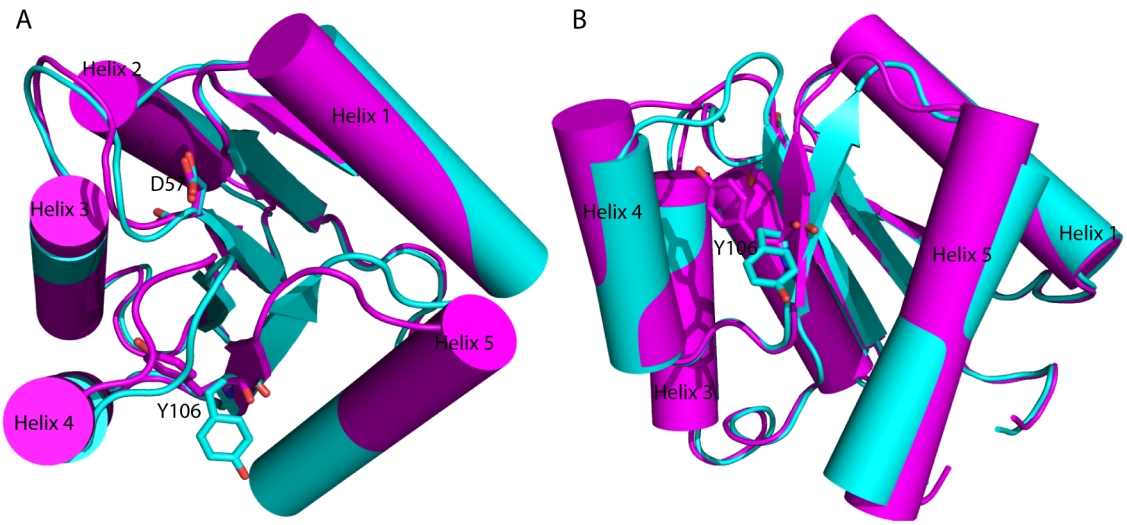

Figure 1.11: Comparison of CheY-BeF_3^- (pdb:1FQW) and CheY.Mg^{2+} (pdb:2CHE). BeF_3^- (pdb:1FQW) is magenta and CheY.Mg^{2+} (pdb:2CHE) is cyan. Panel A and B represent different orientations of the same alignment. Helices are shown as cylinders to aid comparison. Sidechains of residues Asp57 and Tyr106 are shown. Atoms are coloured; carbon=parent molecule colour, oxygen=red and nitrogen=blue. Images generated using PyMOL (Delano scientific).

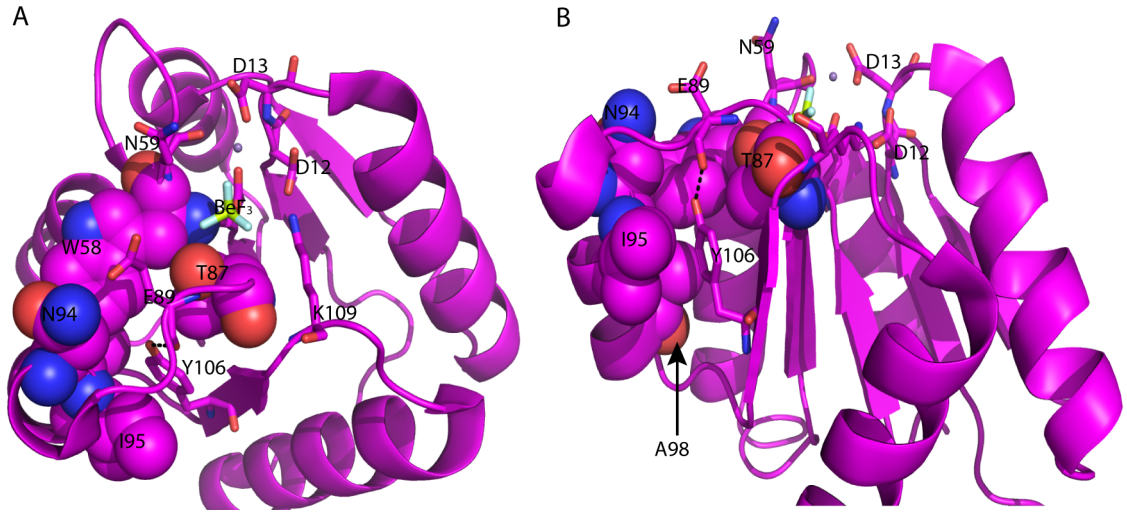

Figure 1.12: Composition of Tyr106 Hydrophobic Pocket in CheY-BeF_3^- (pdb:1FQW). Panel A and Panel B represent different orientations of the same structure. Sidechains of residues Asp12, Asp13, Asp57, Asn59, Glu89, Tyr106 and Lys109 are shown. The hydrophobic pocket residues Trp58, Thr87, Asn94, Iso95 and Ala98 are shown as space filling models. Atoms are coloured; carbon=parent molecule colour, oxygen=red, nitrogen=blue. $BeF_3^-$is shown in white and yellow and Mn^{2+} is coloured magenta. Images generated using PyMOL (Delano scientific).

1.4.2 Conclusion

CheY adopts a stabilised conformation upon activation, conformational changes facilitated by helix 4 propagate from the activated active site towards the carboxyl end of CheY. The flexibility of loop 4 and especially helix 4, ultimately their susceptibility to conformational change, are central to CheY being able to access its active conformation. Strand 5, in particular Tyr106, coupled to the movement of Thr87 out of the hydrophobic pocket formed by helix 4 and strand 5 helps to further stabilise the active conformation. As such, a coordinated ballet of specific movements, bond formation and structural flexibility help activate CheY.

CheY activation effects the conformation of the carboxyl region of CheY; the α_4-β_5-α_5 region. This part of CheY also associates with CheZ, which promotes CheY-P dephosphorylation, and FliM to effect the motor (105) (48).

The proceeding section will explore CheA and how the α_4-β_5-α_5 region interacts with this HPK.

1.5 CheA

CheA is the cognate HPK of CheY, it is composed of 5 domains; P1-P5. These domains segregate the function of CheA into modular components;

- P1, the HPt domain, contains the conserved phosphorylatable histidine, which undergoes autophosphorylation and after associating with CheY transfers this phosphoryl group to the active site aspartate
- P2, specific to CheA type HPKs, this domain binds CheY, providing a higher affinity binding site than P1
- P3 is a dimerisation domain, a four helix bundle composed of two α helices from each monomer
- P4 the ATP kinase domain, containing a hydrophobic conserved pocket to bind ATP and a divalent cation
- P5 a regulatory domain, connecting to receptors via CheW

The P1 domain of CheA is composed of 5 α helices (residues 1-131), 4 of which form a 4 helix antiparallel bundle; helices A-D (63). The phosphorylatable histidine residue resides on α_B of CheA-P1, this location of the His appears to be a common feature in several CheA-P1 structures (8) (62). CheA-P2 runs from residue 159-227 and is flanked by flexible linkers (62). Its structure is that of an open faced β-sandwich. One face of CheA-P2 is formed from a 4 stranded anti-parallel β sheet. The other face, which binds CheY, is composed of two helices, H1 and H2 (62).

1.5.1 CheA:CheY Binding

Domains P1 and P2 of CheA are involved in binding CheY and phosphotransfer, they are connected by a 23 residue flexible linker, Figure 1.13. The modular nature of CheA means that each of these domains has evolved for particular functions. Consequently, P1 is responsible for phosphotransfer to CheY, interacting with helix 1 and loop 5 of CheY with a K_d of between 218μM and 4.5mM (8) (62). *E.coli* CheA-P1 provides a continuous binding surface for CheY, spread across the amino terminal region of α_A and α_B (62). The interaction surface is only small, burying $\approx$ 700Å^2 of solvent accessible surface area. The interface is characterised by two patches of interactions, the larger of the two, patch 1, is formed by residues from P1 helix A and CheY helix 1. A smaller interaction, patch 2, is formed by loop 5 of CheY and 1 residue each from the loop preceding α_A, α_A itself and α_B of CheA-P1.

P2, on the other hand, provides a higher affinity site for CheY docking to CheA, the K_d of CheA-P2:CheY complex falls between 90nM and 1700nM (83) (85). The interaction between P2 and CheY is mediated by the α_4-β_5-α_5 region of CheY and the helices and loops of P2. By binding to different areas of CheY, the RR is sandwiched between P1 and P2 domains of CheA, Figure 1.13.

The interaction between CheY and CheA-P2 is mainly hydrophobic and buries $\approx$1,200Å^2 of surface area from the solvent (58) (97) (31). The interaction surface is composed of a hydrophobic patch with contributions from H2 of CheA-P2 and α_4 and β_5 from CheY. The hydrophobic patch is flanked apically and laterally by stabilising hydrogen bonds, which orignate from α_4, β_5 and α_5 of CheY and from H1, H2 and the loop following H2 of CheA-P2. It is worth noting that CheA-P2 residue Phe214 projects into the space between the carboxyl terminal end of helix 4 and the amino terminus of strand 5 of CheY, which precludes the sidechain of CheY residue Tyr106 from adopting an inward and down position. Consequently, Tyr106 in the CheY:CheA-P2 complex points out and up, stabilised by a hydrogen bond to either Glu178 or His181 on H2 of CheA-P2. The stabilisation of the outward rotomer of Tyr106 maybe a prerequisite for successful CheY binding. Additionally, it has been observed that binding of CheY to CheA-P2 causes the solvent accessible surface area of Asp57 of CheY to increase 2 fold, from 8 to 16Å^2 (97) (58). This is caused by the expansion of the helices away from the active site and a rotation of the sidechain of Phe14 away from Asp57. This is thought to provide a phosphotransfer primed CheY conformation.

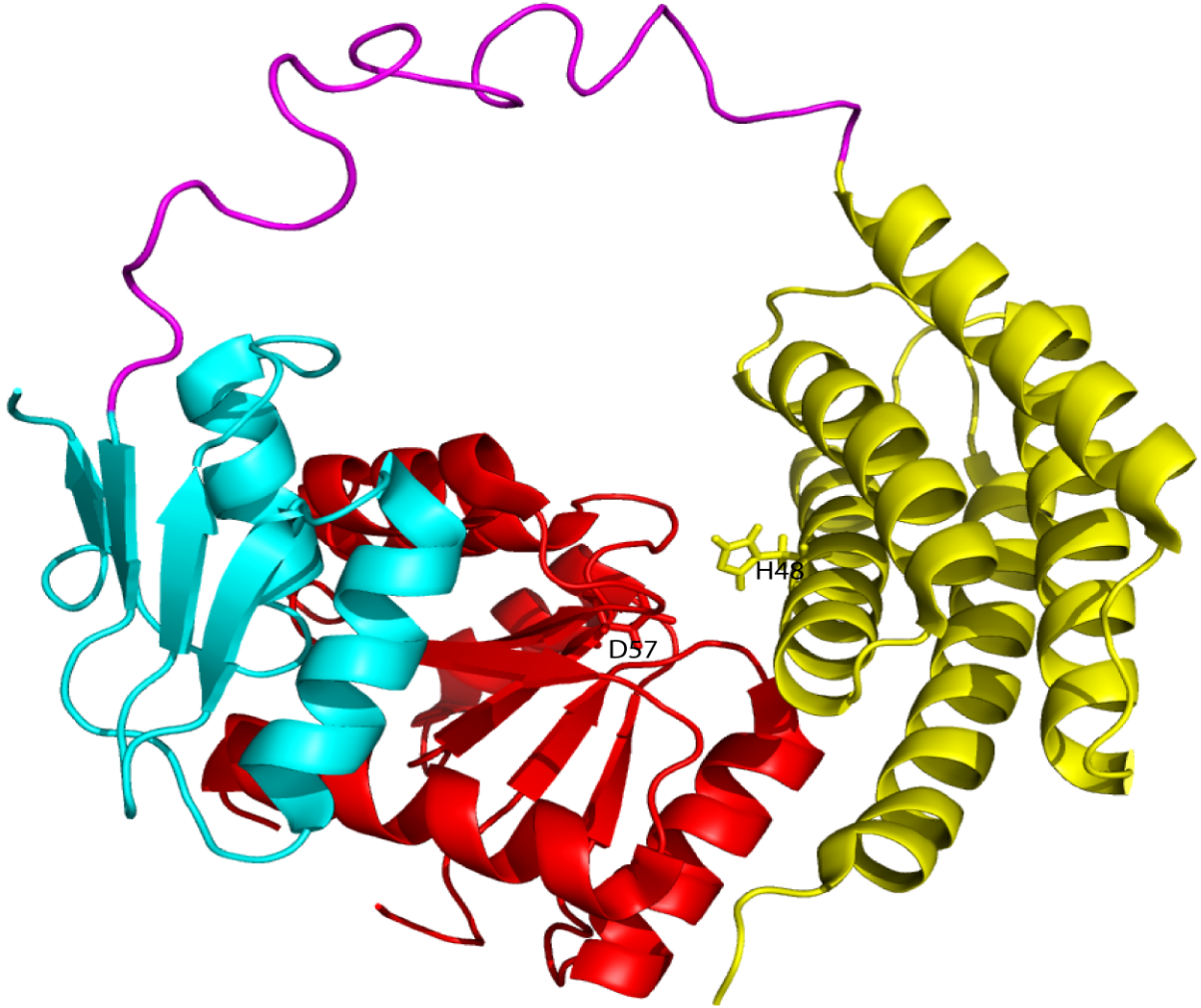

Figure 1.13: Structure of the *E. coli* CheA-P1P2:CheY Complex (pdb:2LP4). CheY is coloured red, P1 yellow, the P1P2 linker is purple and P2 cyan. The conserved histidine (His48) on P1 and aspartate of CheY (Asp57) have their sidechains displayed. Images generated using PyMOL (Delano scientific).

The dissociation constant of CheA P1, P2 and P1P2 domains, as well the full length CheA and a CheA-CheW-Tar complex have been determined for CheY (83) (8) (85) (50) (62) (75) (56). Table 1.1 compares the K_d of the complexes discussed.

The calculated K_d ($K_d = K_{dissociation}/K_{association}$) of full length CheA-CheW-Tar for CheY-Y51C is 30nM (75). The interaction between CheY and CheA-CheW-Tar was characterised by a slow association rate of 368 M^{-1} s^{-1} and even slower dissociation rate 1.14 X 10^{-5} s^{-1} (75). This basal dissociation rate could be increased up to 75 times by the addition of ATP to the CheY:CheA-CheW-Tar complex, indicating that CheY-P has a decreased affinity for CheA. Similarly, it has been demonstrated that CheY-P has a 6 fold lower affinity for CheA-P1P2 than apo-CheY (50).

A liberated P1 domain cannot bind to CheY-Y51C to any significant level (83). A low affinity complex formed by CheY and CheA-P1 was observed in NMR titration experiments where a K_d of 4.5mM was reported (62). These results were obtained with *E. coli* CheA-P1 and CheY, and the low affinity could stem from the small surface area of interaction observed, ≈ 700Å^2 (62). The low affinity with *E. coli* CheA-P1 and CheY indicate that high affinity binding between CheA and CheY is mediated by the CheA-P2 domain. Interestingly, a lower K_d of 218μM was measured with SPR between *R. sphaeroides* $CheA_3$-P1 and $CheY_6$, although this complex buries less surface area at the interface than the *E. coli* complex; 530Å^2 (8). $CheA_3$ lacks a high affinity P2 domain, whereas P2 is present in *E. coli*, and as such the $CheA_3$-P1 domain is solely responsible for $CheY_6$ binding. Consequently, $CheA_3$-P1 could have developed a higher affinity site to compensate for the lack of a P2 domain, a more in-depth discussion of the $CheA_3$-P1:$CheY_6$ complex is undertaken in section 1.2.3 and includes the contributions to the interface from $CheY_6$. Additionally, the higher affinity measured with SPR for the *R. sphaeroides* chemotaxis proteins could be due to a modern machine being used compared with the SPR results obtained with *E. coli* (83) (8).

Significant binding has been observed between CheA-P1P2 and CheY, with a calculated K_d of 370nM (83). This K_d is about 10 fold greater than the K_d for the CheA-CheW-Tar:CheY complex. Taking the weak binding by P1 into account, these results further indicate that P2 provides the contacts for a high affinity CheY binding site in *E. coli*. Results from ITC experiments using CheA-P1P2 (1-233) and wild-type CheY demonstrated that the isolated domains have a lower K_d for CheY than the full-length CheA protein (50). Although the ITC results contrast with SPR

Method	**Fragments**	**K_d**	**Reference**
NMR titration	CheY:CheA1-134	4.5mM	(62)
SPR	$CheY_6$:$CheA_3$-P1	218μM	(8)
Fluoresence titration	CheY:CheA124-257	1.7μM	(83)
Fluoresence titration	CheY:CheA159-229	90nM	(85)
SPR	CheY-Y51C:CheA1-233	370nM	(83)
ITC	CheY:CheA1-233	1.2μM	(50)
ITC	CheY.Mg^{2+}:CheA1-233	1.2μM	(50)
ITC	CheY-P:CheA1-233 + EDTA	2.6μM	(50)
ITC	CheY-P:CheA1-233	6.6μM	(50)
ITC	CheY:CheA	1.9μM	(50)
Fluoresence titration	CheY:CheA	170nM	(85)
Fluoresence titration	CheY:CheA	2μM	(56)
SPR	CheY-Y51C:CheA-CheW-Tar	30nM	(75)

Table 1.1: Comparison of Different CheY:CheA Complexes K_d's. The table is split by blank rows into P1, P2, P1P2, full length CheA and full length CheA + CheW + Tar binding with CheY.

experiments, they further demonstrate that the contacts for binding are localised to the CheA-P1P2 domains. Taking the SPR and ITC results together supports the assertion of CheA modularity, where CheA-P1 provides a low affinity site for CheY association but is the site of phosphotransfer, whilst, CheA-P2 provides a high affinity site for CheY docking prior to phosphotransfer from CheA-P1.

1.5.2 CheA:CheY Phosphotransfer Kinetics

Two phases of phosphotransfer have been observed when mixing CheA-P and CheY (56). Phosphotransfer from CheA-P to CheY occurs over the initial 20ms, the complex formed has a K_d of 7 ± 2 μM, a rate of phosphotransfer (K_{phos}) of 750 ± 100 s^{-1} and a K_M of 6.5 ± 2 μM (56) (79). The phase proceeding over the next 50-100ms, is driven by CheY-P autodephosphorylation and has a rate constant of $0.04s^{-1}$. It has been demonstrated that when CheY is in a molar excess of at least 4 with respect to CheA-P, phosphotransfer will effectively be complete in less than 1s, while CheY-P auto-dephosphorylation is complete by 1 minute (79). When contrasted with the reaction kinetics of VanS and VanR, the vancomycin resistance mediating Class 1 TCS, these data demonstrate the enhanced speed at which phosphotransfer occurs between CheA-P and CheY (25). The K_{phos} from VanS-P to VanR is $1.6s^{-1}$ which is over 450 fold slower than the value for CheA-P:CheY, furthermore the K_M for VanS-P:VanR is 3μM half the corresponding value for CheA-P:CheY (25).

The peculiarities of the HPK CheA, the modular nature of the higher affinity CheY binding and lower affinity phosphotransfer domains, could well facilitate fast phosphotransfer kinetics. CheY is bound by CheA-P2 with a K_d of $\approx$ 90nM whilst CheY is phosphorylated by CheA-P1-P with a K_d in the μM-mM range. CheY-P is therefore not restrained between two high affinity sites, potentially facilitating a fast dissociation of CheY-P from the CheA-P1P2 complex. Contributing to this mechanism, the dissociation of CheY-P from the high affinity P2 domain is rapid, with a rate constant of $\approx$650 ± 200 s^{-1} (79). The rapid dissociation of CheA-P2 and CheY-P could be due to the interactions of helix 4 and Tyr106 on CheY-P and Phe214 on CheA-P2. As previously discussed, activation of CheY causes Tyr106 to adopt an internal rotomer pointing upwards towards loop 4. Additionally, the amino terminus of helix 4 moves up and out while the carboxyl terminus moves inwards towards the amino end of strand 5, precluding Tyr106 from pointing down in its internal rotomer. When bound to inactive CheY, Phe214 on CheA-P2 points downwards between the

carboxyl end of helix 4 and amino end of strand 5. Consequently, the activation of CheY would produce a movement of helix 4 that would remove Phe214 from between α_4 and strand 5.

Phe214 forms an anchor residue to CheY; a residue that provides a large share of the buried surface area at the interface and thus is a central mediator of binding (85). A Phe214Ala mutation in full length CheA causes a decrease in affinity for CheY of more than 400 fold, causing phosphotransfer to proceed 10 fold slower compared to wild type CheA. The Phe214Ala mutation had an even greater effect in the isolated P2 domain, causing a greater than 1300 fold decrease in affinity (85). The dramatic change in affinity by removing Phe214 from the CheA-P2:CheY interface illustrates the potency of this mechanism for rapid dissociation following CheY activation. However, it is interesting to note that such a large change in affinity does not cause a similar change in the speed of phosphotransfer. This indicates that the remaining residues in the P2 domain can potentially compensate for the loss of the anchor Phe214. These data also highlight the importance of the CheA-P2 high affinity binding site and the associated mechanism of rapid CheY-P dissociation to the speed of phosphotransfer between CheA-P and CheY.

1.5.3 Conclusion

CheA provides two modular binding sites for CheY, both of which involve bonds to the the α_4-β_5-α_5 region of CheY. Based on the evidence, CheA-P1 is optimised for phosphotransfer to CheY whilst CheA-P2 provides a high affinity site to not only bind CheY but to prime the RR for phosphotransfer and aid rapid dissociation upon CheY activation.

1.6 Osmosensing

The osmosensing TCS responds to changes in external osmolarity, modulating the expression of outer membrane porin proteins, OmpF and OmpC (Figure 1.14). The porins select for osmolytes based on size and charge (64). OmpC, the smaller porin, is expressed when *E. coli* is in the gastrointestinal tract, a high osmolarity condition when bile salts, micelle forming detergents that emulsify fats, need to be blocked from accessing the cells inner membrane (81).

EnvZ, the HPK of the osmosensing TCS, is bifunctional in that it is capable of both phosphorylating and dephosphorylating the RR OmpR (36) (6). The kinase and phosphatase functions are interdependent, relying on overlapping residues in the DHp and CA domain for their functions (5) (21) (108) (34). It has been demonstrated that the switch between EnvZ kinase and phosphatase functions originates from the periplasmic domain of the HPK, where residue Pro159 is central to the signal to change function (88). Increasing medium osmolarity produces an increase in the kinase function over the phosphatase function of EnvZ (88). Phosphorylation of OmpR by EnvZ results in a conformational change in the RR that allows it to bind the promoters for OmpF and OmpC with a higher affinity than when unphosphorylated (45). Differential expression of porins, dependent on medium osmolarity, is accomplished through the concentration of phosphorylated OmpR (OmpR-P), (Figure 1.14) (5). A small increase in osmolarity cause a small increase in the kinase activity of EnvZ, resulting in low levels of OmpR-P which preferentially binds to the *ompF* promoter due to its higher affinity binding sites compared to the *ompC* promoter (104). As osmolarity increases, EnvZ kinase activity increases and so does the level of OmpR-P. A greater amount of activated OmpR is available to bind to DNA, allowing binding to the lower affinity sites of the *ompC* promoter and to a lower affinity *ompF* promoter site that blocks transcription of OmpF (Figure 1.14) (6) (5) (104) (77).

1.7 OmpR

OmpR is a two domain RR belonging to the OmpR/PhoB family of RRs. Its amino terminal domain (NTD) is a classical REC domain, containing all of the conserved active site residues, see Figure 1.4. It has been demonstrated that OmpR homologues, members of the OmpR/PhoB family, share the mechanism of activation of CheY (89)

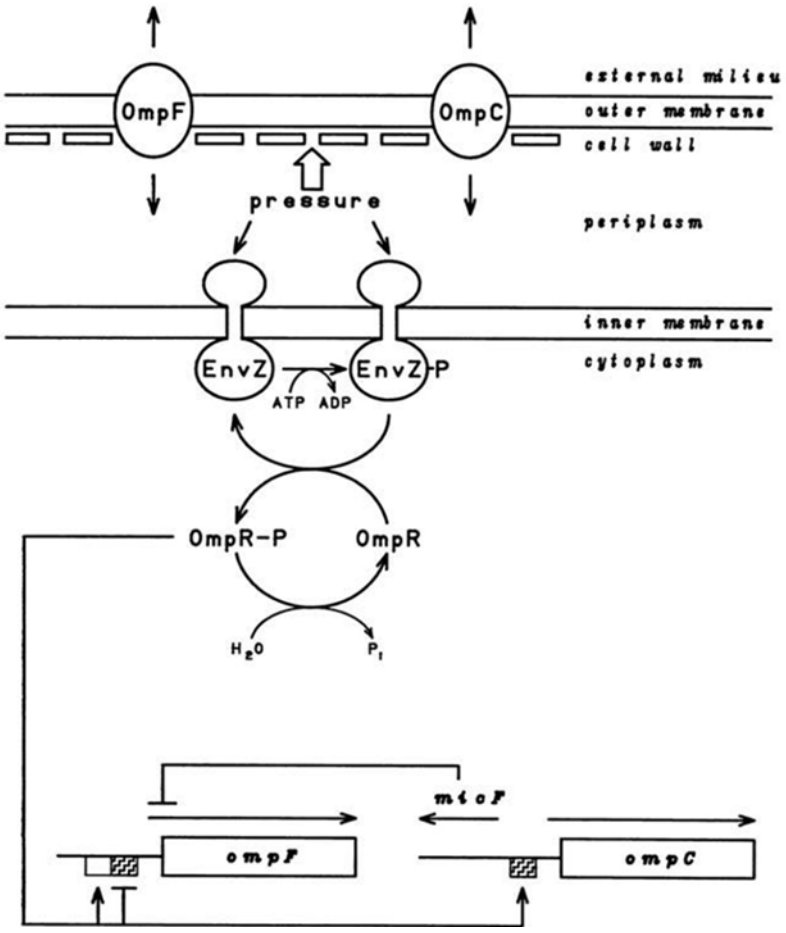

Figure 1.14: Schematic of Osmosensing System. EnvZ phosphorylates OmpR. Low osmolarity produces low levels of OmpR-P, activating transcription from *ompF* high-affinity promoter sites (open box). High osmolarity produces higher concentrations of OmpR-P that repress *ompF* transcription and activate *ompC* transcription. Transcription from pOmpC also activates transcription of *micF* RNA, which can inhibit the synthesis of OmpF. Image adapted from (81).

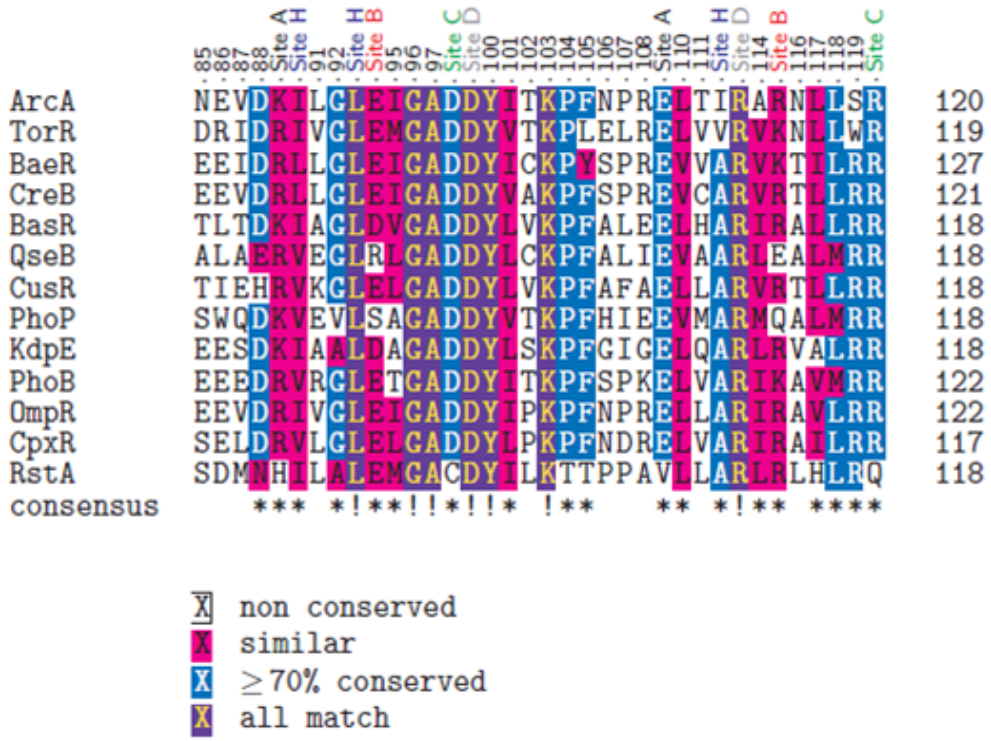

Figure 1.15: *E. coli* OmpR/PhoB family α_4-β_5-α_5 alignment. Sequence conservation across the α_4-β_5-α_5 region of the OmpR/PhoB family is shown, shading represents; similarity by property of residue, highly conserved in more than 70% and absolutely conserved in 100% of the sequences. Sites A-D pairs form inter-protein salt bridges, site H pairs form inter-protein hydrophobic contacts (29). Alignment generated in Clustal W (46).

(90) (60) (2) (26). The NTD is connected to the CTD via a 15 amino acid flexible linker, spanning residues 123-137. Data suggests a role for the linker in propagating the conformational change associated with REC domain phosphorylation to the CTD, implying it could undergo a change upon activation (40).

It has been demonstrated that the α_4-β_5-α_5 region of OmpR/PhoB members is conserved, with a sequence identity of 60%, much greater than the conservation over the rest of the domain, at 20-30% (Figure 1.15) (29). This is a particular feature of the OmpR/PhoB family (89). The reason for this conservation is due to its use in a conserved mechanism of REC domain dimerisation seen exclusively in the OmpR/PhoB family (29).

Å^2 Crystallised members of the OmpR/PhoB family ArcA, KdpE, TorR, PhoP, PhoB and MtrA all display the same mechanism of dimerisation (Figure 1.16) (89)

(90) (60) (2) (26). Helix 4 of one monomer packs against helix 5 of the second monomer. In all these structures this is mediated by a hydrophobic patch further stabilised by an extensive network of salt bridges and electrostatic interactions (Figure 1.16 and 1.15). Crystallised OmpR/PhoB homodimers bury a similar amount of surface area at the interface per monomer; ArcA 850Å^2, KdpE 900Å^2, TorR 1000Å^2, PhoP 890Å^2 , PhoB 890Å^2 and MtrA 800Å^2, indicative of α_4-β_5-α_5 conservation in the OmpR/PhoB family (89) (90) (60) (2) (26). Based on these data a common mechanism has been proposed for OmpR/PhoB family member activation (89). The model proposes that activation drives dimerisation via the stabilisation of loop 4 and Y/T coupling, where activation breaks any NTD contacts with the linker. This allows the NTD the freedom to dimerise via the α_4-β_5-α_5 region in a conserved mechanism. The removal of NTD-linker contacts and the process of NTD dimerisation results in CTD-linker contacts breaking, thus allowing the CTD to become active. This model could be applicable to OmpR, indeed dimerisation appears to be a pre-requisite to DNA binding and many orientations of NTD-linker-CTD contacts have been described, indicating that structural differences are not a barrier to this common mechanism of regulation (4) (29) (89) (90) (60) (2) (26).

It has been shown that some *E. coli* OmpR/PhoB family members can heterodimerise, although there is a kinetic preference for homodimerisation (29). OmpR-P homodimerises with a rate constant of 3.8 X 10^{-3} s^{-1}, a rate constant for heterocomplex formation is not reported although it is noted to be weak compared to homodimerisation (29). CpxR appears to be a particularly promiscuous heterodimeriser, however, given the kinetic preference for homodimerisation observed the likely *in vivo* occurrence of heterocomplexes of the OmpR/PhoB family in *E. coli* is questionable. It is worth noting that members of other RR families, such as NtrC and NtrN, were not observed to homodimerise at all (29).

The native linker of OmpR contains a mix of amino acid types and sizes but two proline residues stand out (sequence: GlnAlaAsnGluLeuProGlyAlaProSerGlnGluGlu AlaVal). Proline preferentially forms cis peptide bonds with the preceeding residue, this type of bond increases the flexibility of the peptide chain by diminishing the resonance stabilisation of the peptide bond between carbonyl and amino groups, also, the backbone amino groups of prolines cannot take part in hydrogen bonding (18). As a result of these properties, prolines are favoured in turns where they can contribute to the flexibility required to bend the peptide chain and not contribute

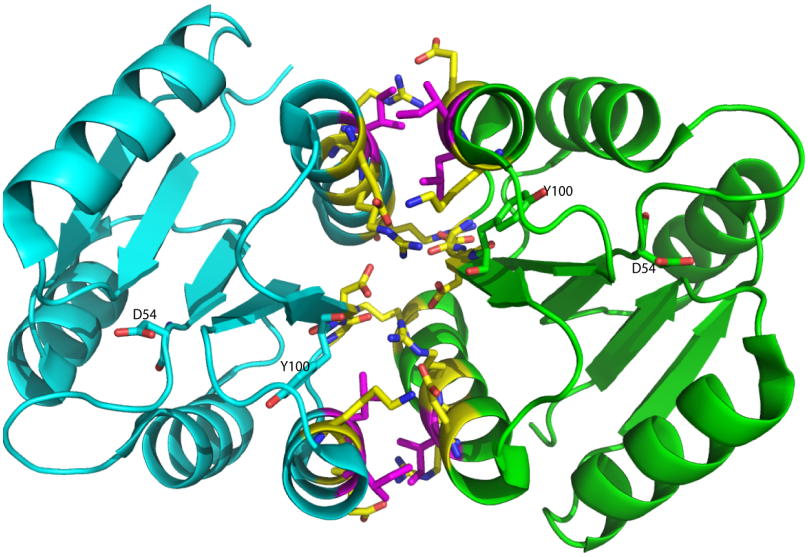

Figure 1.16: The residues of the $ArcA_N$-BeF_3^- dimer interface (pdb:1XHF). One monomer of $ArcA_N$-BeF_3^- is cyan, the other is green. Sidechains of residues that form salt bridges are coloured yellow, those that form the hydrophobic part of the interface are magenta. The sidechains of Asp54 and Tyr99 are shown as well. Residues are coloured; carbon=parent molecule colour, oxygen=red and nitrogen=blue. Images generated using PyMOL (Delano scientific).

hydrogen bonds, which stabilise the turn motif either side of the bend (18). It is possible that the LeuProGlyAlaProSer sequence could create a turn in the linker with a hydrophobic character; the two prolines would form cis bonds between Leu-Pro and Ala-Pro, while the prolines themselves would not be involved in hydrogen bonding, causing 4 residues in this turn to not hydrogen bond. The flanking Leu and Ser could hydrogen bond to bring stability to this feature. This structure, in the middle of the linker, could be involved in the information transfer from an activated NTD to the CTD, discussed in greater detail below.

The CTD DNA binding domain is the only part of OmpR for which structural data is available (54) (44). Figure 1.17 shows the DNA binding domain of OmpR, which is classified as a winged Helix-Turn-Helix (wHTH) domain. It is composed of an amino terminal 4 stranded antiparallel β sheet, which is a particular feature of the OmpR/PhoB family of RRs. The proceeding α helices, which form the helix-turn-helix motif composed of α_2-loop-α_3, pack against the antiparallel β sheet. Carboxyl to the helices is a β sheet that packs against the helical structure, as such, the helices are sandwiched between the sheets. The carboxyl β sheet forms the wing of the

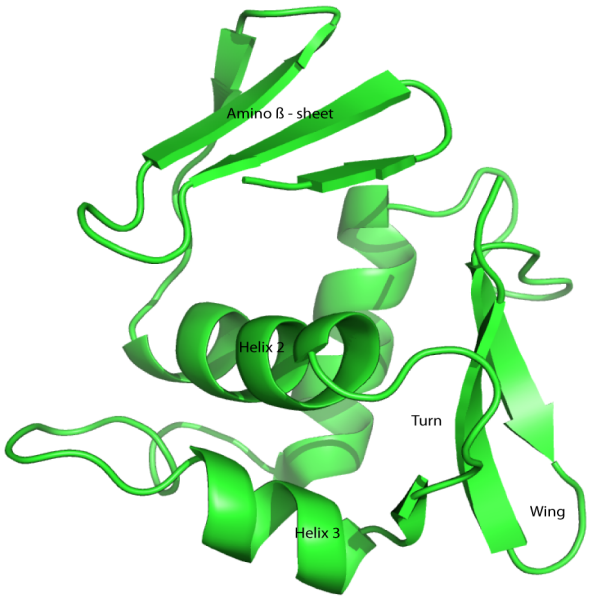

Figure 1.17: OmpR DNA Binding CTD. The general fold of the CTD of OmpR, secondary strucutre elements have been labelled. pdb:1OPC. Image generated using PyMOL (Delano scientific).

domain, specifically, β_6-loop-β_7. Functionally, both helix 3 and the loop between β_6 and β_7 interact with DNA (54).

OmpR can bind to the promoter sequences of *ompF* and *ompC*, an activity which is regulated by osmolarity. The porin OmpF is transcribed under low osmolarity, becoming downregulated with increasing osmolarity. OmpC is transcribed under conditions of increasing osmolarity (6) (5) (104) (77). It has been demonstrated that the *ompF* promoter consists of 4 sites, F1, F2, F3 and F4, additionally, the *ompC* promoter has 3 sites, C1, C2 and C3 (104) (35) (77). Each individual site contains two half sites, a and b, defined based on differences in the consensus sequence, each half site binds one OmpR protein (104) (4). The F1 and C1 sites both have the highest affinity for OmpR-P, while F2, F3, C2 and C3 are lower affinity sites, Table 1.2 (32). It can be argued that the high affinity sites, F1 and C1, are the catalyst for binding to the lower affinity sites. A comparison of the affinities of the isolated F2, F3, C2 and C3 sites with composite sites containing F1 or C1 demonstrates that the presence of F1 or C1 increases the affinity of OmpR/OmpR-P for the lower affinity sites, Table 1.2. This could indicate that upstream sites act cooperatively

with downstream sites to facilitate DNA binding. Further, it has been observed that half sites act cooperatively, only after the higher affinity b site is bound can site a be filled (104).

Based on the relative affinities and cooperativity of promoter binding, the galloping model has been proposed (104). *In vivo*, the relative affinities of the different promoter sites determines that the a and b sites of F1-3 are bound by OmpR-P before C2 and C3 are bound, and, that the C1 and F1 sites are filled at the same time. As such several steps are proposed for binding and expression from the promoters;

- F1 and C1 are filled - no expression
- F1-F2, C1 are filled - *ompF* expression
- F1-F2-F3, C1 are filled - *ompF* expression
- F1-F2-F3 + F4, C1-C2-C3 are filled - *ompF* repression, *ompC* expression.

These steps are dependent on increasing osmolarity to increase the population of OmpR-P, allowing lower affinity sites to be filled once higher affinity sites are full.

OmpR or OmpR-P cannot bind an isolated b site, indicating that OmpR/OmpR-P binds as a dimer in a cooperative manner (4). This agrees with the conjecture that OmpR dimerises similarly to other OmpR/PhoB RRs. It has been demonstrated that phosphorylation of OmpR decreases its affinity for EnvZ, from 519nM to 1.6μM, and increases its affinity for F1 DNA when compared to unphosphorylated OmpR, from 2μM to 150nM (6) (4) (41) (45) (51). Furthermore, OmpR activation decreases the K_D of OmpR homodimers, from 1.1mM to 7μM (4), indicating that activation of OmpR drives not only dissociation from its HPK, similarly to CheY activation, but also homodimerisation of OmpR monomers for promoter binding. The driving force behind DNA binding by activated OmpR appears to be its coupling to OmpR dimerisation. Evidence suggests that the change in free energy of OmpR-BeF_3^- binding to DNA, $\Delta\Delta G_{binding}$, is 1.6 kcal mol^{-1}, which is identical for the C1 and F1 promoter sites. The change in free energy of OmpR-BeF_3^- dimerisation, $\Delta\Delta G_{dimerisation}$, is 3.3 kcal mol^{-1} (4). The difference in the $\Delta\Delta G$ of these processes could serve as the driving force for more stable DNA binding by OmpR-P. This $\Delta\Delta G$ difference could help explain the binding affinities of OmpR and OmpR-P, a decrease in the $\Delta\Delta G_{dimerisation}$ from active to inactive OmpR monomers could affect the free energy available to drive and stabilise DNA binding by inactive OmpR.

DNA	OmpR K_d (nM)	OmpR-P K_d (nM)
F1	194 ±59.5	6.5 ±2.0
F2	NSB	270.9 ±27.8
F3	NSB	301.2 ±56.4
F4	NSB	NSB
F1-F2	180.4 ±31.4	10.7 ±5.1
F1-F3	183.1 ±59.1	21.9 ±1.3
F1-F2-F3	496.5 ±60.9	15.4 ±3.5
C1	101.4 ±59.1	7.7 ±4.8
C2	NSB	284.8 ±124.7
C3	NSB	NSB
C1-C2-C3	86.7 ±32.5	31.4 ±8.0

Table 1.2: Comparison of K_d of *ompF* and *ompC* promoter sites. Different concentrations of OmpR or OmpR-P, previously phosphorylated with acetyl phosphate and the level of phosphorylation quantified, were titrated with fluorescein tagged promoter DNA. NSB, non specific binding where K_d is $> 1.4\mu$M. Table reproduced from (32).

1.7.1 Conclusion

Based on the evidence from the OmpR/PhoB RR family, it is highly probable that the α_4-β_5-α_5 region of OmpR is involved in interdomain contacts to inhibit the active conformation of the DNA binding domain. Evidence indicates that the α_4-β_5-α_5 region of the OmpR/PhoB family of RRs has been adapted for a function specific for their action, instead of forming a binding site for a HPK, as in the case of CheY, it has been used to regulate activation and help stabilise the activated state via homodimerisation.

1.8 EnvZ

EnvZ, the cognate kinase of OmpR, is a bifunctional Class I HPK having both kinase and phosphatase activity (36) (6). EnvZ is an integral membrane protein, its domains consist of;

- Transmembrane domain 1 (TM1) - residues 16-47
- Periplasmic domain - residues 48-162
- Transmembrane domain 2 (TM2) - residues 163-179
- Cytoplasmic - resiudes 180-450

The TM domains help anchor the periplasmic sensor domain, while the cytoplasmic domain interacts with OmpR (72) (67). The cytoplasmic domain of EnvZ (EnvZc) exists as a dimer and is phosphorylated at a conserved histidine, His243 (72) (67). As such EnvZc, residues 223-450, can be divided into the DHp domain, residues 223-289, and a CA domain, residues 290-450 (67) (109). It has been demonstrated *in vivo* that an increase in osmolarity causes an increase in localisation of OmpR to EnvZ at the poles of the cell (6). The DHp domain of EnvZ can act as a phosphatase for OmpR on its own, however, the presence of the CA domain is required for maximal EnvZ phosphatase activity, as is Mg^{2+} and ADP (67) (109). Furthermore, the phosphorylatable histidine, His243, is required for both phosphatase and kinase functions (67) (109) (34).

The homodimeric core of EnvZc, the DHp domain, is the main site of OmpR interaction (84). It has been demonstrated that OmpR binds at the base of the 4 helix bundle formed by the 2 EnvZc monomers (84). This correlates with the specificity data generated using coevolution and verified both *in vitro* and *in vivo* (Section 1.2.3) (76). Binding studies between EnvZ and OmpR have reported a range of results from nanomolar to micromolar for the K_d of the complex, Table 1.3. The differences observed are likely to be due to differences in the conditions and methods of measurement used.

Based on the data in Table 1.3 and above a model can be proposed where increased osmolarity shifts the HPK's activity to kinase dominant causing EnvZ to autophosphorylate, OmpR localisation with EnvZ increases and OmpR undergoes phosphotransfer. Activation allows phosphorylated OmpR monomers to dimerise

with a higher affinity compared with inactive monomers, and releases the OmpR CTD from inhibitory interactions with the linker/NTD. The difference in $\Delta\Delta G$ between OmpR-P dimerisation and DNA binding provides the driving force for stable dimeric DNA binding; the $\Delta\Delta G_{binding}$ to DNA appears to be independent of promoter site. As osmolarity increases, a greater proportion of the OmpR population becomes phosphorylated, thus, greater free energy from $\Delta\Delta G_{dimerisation}$ would be available to drive DNA binding, which could explain the cooperativity seen between adjacent promoter sites. As osmolarity decreases, EnvZ becomes phosphatase dominant dephosphorylating OmpR-P, this process is enhanced by the presence of Mg^{2+} and ADP which are coordinated by the G2 box of the CA domain and a water molecule catalyses the dephosphorylation of OmpR-P.

Experiment	Conditions	Fragments	K_d	Reference
Fluorescein titration	Mg^{2+}	FL-OmpR:EnvZc	425 ±127 nM	(55)
Fluorescein titration	Mg^{2+} + OmpR-P	FL-OmpR-P:EnvZc	undetected	(55)
Fluorescein titration	Mg^{2+}	FL-OmpR:EnvZc:C123 DNA	385 ±162 nM	(55)
Fluorescein titration	Mg^{2+}	FL-OmpR:EnvZc	1.96 ±0.28 μM	(102)
Fluorescein titration	Mg^{2+} and ATP	FL-OmpR:EnvZc	0.78 ±0.064 μM	(102)
Ni-NTA agarose SDS-PAGE		His_{10}OmpR:EnvZc	1.2 ±0.17 μM	(12)
Ni-NTA agarose SDS-PAGE	Mg^{2+} and ADP	His_{10}OmpR:EnvZc	1.17 ±0.15 μM	(12)
FRET		EnvZ:OmpR-P	1.6μM	(41)
FRET		EnvZ:OmpR	519 nM	(41)

Table 1.3: K_d Comparison of Different OmpR:EnvZ Complexes. Conditions refers to additions that can influence binding, Mg^{2+} and ATP/ADP, a blank in this column indicates that these cofactors were ommitted from the reaction. In row 2, OmpR-P was phosphorylated with phosphoramidate to $> 95\%$ homogeneity.

1.9 Aims of This Study

The conserved RR REC domain is involved in every function of CheY and OmpR; HPK binding, phosphotransfer and activation, output response and dephosphorylation. Synthetic biology approaches have produced functional circuits from TCS components, although chimeric systems of class I and class II TCS have not been explored. This study will aim to create a synthetic TCS from both class I and class II components. A system where chemotactic stimuli drive transcription via a chimeric RR composed of CheY and OmpR, such a system linking taxis and transcription could be used as a motile biosensor.

To successfully fuse chemotactic sensing, which is capable of adaptation, to transcription from the OmpF and OmpC promoter sites, which produce a graded signal in response to the level of OmpR-P, the chimeric CheY-OmpR RR will need to preferentially bind CheA and become phosphorylated. To bind to the OmpF and OmpC promoter sites the chimeric RR will need to be stably phosphorylated and transduce REC domain phosphorylation into CTD activation. Consequently, these functional aspects of the chimeric RRs will be assayed; HPK binding, phosphorylation by HPK-P plus auto-dephosphorylation and DNA binding. Fusing only the RRs of the chemotaxis and osmosensing system should allow the preservation of the adaptation function regulated by upstream chemotaxis components and the graded transcriptional output from the downstream OmpF and OmpC promoter sites.

Furthermore, CheY is the archetypal REC domain and has been thoroughly studied, a large volume of data is available concerning CheY's structure, interaction with CheA and phosphotransfer and dephosphorylation kinetics. In comparison OmpR is less well studied, for example the structure of OmpR's REC domain has not been resolved. The chimeric CheY-OmpR RRs will be fused at sites across the α_4-β_5-α_5 region, an area implicated in OmpR dimerisation. Consequently, the synthetic RRs may help elucidate the mechanism of OmpR homodimerisation and highlight how activation of the REC domain is transmitted to the DNA binding domain.

The aims of this study are;

- To determine the optimum fusion site between CheY and OmpR, a number of fusion sites across the α_4-β_5-α_5 region will be created and their structures characterised by circular dichoism and ESI-MS.

- To determine the HPK binding affinity of the fusion constructs, assayed by

surface plasmon resonance.

- To determine the phosphotransfer capabilities of the fusion constructs, assayed by *in vitro* phosphotransfer with a HPK-P.
- To determine the *ompC* and *ompF* binding capabilities of the constructs, assayed by fluorescence anisotropy.

Chapter 2

Materials and Methods

2.1 General Experimental Protocols

The composition of all buffers and reagents are available in Chapter 8. Primer sequences and PCR programme details are available in Chapter 9.

2.1.1 Strains and Plasmids

Strains are summarised in Table 2.1, plasmids in Table 2.2. For plasmid propagation, strains were grown aerobically with shaking at 225rpm in Luria-Bertani broth (LB-broth), for protein expression, strains were grown in 2xTY. Where appropriate the following antibiotics, were added:

- Ampicillin at 100μg/ml or Carbenicillin at 50μg/ml dissolved in water
- Kanamycin at 25μg/ml dissolved in water
- Chloramphenicol 30μg/ml dissolved in 95% ethanol

***E. coli* Strains**	**Description**	**Source**
RP437	Wild-type chemotaxis *E. coli* strain	JS Parkinson
XL-1 Blue	General cloning strain for amplification of plasmid DNA, Tet^r, *lacI*	Stratagene
M15pREP4	Protein expression strain for pQE-60 vector, contains pREP4, Kan^r	Qiagen
BL21(DE3)pLysS	Protein expression strain for pQE-80 vector, contains pLysS, Cm^r	Promega

Table 2.1: Strains

Table 2.2: Plasmids

Plasmid	**Description**	**Source**
pQE-60	Introduces a C-terminal 6 x His-tag, Amp^r	Qiagen
pQE-80	Introduces a N-terminal 6 x His-tag, Amp^r	Qiagen
pGEX-6P1	Introduces an N-terminal Glutathione S-transferase tag, Amp^r	GE Healthcare
pQE-60-F1	C-terminal 6 x His-tag, Amp^r, F1 CheY OmpR fusion	This study
pQE-60-F2	C-terminal 6 x His-tag, Amp^r, F2 CheY OmpR fusion	This study
pQE-60-F3	C-terminal 6 x His-tag, Amp^r, F3 CheY OmpR fusion	This study
pQE-60-F4	C-terminal 6 x His-tag, Amp^r, F4 CheY OmpR fusion	This study
pQE-60-CheY	C-terminal 6 x His-tag, Amp^r, wild-type *E. coli* CheY	This study
pQE-60-OmpR	C-terminal 6 x His-tag, Amp^r, wild-type *E. coli* OmpR	This study

Table 2.2: Plasmids

Plasmid	**Description**	**Source**
pQE-60-CheA	C-terminal 6 x His-tag, Amp^r, wild-type *E. coli* CheA	This study
pQE-60-EnvZc	C-terminal 6 x His-tag, Amp^r, wild-type *E. coli* EnvZc	This study
pQE-60-mEnvZ	C-terminal 6 x His-tag, Amp^r, mutant EnvZc-L288P	This study
pQE-80-CheAP1	N-terminal 6 x His-tag, Amp^r, biotinylation-tagged CheAP1 derived from pQE-60-CheA	This study
pQE-80-CheAP2	N-terminal 6 x His-tag, Amp^r, biotinylation-tagged CheAP2 derived from pQE-60-CheA	This study
pQE-80-CheAP12	N-terminal 6 x His-tag, Amp^r, biotinylation-tagged CheAP12 derived from pQE-60-CheA	This study
pQE-80-bmEnvZ	N-terminal 6 x His-tag, Amp^r, biotinylation-tagged mEnvZ derived from pQE-60-mEnvZ	This study

2.1.2 Long Term Storage of Strains

Strains were stored at -80°C as a 1:1 mixture of stationary phase culture and 50% (v/v) glycerol.

2.1.3 Competent Cells

To prepare RbCl-competent cells, 1ml of stationary phase starter culture was sub-cultured into 50ml LB-broth, grown to an OD_{600} between 0.3 and 0.5 and chilled on ice for 15-30 minutes. Chilled cultures were spun at 2000rpm for 10 minutes at 4°C, resuspended in 16ml TFBI and chilled for a further 30 minutes. Cells were centrifuged again at 1700rpm for 10 minutes at 4°C, the resulting pellet was resuspended in 2ml TFBII. 200μl aliquots of this suspension were flash frozen in liquid nitrogen and stored at -80°C.

2.1.4 DNA Manipulation

Plasmid DNA was extracted from stationary-phase cultures using either the QIAPrep Spin Miniprep kit or the HiSpeed Plasmid Midiprep kit (both Qiagen), following the provided protocols. Chromosomal *E. coli* DNA was extracted using the GenElute Bacterial Genomic DNA Kit (Sigma), following the provided protocols.

2.1.5 Polymerase Chain Reaction

Polymerase chain reaction (PCR), to obtain DNA for cloning purposes, was carried out using Pfu DNA polymerase (Promega), with the following mixture for 1 reaction:

- 1μl template DNA
- 5μl each of two 100μM primers
- 5μl 2.5mM dNTPs
- 5μl 10x Pfu polymerase buffer (Promega)
- 1μl (2 units) Pfu DNA polymerase (Promega)
- 2.5μl DMSO
- to 50μl with MilliQ water

A gradient PCR identified the annealing temperature for optimum extension conditions, after which PCRs were completed with the appropriate annealing temperature.

2.1.6 Site Directed Mutagenesis PCR

Primer design, the PCR programme and *Dpn*I digestion were carried out as per the manufacturers protocol (Stratagene), with the following mixture for 1 reaction:

- 1μl template DNA
- 5μl each of two 100μM primers
- 5μl 2.5mM dNTPs
- 5μl 10x Pfu polymerase buffer (Promega)
- 1μl (2 units) Pfu DNA polymerase (Promega)
- 2.5μl DMSO
- to 50μl with MilliQ water

Template DNA consisted of the wild-type gene inserted in to a plasmid. Gradient PCR was not used given the low annealing temperature of the primers. PCR was followed by a 1 hour incubation at 37°C with the addition of 1μl of *Dpn*I (NEB) to digest the methylated and hemimethylated template DNA. 1μl of this mixture was transformed into XL-1 Blue competent cells using the standard protocol (Section 2.1.13).

2.1.7 Overlap-Extension PCR

Overlap extension PCR (OE-PCR) was used to make the chimeric proteins F1, F2, F3 and F4. In OE-PCR two rounds of PCR are undertaken and 4 primers are designed, 1-4, to amplify the native DNA. Two primers have complementary 5' sequences allowing their amplified sequences to anneal in the second round of OE-PCR to produce a chimeric sequence. In this study, for example, in the first round of PCR forward primer 1 and reverse primer 2 amplified *cheY* and forward primer 3 and reverse primer 4 amplified *ompR*. The 5' end of primers 2 and 3 are complementary. During

the second round of PCR their products can anneal and are amplified by primers 1 and 4 producing chimeric DNA containing textitcheY fused with *ompR*. The reaction mixture for an OE-PCR is as above for PCR.

2.1.8 DNA Electrophoresis

DNA fragments were separated by size in 0.8% to 2% (w/v) agarose (Roche) made up in 0.5 x TBE solution. 5 x DNA loading dye was added to each sample. The gels were run at 80 - 140v, dependent on the size of the gel, then stained in ethidium bromide solution (1ng/ml) for 20 minutes and viewed with a UV transilluminator.

2.1.9 Extraction of DNA from Agarose Gels

The Genelute Gel Extraction kit (Sigma) was used to extract DNA from the bands excised from gels following the manufacturers protocol.

2.1.10 PCR DNA Restriction

PCR DNA restriction reactions were incubated for 3 hours at 37°C, each 100μl reaction contained:

- 50μl purified PCR product
- 1μl BSA
- 10μl 10 x Buffer
- 3μl each of two restriction enzymes
- 33μl Water

Purification of the restricted PCR DNA was accomplished with Genelute Gel Extraction kit (Sigma), as per the manufacturer's protocol.

2.1.11 Plasmid DNA Restriction

Plasmid DNA restriction reactions were incubated at 37°C for 2 hours, each 20μl reaction contained:

- 2μl plasmid DNA

- 0.5μl BSA
- 2μl 10 x Buffer
- 0.5μl each of two restriction enzymes
- 14.5μl Water

Purification of the restricted plasmid DNA was accomplished with Genelute Gel Extraction kit (Sigma), as per the manufacturer's protocol.

2.1.12 DNA Ligation Reactions

Vector and insert DNA were mixed in a 1:3 molar ratio with 3μl DNA ligase (NEB) and the appropriate buffer to a total reaction volume, with water, of 20 μl. The reaction mixture was incubated for 16 hours at 16°C, then transformed into previously-prepared competent cells.

2.1.13 Transformation Of Competent Cells

Competent cells were transformed with up to 3μl of plasmid DNA or, for ligations, 5μl of the ligation mixture. Aliquots of competent cells were defrosted on ice for 25 minutes, then DNA was incubated with competent cells for 30 minutes on ice. The transformation mixture was heat-shocked at 42°C for 2 minutes, then incubated for 2 minutes on ice. 800μl of LB-broth was added to the transformation mixture, followed by a 1 hour incubation at 37°C. The transformation mixture was spread onto LB-agar plates containing appropriate antibiotics and incubated overnight at 37°C.

2.1.14 DNA Sequencing

DNA sequencing was done by the Automated DNA Sequencing Service provided by Source BioScience Lifesciences. The BigDye dye termination method (PE Biosystems) was used on a 3730 DNA sequencer (Applied Biosystems). Sequences were analysed using Clone Manager Professional version 9 (Sci Ed Central).

2.1.15 SDS-PAGE

10μl of eluted protein was mixed with 20μl 5xSDS Buffer and boiled for 10 minutes. Subsequently, samples were centrifuged briefly in a Tomy Capsule HF-120. 15μl of each sample and a ladder (BenchMark Prestained Protein ladder from life technologies) were loaded on to a 4-20% RunBlue SDS Precast Gel from Expedeon. Gels were run in 20 x Reducing buffer for 1 hour at 175V, 110mA/gel and 50W. Gels were stained with InstantBlue (Expedeon), and visualised using a G:Box from Syngene.

2.2 Overexpression and Protein Purification

2.2.1 CheA, CheY, OmpR and Fusion Proteins

100ml starter cultures were grown at 37°C in 500ml flasks in 2xTY media, with the appropriate antibiotics, to an OD_{600} between 0.3 and 0.5. 25ml was subcultured into 500ml of 2xTY media, with the appropriate antibiotics, in 2L flasks . These were grown to an OD_{600} between 0.3-0.5. Cultures were then induced with 200μM of IPTG and grown for 4 hours at 37°C. Cells were harvested by centrifugation at 7000g for 10mins, weighed and the pellets frozen at -80°C. Pellets were defrosted at room temperature then resuspended in His-Tagged Protein Lysis buffer at 5ml/g of cells. This mixture was sonicated (Vibracell Sonics Materials Incorporated) for 6 minutes with a regime of 5 seconds on, 5 seconds off at 60% of maximum. Lysates were centrifuged at 35000g for 30 minutes to remove insoluble material and cell debris. The cleared lysates were applied to Nickel-NTA Agarose resin (Qiagen) equilibrated with His-Tagged Protein Lysis buffer. Columns contained 1ml Nickel-NTA Agarose per 6L of culture. Columns were washed with 20ml of His-Tagged Protein Wash Buffer I followed by 4ml of His-Tagged Protein Wash Buffer II. Columns were incubated with 8ml of His-Tagged Protein Elution Buffer for 5 minutes, after which 0.5ml fractions were collected and stored on ice. Where proteins precipitated during elution, aliquots were diluted 1:1 with a volume of elution buffer and spun for 10 minutes at 17000g at 10°C, the supernatant was removed to separate the precipitate from the soluble protein.

Proteins were further purified using an ÄKTApurifier with a HiLoad 16/60 Superdex 75 column, running Unicorn version 5.11 (GE Healthcare). Fresh running buffer was made for each new run. Elution times were calculated based on the stan-

dards provided for the column by GE Healthcare. Eluted fractions were stored on ice and their concentration measured using a Bradford based assay (BioRad) using BSA as a standard. To verify the purity and molecular weight of the fractions collected, SDS-PAGE was used. Subsequently, proteins were concentrated in a vivaspin 15ml concentrator (Sartorius Stedim biotech), concentrators were equilibrated with 1ml running buffer at 3000g for 5 minutes at 10°C. Proteins were concentrated to greater than 1mg/ml, assayed by Bradford. Proteins were characterised using ESI-MS to verify the molecular weight and the dominant species

2.2.2 EnvZ GST

Overexpression and cell harvesting procedures for the EnvZ-Glutathione S-transferase (GST) tagged protein were as above for His-tagged wild-type and chimeric proteins. Frozen cell pellets were defrosted at room temperature and resuspended in GST-Tagged Protein Binding Buffer at 5ml/g of cells, before sonication and centrifugation as above. The cleared lysates were applied to a gravity flow column containing Glutathione Sepharose 4B (GE Healthcare), equilibrated with GST-Tagged Protein Binding Buffer. The column contained 1ml of Glutathione Sepharose 4B per 6L of culture. The column was washed with a total of 15 column volumes of GST-Tagged Protein Binding Buffer. Protein was eluted by applying 0.5ml of GST-Tagged Protein Elution Buffer per ml of Glutathione Sepharose 4B, the elution step was repeated three times. 0.5ml fractions were collected and stored on ice.

Further purification of EnvZ-GST followed the protocol optimised for His-tagged proteins, above. The purification of EnvZc-L288P (mEnvZ), a phosphatase null mutant of EnvZ, followed the purification procedures outlined in this section for wild-type EnvZ.

2.2.3 Biotinylated HPKs

For surface plasmon resonance (SPR) experiments, biotinylated HPKs (the ligands) were attached to a streptavidin hybridised sensor surface. CheA-P1, CheA-P2 and CheA-P1P2 and mEnvZ were inserted into the pQE80 plasmid, with an amino terminal His-tag. A minimal biotinylation tag used for immobilisation was engineered to the carboxyl terminii of the HPKs; (GlyGlyGlyLeuAsnAspIsoPheGluAlaGlnLysIsoGlu TrpHisGlu) where the lysine residue is the site of biotinylation (7).

All HPK constructs were transformed into competent BL21(DE3)pLysS cells. The overexpression protocol for each HPK followed the standard heat shock protocol followed by spreading on to LBA plates containing biotin at 2% (w/v), to ensure *in vivo* biotinylation of the HPK constructs. Biotin was used at this concentration based on unpublished observations by Dr Mostyn Brown. Colonies were cultured at 37°C for 18 hours in 100mls of 2xTY , with the appropriate antibiotics and 2% (w/v) of biotin. Subsequently, 50ml was subcultured in to 500ml 2xTY with 2% (w/v) of biotin, grown at 37°C to OD_{600} between 0.3-0.5 after which they were induced with 200μM IPTG for 4 hours at 37°C.

Centrifugation and purification procedures were the same as for unbiotinylated CheA and mEnvZ. Biotinylated proteins were not further purified using an ÄKTApurifier, additional purification took place via binding these biotinylated proteins to the chip for SPR.

2.3 Circular Dichroism

Circular dichroism (CD) experiments were used to ascertain the structural characteristics of CheY, OmpR and the fusion proteins. Experiments were performed on a Jasco J-720 Spectropolarimeter with a 1mm path length. Proteins were buffer exchanged into Cicular Dichroism Buffer using a PD SpinTrap G-25 as per the manufacturers instructions (GE Healthcare). After buffer exchange, protein concentration was adjusted to 0.123mg/ml. Spectra were collected from 190-260nm over a temperature range of 20° to 90° to monitor the denaturing behaviour of wild-type and chimeric RRs.

2.4 Phosphotransfer Assays

HPK was autophosphorylated at room temperature for 30 minutes in Histidine Kinase Autophosphorylation Buffer, which contained 0.67mM of [γ-^{32}P] ATP (final concentration) with a specific activity of 14.8 GBq/mmol. Phosphotransfer reactions from HPK to wild-type or fusion RRs were performed in 1 x Phosphotransfer Assay Buffer at room temperature. 10μM of wild-type or fusion RR were incubated with 5μM of the phosphorylated HPK (final concentrations), aliquots of this mixture were removed at the specified time points, quenched in Phosphotransfer Loading Dye and

stored on ice. Quenched samples underwent SDS gel electrophoresis on 15% polyacrylamide gels, at 4°for 45 minutes. Gels were dried, exposed to phosphor screens (Kodak) and analysed using an SF-phosphorimager with ImageQuantTL software (version 7.0, GE Healthcare), correcting for the background present in each lane. [γ-^{32}P] ATP standards of 5, 4, 3, 2, 1, 0.5, 0.4, 0.3, 0.2, 0.1 and 0.05 pmol/μl were included.

2.5 Surface Plasmon Resonance

Experiments were performed at 25°C on a BIAcore T200, using a Series S Sensor Chip CAP (GE Healthcare) with a Biotin CAPture kit (GE Healthcare) as per the manufacturers instructions. Biotinylated HPKs, mEnvZ, CheA-P1, CheA-P2 and CheA-P1P2 (the ligands) were diluted to a 1μM stock in SPR Buffer. Serial dilutions of the wild-type and fusion RRs (the analytes) were made from 3μM to 0.01μM in SPR Buffer. Ligands were attached to the sensor chip using the Biotin CAPture Reagent (GE Healthcare), analytes were flowed over the surface at a rate of 2μl per minute. The sensor surface was regenerated after each cycle using the Regeneration Solution, after which fresh ligand was attached to the sensor chip. kD values were generated from reference subtracted sensorgrams using a steady-state surface bound affinity model using the default settings (T200 Evaluation Software, GE Healthcare).

2.6 Fluorescent Anisotropy

C1-C2-C3 and F1-F2-F3 composite promoter sites tagged with fluorescein and complimentary untagged strands (both Sigma, purified via HPLC) were annealed in Oligo Annealing Buffer. To verify annealing, 10μl aliquots of each single stranded oligo and the annealed reaction were mixed with 5μl of 5 x DNA Loading Dye and run on 20% RunBlue Native Precast Gels (Expedeon) in 1 x Native Running Buffer.

Both phosphorylated and unphosphorylated wild-type and chimeric RRs were assayed for DNA binding activity. To increase accuracy at low protein concentrations Biotix lo-bind tips were used for all stages of the phosphorylated and unphosphorylated assay.

Unphosphorylated RRs were diluted to stock concentrations of 1μM and 0.1μM in Anisotropy Buffer, diluted to reaction concentrations and aliquotted in to a 96 well

plate to a final volume of 100μl per well, using 3 wells per concentration.

Phosphorylated RRs were obtained by incubation with a phosphorylated HPK; wild-type RRs were incubated with their cognate HPK and chimeric RRs were incubated with a suitable HPK to achieve maximal phosphorylation over the course of the assay.

5μM of HPK was autophosphorylated at room temperature for 30 minutes in Anisotropy Buffer containing 5mM ATP. CheY, OmpR and fusion RRs were diluted to stock concentrations of 1μM and 0.1μM. Phosphorylated HPKs were mixed in a 2:1 ratio with RR stock concentrations. Reactions were incubated for at least 10 minutes to ensure the phosphotransfer reaction had reached its end-point. These were then diluted with Anisotropy Buffer to the specified concentrations and aliquotted in to a 96 well plate to a final volume of 100μl per well, using 3 wells per concentration. To ensure that ATP was not exhausted between assay preparation and assay measurement a ratio of HPK:ATP of 1:1000 was chosen. CheY-P, the RR with the fastest autodephosphorylation rate used in this study, has a $t_{\frac{1}{2}} \approx 20$s, equating to 90-135 half lives over the 30-45 minutes required to complete the assay. Taking the multiple dilution steps into account results in a final ratio of HPK:ATP of 1:700. Consequently, ATP should not be exhausted over the course of the anisotropy experiment ensuring that RRs are phosphorylated when measurements are taken.

Data analysis was done using the MARS Data Analysis software version 2.1 (BMG Labtech). Blank subtracted anisotropy was calculated for each well, using the following equation (2.1) for anisotropy,

$$Anisotropy = 1000 * (parallel - perpendicular)/(parallel + 2 * perpendicular) \quad (2.1)$$

These values were plotted using Sigma Plot version 12 (Systat Software Inc.), and fitted to a Single Rectangular 2 Parameter Hyperbola model.

Chapter 3

Chimeric Protein Design

3.1 Chapter Overview

This chapter will address chimera design issues that could affect HPK binding, phosphotransfer, auto-dephosphorylation and DNA binding. This chapter will then assess the physical properties of the chimeras and whether they are suitable to use for experimentation.

3.1.1 Chimera Design Considerations

RRs CheY and OmpR have a conserved REC domain in common, this NTD runs from β_1 to α_5 with alternating β strands and α helices. The conserved residues of the REC domain are therefore common to both RRs, these comprise the active site required for phosphotransfer. Primarily, differences between CheY and OmpR occur in residues that mediate the other functions such as HPK binding, auto-dephosphorylation and output modulation, Figure 3.1.

The SDRs of OmpR are located in helix 1 and loop 5 of the REC domain. In CheY, binding to CheA occurs via helix 1 and across the whole α_4-β_5-α_5 region of the REC domain. Activation of both CheY and OmpR results in conformational changes that occur in the α_4-β_5-α_5 region of the REC domain. Activation of OmpR leads to monomer dimerisation, the residues for which lie across the α_4-β_5-α_5 region of the REC domain. CheY activation results in the α_4-β_5-α_5 region binding to FliM of the motor or to the phosphatase CheZ, these residues are not shown in Figure 3.1 since they are not of direct interest to this study. Auto-dephosphorylation residues are located in conserved positions in the REC domain. The difference between these residues results in CheY-P auto-dephosphorylating faster than OmpR-P, the $t_{\frac{1}{2}}$ for CheY-P is $\approx$ 20s and for OmpR-P it is $\approx$ 90min.

The different functions of the REC domains of CheY and OmpR dictated the design of the chimeras. The rationale for the chimeric RRs composed of CheY and OmpR was that the CheY component would bind to CheA and undergo phosphotransfer to the active site. Similarly to wild-type RRs, phosphorylation would be transduced into a conformational change transmitted to the α_4-β_5-α_5 region of the chimeric REC domain where the OmpR component would dimerise and mediate the output of DNA binding to *pOmpC* or *pOmpF*. Consequently, a number of fusion sites between CheY and OmpR were investigated to determine which one would produce optimal binding, phosphotransfer and signal transduction for the chimeric RR.

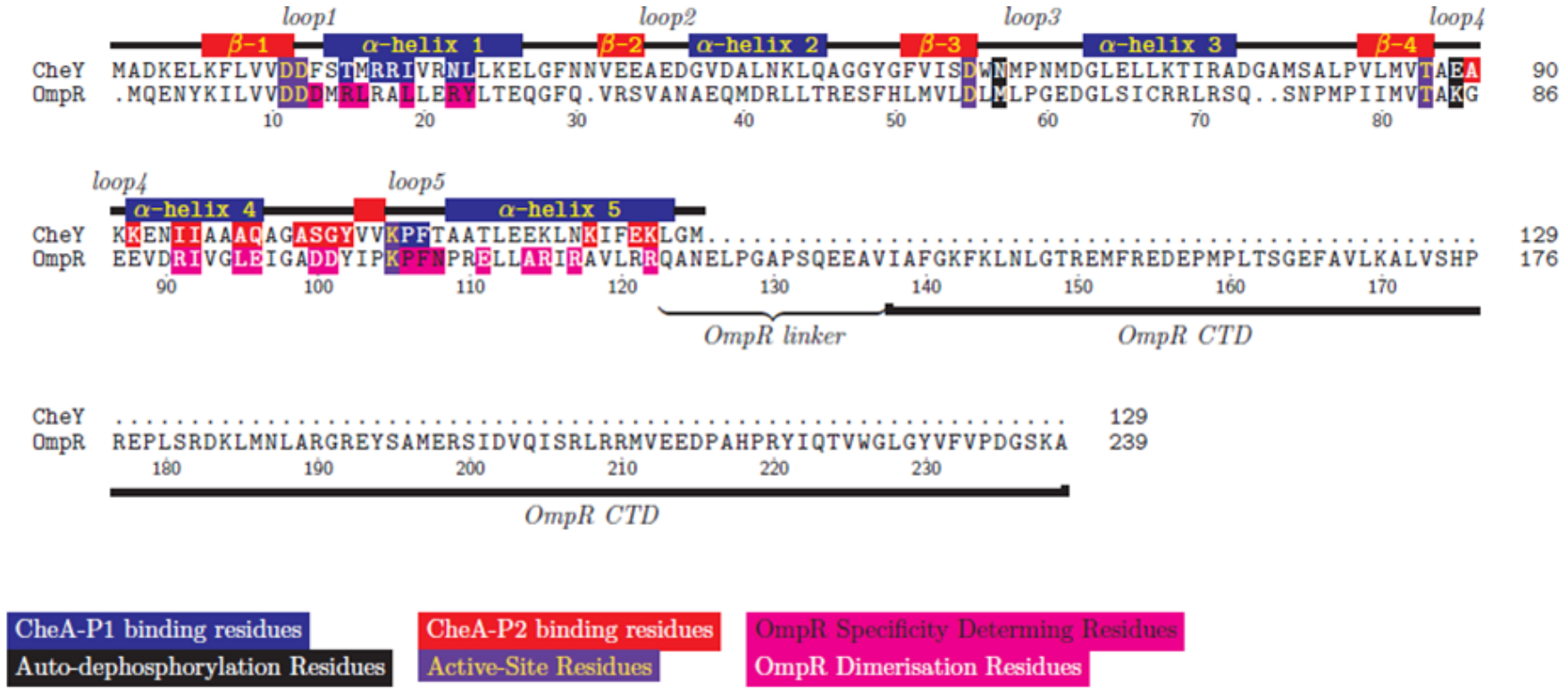

Figure 3.1: Alignment of CheY and OmpR highlighting features of the REC domain. Highlighted on both RRs are the conserved active site and auto-dephosphorylation residues. Highlighted on CheY are the CheAP1P2 binding residues. The OmpR sequence shows SDRs for EnvZ and the OmpR/PhoB NTD dimerisation residues. See legend for details. Secondary structure depicted is that of CheY. Alignment performed with Clustal W (46).

Figure 3.2 shows an alignment of CheY, OmpR and Fusions 1-4 (F1-4) and Figure 3.3 shows a schematic of the fusion sites. The alignment highlights features of the wild-type REC domain of CheY and OmpR. Highlighted on both are the conserved active site and auto-dephosphorylation residues. Highlighted on CheY are the residues involved in CheA-P1P2 binding. Highlighted on OmpR are OmpR SDRs for EnvZ and the OmpR/PhoB NTD dimerisation residues. The sequences of F1-4 can be observed, each shares features with CheY and OmpR, and fusion sites between these sequences are highlighted. All the fusion sites between CheY and OmpR occur in the α_4-β_5-α_5 region. Common to each fusion is the OmpR linker and CTD. Highlighted on F1-4 are the REC domain residues that each has in common with CheY and OmpR.

F3 is composed of the entire CheY sequence fused to a truncated OmpR linker and full CTD. Due to an earlier alignment error, the first 3 OmpR linker residues have been clipped (GlnAlaAsn, residues 123-125). F4 contains the entire CheY protein fused to the OmpR linker and CTD, F4 was created to correct the mistake made with F3. Consequently, the REC domains of F3 and F4 contain only CheY residues. As synthetic RRs, it is unlikely that REC domain activation of F3 and F4 will lead to activation of the downstream OmpR components, especially since dimerisation is required for OmpR DNA binding.

F2 is a REC domain fusion between loop 5 of CheY and OmpR. The wild-type RRs have conserved residues in loop 5, consequently, this region was chosen as a suitable fusion site to minimise structural disruption to the mutant. F2 contains the auto-dephosphorylation residues of CheY, all the CheA-P1 binding residues of α_1 and loop 5, the CheA-P2 binding residues of α_4 and β_5 and the OmpR dimerisation residues of helix α_5. In addition, F2 has one OmpR SDR, Asn108 in α_5. As such, F2 is missing the α_5 CheA-P2 binding residues, the α_4 and β_5 OmpR dimerisation residues and the α_1 SDRs for EnvZ. As a synthetic RR connecting chemotaxis to transcription, it is arguable that F2 could bind to CheA-P1, although the loss of the α_5CheA-P2 binding residues could result in reduced affinity for CheA. The position of the fusion site in F2 could produce CheY-type phosphorylation, dephosphorylation and conformation change behaviour in the REC domain. F2 contains a reduced number of OmpR NTD dimerisation residues, although these could be sufficient for dimerisation upon activation. However, this effect would depend on successfully transmitting CheY activation into a conformational change that produces OmpR dimerisation. Furthermore,

if F2 auto-dephosphorylates similarly to CheY the activation signal maybe too short lived to lead to dimerisation and DNA binding. However, evidence suggests that the conformational change due to phosphorylation can block auto-dephosphorylation by producing stabilising interactions, indicating that if F2-P dimerises it could have a longer half-life than CheY-P (69).

F1 is a REC domain fusion between β_4 and the amino terminii of loop 4 of CheY and OmpR. The wild-type RRs are also completely conserved at this fusion site, which could minimise disruption to the mutant RR's structure. F1 contains all the CheA-P1 binding residues of α_1 and loop 5. The sequence conservation between loop 5 of CheY and OmpR means that although all of the α_4-β_5-α_5 region of F1 is constituted solely from OmpR it retains the CheA-P1 binding residues; Lys109 and Phe111 (CheY numbering). F1 contains no CheA-P2 binding residues but all of the OmpR NTD dimerisation residues. In addition, F1 has one OmpR SDR, Asn108 in α_5. As such F1 is missing the α_1 SDRs for EnvZ. F1 contains one auto-dephosphorylation residue each from CheY and OmpR. F1 maybe able to bind to CheA-P1 and undergo phosphotransfer, although the lack of CheA-P2 binding residues may hamper this process. F1 could dimerise via its OmpR α_4-β_5-α_5 region but only if phosphorylation induces a conformational change in the OmpR component. If phosphorylation is transduced into a conformational change, F1 could have a half-life similar to OmpR. It has been demonstrated that the positive charge of the OmpR auto-dephosphorylation residue, lysine 85, can cause an extension of RR half-life (86) (69).

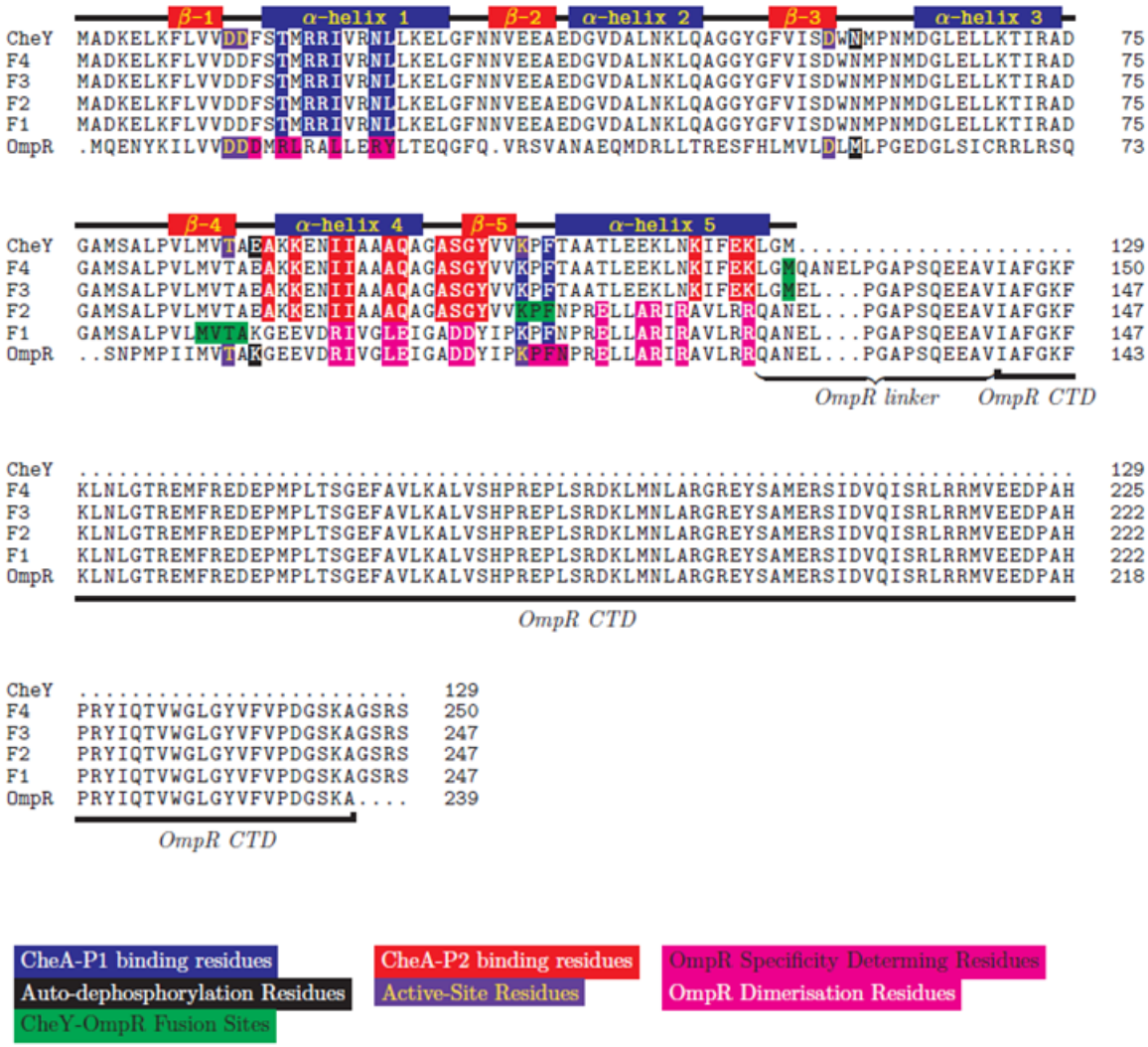

Figure 3.2: Alignment of CheY, OmpR and Fusions 1-4. See text and legend for details. Secondary structure depicted is that of CheY. Alignment performed with Clustal W (46).

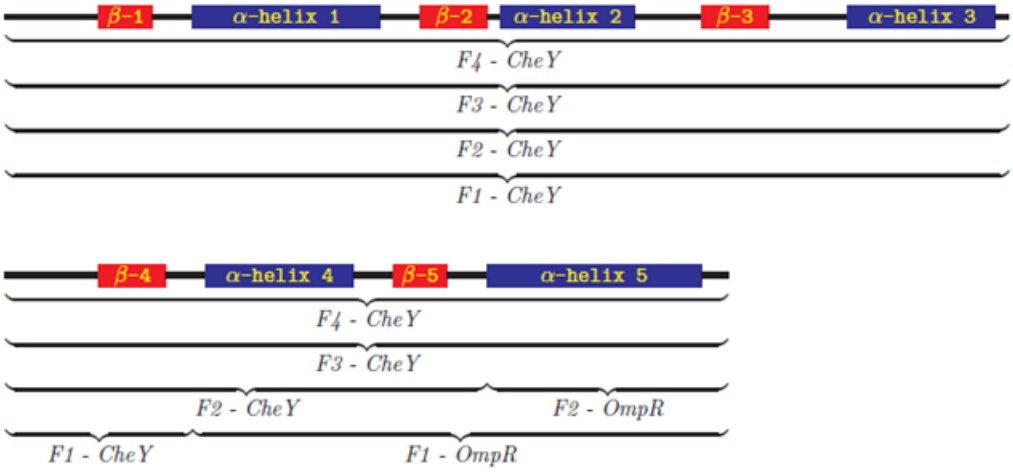

Figure 3.3: Schematic of F1-4 fusion sites. Below the REC domain structure of CheY is a schematic of F1, F2, F3 and F4 fusion sites labelled with their CheY and OmpR components. F4 and F3 are composed of only CheY, F2 and F1 contain both CheY and OmpR. The OmpR linker and CTD are common to each fusion, therefore, these are not shown on the schematic.

3.2 Chimeric Protein Over-expression

Chimeric proteins proved difficult to purify. Using a standard protocol for over-expression it was observed that strains carrying F1 and F2 had lower and inconsistent growth, as measured by the time taken for a starter culture to reach an OD_{600} between 0.3-0.5. Less severe effects were noted for F3 and F4, ultimately the toxicity of the chimeric RRs impacted protein yield. Consequently, a new protocol had to be developed and optimised to maximise protein expression while minimising toxicity to over-expression strains. This protocol aimed to reduce the number of generations between the starter culture and the end of induction. Steps taken to optimise expression conditions included;

- Over-expression over a shorter 12 hour period
- Over-expression cultures grown in a richer medium to maximise growth over the short time period
- Scaling up over-expression to 12L of media per protein
- Less media used per flask to increase oxygenation of the cultures
- More IPTG used at induction

As a result of this approach, growth increased between 3 and 12 fold depending on the protein expressed, assayed by mass of cell pellets from 1L of culture. Due to the success of this protocol all proteins used in this study were over-expressed in this way. The full protocol for over-expression is available in Materials and Methods, Section 2.2. Using the new protocol, over-expression strains containing wild-type proteins, CheY and OmpR, and F3 and F4 exhibited the highest expression levels. F2 and F1 consistently managed lower levels of expression. The relative levels of expression between the proteins could be expressed as CheY = OmpR = F4 = F3 $\gg$ F2 $>$ F1. Indicating that the OmpR additions to CheY in F4 and F3 were not deleterious to expression. However, changes to the REC domain in F2 and F1 had more severe effects.

3.3 Chimeric Protein Characterisation

Proteins were purified with an AKTApurifier with a HiLoad 16/60 Superdex 75 column, the elution profiles of OmpR and F2 are displayed in Figures 3.4 and 3.5. OmpR, F4 and F3 elute with identical profiles, a peak corresponding to elution of RR monomers can be observed between fractions 60 and 75 (Figure 3.4). Only a small fraction of the eluted protein is potentially dimeric, RR dimers would elute between fractions 50 and 55. Figure 3.5 represents the elution profile for F2, approximately fives times less monomeric F2 is eluted compared to OmpR indicative of the expression issues with this chimeric RR. Similarly to OmpR, little dimeric F2 is eluted between fractions 50 and 55. Only fractions between 60 and 75 were collected and used for further experimentation.

After purification, proteins were characterised using ESI-MS to verify the molecular weight and the dominant species, and further characterised with heat denaturing CD to investigate their structural characteristics. These data are summarised in Table 3.1.

Each protein used in the study was subjected to ESI-MS, Table 3.1. The predicted molecular weight was calculated based on the DNA sequencing results, submitting these to the ExPASY translate (web.expasy.org/translate/) and ProtParam (web.expasy.org/protparam/) servers. Sequences included affinity tags and biotinylation tags, where appropriate.

CheA ESI-MS matches its predicted molecular weight within the limits of the

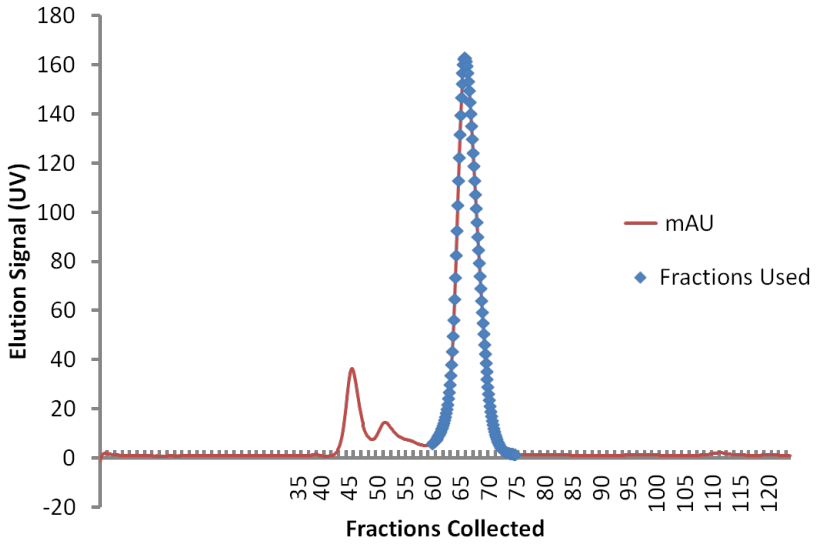

Figure 3.4: OmpR elution profile from AKTApurifier using a HiLoad 16/60 Superdex 75 column. Fractions collected are highlighted in red, fractions used for further experiments are highlighted in blue between fractions 60 and 75. Higher molecular weight complexes can be observed, dimers would elute between fractions 50 and 55. The peak between 40-47 is likely to be from buffer exchange (based on unpublished observations by Dr K. Scott).

technique. mEnvZ undergoes an addition of +80, which is most likely due to phosphorylation.

Mass spec results for biotinylation tagged CheA-P2 (bCheA-P2) and biotinylation tagged CheA-P2 mEnvZ (bmEnvZ) match their predicted molecular weights. However biotinylation tagged CheA-P1 (bCheA-P1) undergoes a reduction of 950 and biotinylation tagged CheA-P1P2 (bCheA-P1P2) undergoes an addition of 133. The decrease in mass of bCheA-P1 cannot be accounted for by a single change. A common cleavage is the 5' methionine start site, this would account for only 131-149 Da (http://www.abrf.org/) of the mass change. Cleavage of the start site, the proceeding residues and 4 histidines of the 6x His-tag would decrease the mass of bCheA-P1 by 980 Da. However, no affect on protein yield was observed compared to other biotinylation tagged proteins, which would be expected with a truncation of the His-tag.

The addition to bCheA-P1P2 cannot be explained by biotinylation of the construct, which has a mass of 226-354Da (http://www.abrf.org/). Part of the mass could be due to phosphorylation of the CheA-P1 histidine, which would increase the

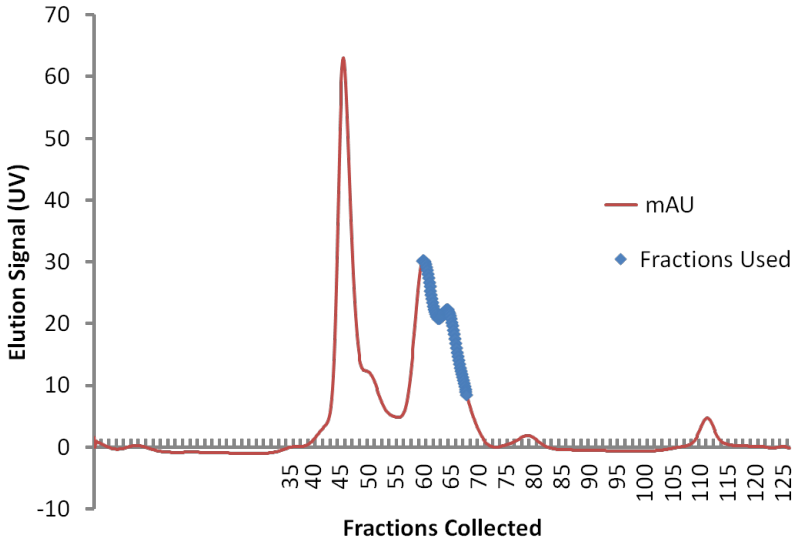

Figure 3.5: F2 elution profile from AKTApurifier using a HiLoad 16/60 Superdex 75 column. Fractions collected are highlighted in red, fractions used for further experiments are highlighted in blue between fractions 60 and 70. Higher molecular weight complexes can be observed, dimers would elute between fractions 50 and 55. The peak between 40-47 is likely to be from buffer exchange (based on unpublished observations by Dr K. Scott).

mass by 80 Da. The cause of the remaining 50 Da change in mass is difficult to determine. Oxidation of cysteine results in a +48 Da mass change, although this is unlikely because reducing conditions were maintained during purification. Another potential modification is acetylation of either a lysine or serine residue. Acetylation results in a mass change of 42 Da.

The results of ESI-MS with the biotinylation tagged proteins indicate that none of the dominant species are biotinylated. The lack of biotinylation observed in MS data is most likely due to use of *in vivo* biotinylation by *E. coli*, rather than *in vitro* enzymatic biotinylation by BirA.

The measured CheY mass is 469 Da more than the predicted mass based on DNA sequencing results. CheY can be phosphorylated, which would add 80 Da, however the CheY-P $t_{\frac{1}{2}} \approx 20$s, discounting phosphorylation as a modification. CheY has been shown to undergo acetylation at 6 lysines (101) (3). Acetylation acts similarly to phosphorylation, allowing CheY to change the motor direction from CCW to CW (101). Acetylation of all 6 sites has only been observed *in vitro* but would results in a change in mass of 252 Da (3). *In vivo* acetylation at 1-3 lysines is most common, 3

acetyl groups would change CheY's mass by 126 Da (101). Assigning the remaining 343 Da to a modification is difficult, and there is no evidence that CheY can be modified other than by acetylation and phosphorylation.

Protein	Predicted MW	ESI-MS dominant species MW	T_m °C	Used
CheA	72458.4	72456	N/A	Yes
mEnvZ	56406.8	56486	N/A	Yes
bCheA-P1	20096.3	19146	N/A	Yes
bCheA-P2	17812	17818	N/A	Yes
bCheA-P1P2	31715.4	31848	N/A	Yes
bmEnvZ	33175.5	33176	N/A	Yes
CheY	15307.6	15776	51.5	Yes
OmpR	28563.8	28572	55.8	Yes
F1	28514.7	NDS	58	No
F2	28568.9	28192	55	Yes
F3	28206.4	28082	45 and 64	Yes
F4	28519.7	28396	43.5 and 55	Yes

Table 3.1: Summary of Wild-Type, Biotinylated and Chimeric Characterisation. T_m is defined by the temperature corresponding to an folded:unfolded ratio of 1. T_m is calculated as the mid-point value from thermal stability profiles at 222nm. N/A is not applicable, NDS is no dominant species for ESI-MS

CD data indicates that CheY is folded at room temperature, producing an alpha helical dominated spectra, Figure 3.6.A. Figure 3.7.A shows that CheY undergoes a long unfolding phase from ≈ 35 and 65 °C at 222nm, punctuated by small transitions at higher and lower temperatures. It has been demonstrated that CheY has such a profile when under heat or urea denaturing conditions (24). The equilibrium unfolding T_m (the mid-point of the unfolding transition) is calculated at 51.5 °C. These data indicate that CheY is folded

The measured OmpR mass matches that predicted, Table 3.1. Furthermore, CD spectra indicate that OmpR contains secondary structure at room temperature (Figure 3.6.B). Thermal stability profiles demonstrate OmpR undergoes a sudden highly cooperative unfolding event from ≈ 50-60 °C (Figure 3.7.B). Consequently, the equilibrium unfolding T_m of OmpR is 55.8 °C. These data indicate that OmpR is folded.

ESI-MS of F1 could not detect a dominant species, indicating that the toxicity of this fusion may have affected its expression. CD spectra at room temperature indicate that the F1 sample contains weak secondary structure, most likely alpha helical in nature, Figure 3.6.C. The thermal stability profile of the protein in the sample displays a number of features; gradual unfolding occurs between 30-50 °C, a small but rapid transition between 55-60 °C and a transition from 70-80 °C (Figure 3.7.C). The equilibrium unfolding T_m for F1 is calculated at 58 °C, roughly the mid-point of the rapid transition. These phases indicate the protein in the sample occupies multiple equilibria of unfolding. ESI-MS and CD data strongly suggest that protein in the F1 sample is initially partially folded or a heterogenous population of folded proteins.

F2, F3 and F4 undergo truncations relative to their predicted molecular weight, Table 3.1. F3 and F4 lose ≈ 125 Da of mass, which could be due to the cleavage of the amino terminal methionine. This would account for 131-149 Da, the discrepancy is within the error of the measurement (http://www.abrf.org/). F2 is modified by 376.6 Da, if methionine is also lost from F2 the remaining mass would be between 227-250 Da. No single change can account for such a large loss, as such assigning the remaining change in mass is difficult.

The CD spectra of F2, F3 and F4 indicate that these proteins have a folded secondary structure at room temperature, and as with the other RRs they are predominantly alpha helical, Figure 3.6.D, E and F. The thermal stability of F2 follows a gradual non-cooperative unfolding profile, preceded by a small transition at ≈ 20

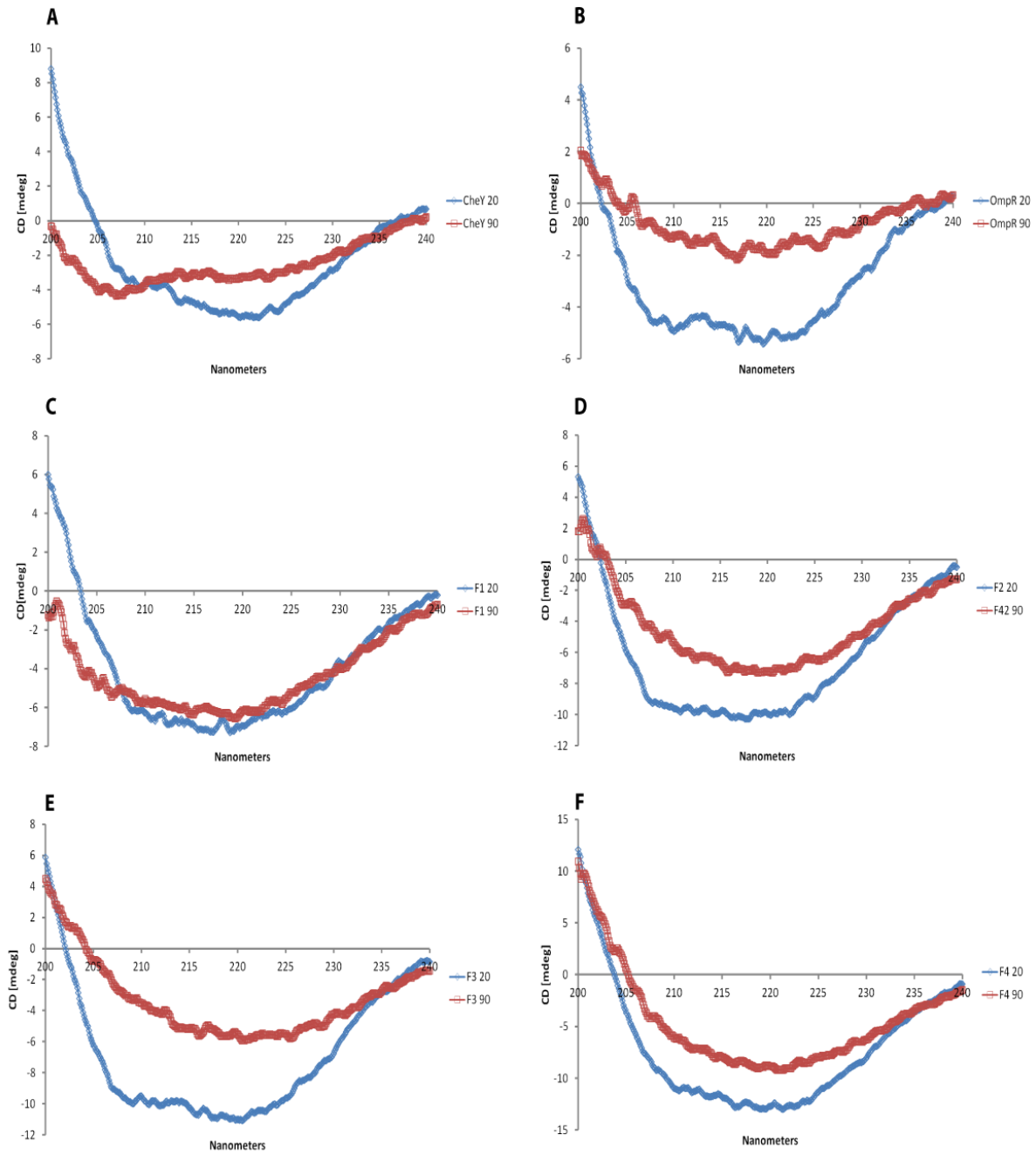

Figure 3.6: CD spectra for CheY, OmpR and F1-4 at 20°and 90°. Panel A: CheY, Panel B: OmpR, Panel C: F1, Panel D: F2, Panel E: F3 and Panel F: F4. CD spectra at 90°C are shown for comparison with room temperature spectra.

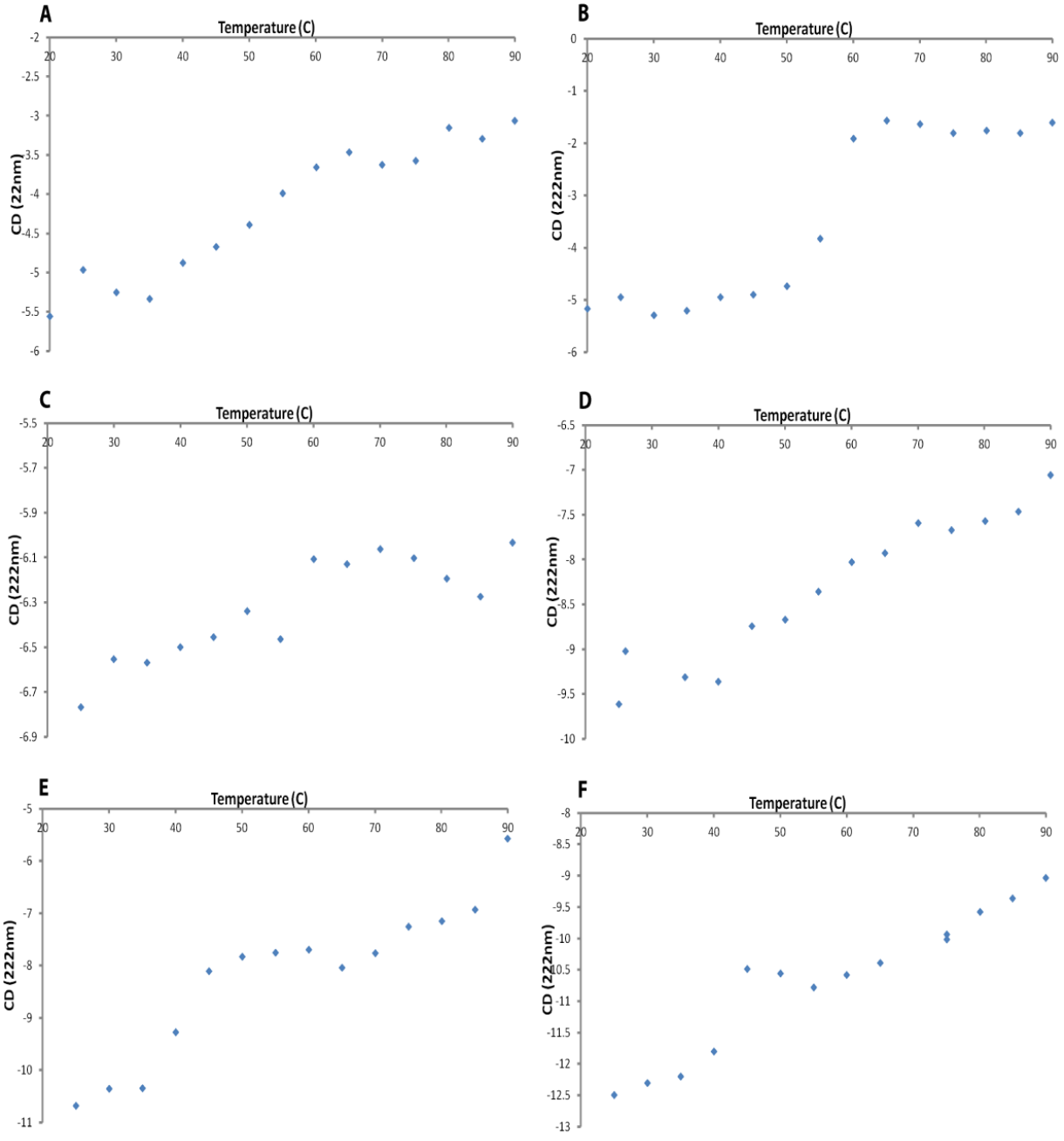

Figure 3.7: CD calculated thermal stability of α helices of CheY, OmpR and F1-4 at 222nm from 20°to 90°C. Panel A: CheY, Panel B: OmpR, Panel C: F1, Panel D: F2, Panel E: F3 and Panel F: F4.

°C (Figure 3.7.D). These data indicating that F2 probably exists as a very flexible structure.

F3's thermal stability profile is dominated by a cooperative unfolding transition between 35-45 °C (Figure 3.7.E). Another sharp transition can be observed from 85 °C. These events are interspersed by slow unfolding. Due to the location of the first cooperative transition, F3 has two calculated T_m at 45 and 64 °C. These data indicate multiple discrete folding/unfolding equilibria for F3, which could arguably be due to the presence of complete CheY and OmpR domains driving different unfolding characteristics at lower and higher temperatures.

F4's thermal stability profile displays a single cooperative unfolding event between 40-45 °C (Figure 3.7.F). There are two calculated T_m values, 43.5 and 55 °C, due to the slope of the curve. The cooperative transition is flanked by gradual unfolding. Similarly to F3, the thermal stability profile of F4 strongly suggests multiple discrete folding/unfolding equilibria, perhaps also due to the presence of complete CheY and OmpR domains.

3.3.1 Conclusion

Data indicate that the wild-type proteins CheY and OmpR can be denatured, indicating they are folded. CheY has undergone a number of modifications *in vivo* affecting molecular weight as assayed by ESI-MS. The exact causes of these are hard to determine but given the large change in mass it is likely to involve multiple changes rather than just one. F1 did not show a dominant species in its ESI-MS spectra and the CD spectra are indicative of either an unfolded protein or a heterogenous population, which cannot be used for further experimentation. F2, F3 and F4 show decreases in mass, demonstrating their toxicity during over-expression could have lead to changes in their recombinant genes. These chimeras are the only ones to give a dominant species and produce thermal profiles indicative of an initially folded state. The evidence from chimeras, F3 and F4, suggests that the addition of the OmpR linker and CTD to CheY do not necessarily lead to misfolding. Further, F2 data indicate that changing small portions of the REC domain and adding the OmpR linker and CTD does not hinder protein folding. However, the failure to purify F1 demonstrates that swapping larger parts of REC domain between RRs, in addition to the OmpR linker and CTD, can affect protein structure.

Chapter 4

Histidine Kinase Binding

4.1 Overview and Aims

ESI-MS and CD established that F2, F3 and F4 are folded, and as a result their functionality as synthetic RRs can be assayed. This chapter will aim to determine the affinity of F2, F3 and F4 for CheA and mEnvZ compared to wild-type RRs, CheY and OmpR. SPR will be used to measure the affinity between the HPKs and RRs.

A synthetic TCS in which chemotactic stimuli drive transcription, where input is linked to output through a chimeric RR, requires that the synthetic RR associates with CheA. The modular binding domains of CheA are CheA-P1 and CheA-P2. In the following experiments, RR affinity is tested against CheA-P1, CheA-P2 and CheA-P1P2. The CheY binding residues for CheA-P1 reside in helix 1 and loop 5, those for CheA-P2 are located across the α_4-β_5-α_5 region of the REC domain. F4 and F3 retain all of these residues, F2 does not have the CheA-P2 binding residues of the α_5 helix, potentially impacting affinity for CheA-P2 and CheA-P1P2. Furthermore, the OmpR linker and CTD, which all chimeric RRs contain, could interfere with association with CheA.

The RRs will also be tested against mEnvZ, the cognate HPK of OmpR. The majority of the OmpR SDRs for mEnvZ are located in helix α_1 and a smaller patch in loop 5. None of the fusions retain α_1 SDRs. The sequence conservation between wild-type RRs CheY and OmpR means that chimeras F4 and F3 contain 75% of the SDRs found on loop 5, and F2 has 100% of these residues. However, the loss of the larger patch of SDRs in α_1 is predicted to have highly detrimental effects on the affinity of the chimeras for mEnvZ.

SPR will be used to measure the affinity between HPKs and RRs *in vitro*. SPR is an optical method that measures the K_d of an interaction due to the change in refractive index at the interface of a sensor chip surface and solution. One protein, the ligand (biotinylated HPKs, bHPK), is immobilised to the sensor chip surface. The partner protein, the analyte (RRs), is flowed over the surface of the chip. Any binding between the analyte and ligand is measured as a change in refractive index and is displayed as a sensogram; a binding curve, which describes the association, binding and dissociation of the complex. SPR can determine the kinetics of association and dissociation to calculate K_d. Alternatively, if association and dissociation are so fast they resemble steps, steady state binding can be used to determine affinity (Biacore Handbook). Additionally, SPR can detect complexes at nanomolar concentrations. As such, it is relatively straight forward and highly sensitive to even weak binding

interactions.

4.2 Preliminary Experiments

Preliminary experiments were undertaken to determine whether binding could be reliably detected between cognate partners, mEnvZ-OmpR and CheA-CheY. CheA has two domains that interact with CheY, P1 and P2. To assay the contributions from each domain to binding, three constructs were created; CheA-P1, CheA-P2 and CheA-P1P2. mEnvZ (EnvZLeu288Pro) was designed to knock-out EnvZ phosphatase function, primarily for phosphotransfer experiments. Leu88 is located in the X-motif, an unstructured carboxyl terminal region on top of the central 4 helix bundle (DHp domain) of EnvZ. OmpR binds to the base of the DHp so the mutation does not act by altering the interaction with OmpR (109). It is thought to act by changing the relative positions of the DHp and CA domains, since it resides in a turn between the two (109). This mutant was used in phosphotransfer experiments, and used in SPR experiments for consistency.

4.2.1 *bm*EnvZ:OmpR Binding

Figure 4.1 displays blank subtracted sensograms for the interaction between immobilised bmEnvZ and increasing concentrations of its cognate RR, OmpR. These data indicate a fast association at the start of the OmpR pulse, steady state binding over the remainder of the injection, the final level of which is proportional to OmpR concentration. OmpR exhibits fast dissociation once the pulse ends.

The decrease in the sensograms at the start of the OmpR pulse and the increase in the sensograms just before the end of the pulse is likely to be an artefact. In this particular experiment, OmpR was passed through a ligand free flow-cell first then the second flow-cell containing bmEnvZ. These artefacts suggest that OmpR is binding to the ligand free flow cell. At A in Figure 4.1, the OmpR of the initial pulse binds firstly to the blank flow-cell thus leaving less to bind to bmEnvZ, when the blank cell signal is subtracted it results in the undershoot observed at 0s. The overshoot at B in Figure 4.1 is arguably due to the opposite phenomenon; there is less OmpR bound to the blank flow-cell than to bmEnvZ. A possible explanation is that as the pulse comes to an end, OmpR is dissociating from the blank flow-cell while still binding to bmEnvZ, causing the overshoot observed once the blank cell signal is subtracted.

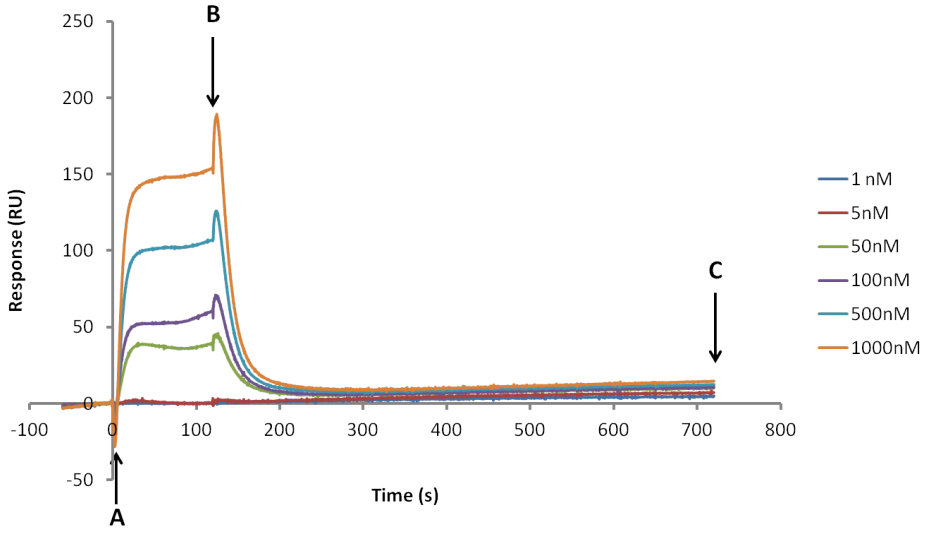

Figure 4.1: bmEnvZ:OmpR blank subtracted sensograms. bmEnvZ immobilised on chip surface (ligand), OmpR (analyte) flowed over surface at different concentrations (see legend for details). A: Analyte injection and capture, B: Analyte injection stop and dissociation and C: Regeneration of sensor surface.

Proceeding experiments adopted simultaneous flow through blank and ligand cells, avoiding artefacts due to the series flow set-up with bmEnvZ:OmpR.

Figure 4.2 displays the fit of these data to a 1:1 steady state affinity model, performed by T200 Evaluation Software. The average K_d generated by fits of 3 independent samples was 305.5 $\pm$121.6 nM. The range of reported results, detailed in Table 1.3, is 425 $\pm$127 nM to 1.96 $\pm$0.28 μM (55) (102) (12) (41). The K_d determined in this study is towards the extreme lower end of this range, but is in agreement with the reported results. SPR experiments were conducted on the latest T200 machine from GE Healthcare, capable of accurately detecting protein-protein interactions with nanomolar sensitivity, potentially explaining the low K_d detected.

Conclusion

The result of preliminary experiments assaying binding between bmEnvZ and OmpR indicate that the biotinylation tag is not detrimental to affinity, the same can be said of the mutation to EnvZ that knocks-out phosphatase activity. The K_d generated from a steady state model of the data is credible with reference to the literature. Consequently, the bmEnvZ construct will be used in further binding experiments with wild-type and chimeric RRs.

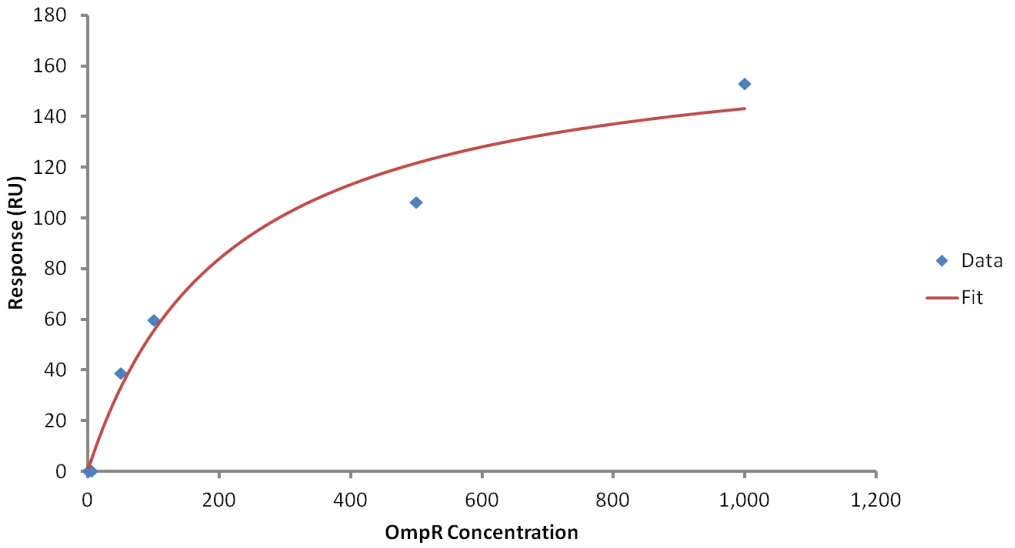

Figure 4.2: Steady state affinity model fit of the bmEnvZ:OmpR sensogram data. Curve represents a fit of OmpR binding to bmEnvZ at steady state; data points for different concentrations are taken are taken 4s before the end of the pulse with a 5s window, before the artefact observed in the sensograms.

4.2.2 *b*CheA:CheY Binding

CheA contains two domains that can interact with CheY; CheA-P1 and CheA-P2. Three CheA constructs were created for SPR experiments; CheA-P1, CheA-P2 and CheA-P1P2. The effect of removing portions of the CheA binding regions of CheY in the chimeras could therefore be assessed.

*b*CheA-P1:CheY Binding

CheY:CheA-P1 binding curves are displayed in Figure 4.3. These sensograms indicate that there is no binding between these two domains. Negative binding can be observed in these blank subtracted sensograms, which strongly suggest that there was more binding of CheY to the reference cell lacking the bCheA-P1 ligand than to bCheA-P1 itself. A close inspection of the raw sensograms for both flow-cells shows that bCheA-P1 does not stably associate with the sensor surface of flow-cell 2, Figure 4.4. The wash after the end of the bCheA-P1 injection removes all of the bCheA-P1 from Fc2, D in Figure 4.4. There is no change in the Fc1 sensogram upon bCheA-P1 injection, as such there is no binding of bCheA-P1 to Fc1. It can be deduced then that the removal of bCheA-P1 from Fc2 by the wash step is total, indicated by

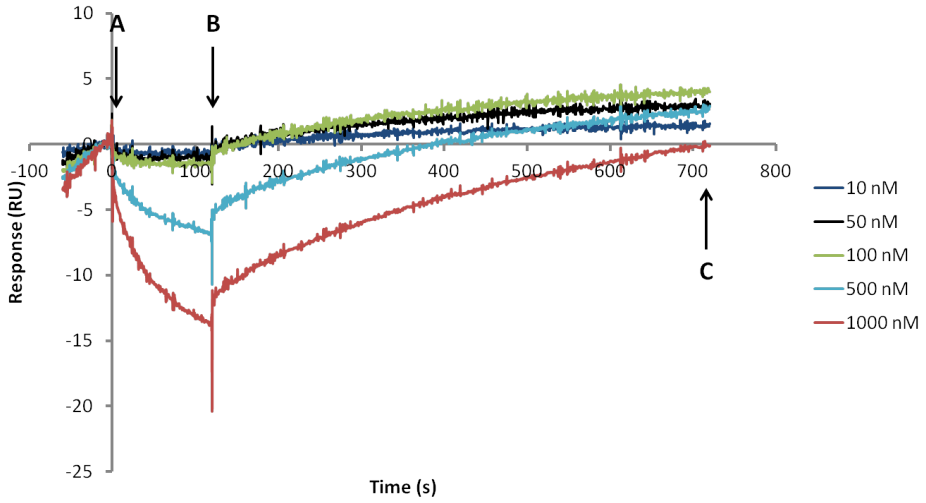

Figure 4.3: bCheA-P1:CheY blank subtracted sensograms. bCheA-P1 domain immobilised on chip surface (ligand), CheY (analyte) flowed over surface at different concentrations (see legend for details). A: Analyte injection and capture, B: Analyte injection stop and dissociation and C: Regeneration of sensor surface.

identical response levels for Fc1 and Fc2 at the wash step end, D in Figure 4.4. There is a decreasing signal for CheY as it is flowed through Fc2, between E and F in Figure 4.4, which could highlight that CheY is not coming into contact with the surface of the sensor. Ultimately, this phenomenon is difficult to explain and is specific to Fc2 in comparison with Fc1, Figure 4.4.

*b*CheA-P1P2:CheY Binding

Figure 4.5 shows the results of CheY binding to bCheA-P1P2. Blank subtracted sensograms display a greater response, therefore more binding, with increasing concentrations of CheY, although, the sensograms vary in their characteristics. Applying 500nM of CheY to bCheA-P1P2 produces a sensogram with fast association when the pulse of CheY starts, steady state binding for the remainder of the pulse and fast dissociation once the pulse stops. However, a number of sensograms, 10nM, 50nM and 100nM, exhibit slower association which occurs over the course of the pulse, followed by slow dissociation. Further, 1000nM of CheY associates quickly when injected, this is followed by two phases of dissociation; a slow phase up to $\approx$ 120s when the pulse stops, indicating more CheY is dissociating than associating, and a fast phase once the CheY pulse is stopped. The difference between the sensograms could

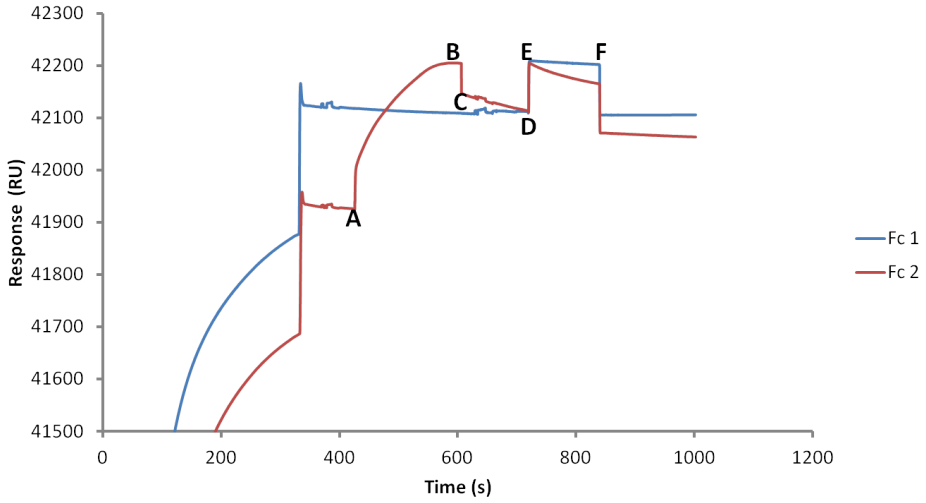

Figure 4.4: bCheA-P1:1000nM CheY Fc1 and Fc2 sensograms. Fc1 blank flow-cell (blue), bCheA-P1 immobilised on Fc2 (red) and CheY (analyte) flowed over surface. A: bCheA-P1 injection and capture, B: injection stop leading to dissociation, C: wash, D: removal of all bCheA-P1 from Fc2 and start of CheY injection and capture, E-F: CheY injection duration and F: CheY injection stop and dissociation.

suggest that CheY concentration has an affect on association and dissociation phases; concentrations up to 100nM exhibit slow phases while 500-1000nM of CheY display fast association and dissociation. No such concentration dependent effect appears to act on equilibrium binding; 500nM CheY displays equilibrium binding while 1000nM does not. Arguably, one would expect equilibrium binding with 1000nM of CheY since it is observed with 500nM. bCheA-P1P2 was immobilised to 140 RU for each run, the calculated Rmax for this is 67.3 RU. The experimental Rmax for this level of immobilisation was 21 RU, highlighting that the bCheA-P1P2 surface only had a ligand activity of 31.2%. However, due to the consistency of the bCheA-P1P2 immobilisation the low activity cannot explain the results obtained. Arguably the presence of the the high affinity P2 and low affinity P1 sites could be acting to produce the different characteristics observed, in this case the P1 and P2 domains appear to be acting independently to bind CheY, suggesting this construct is not functioning as expected.

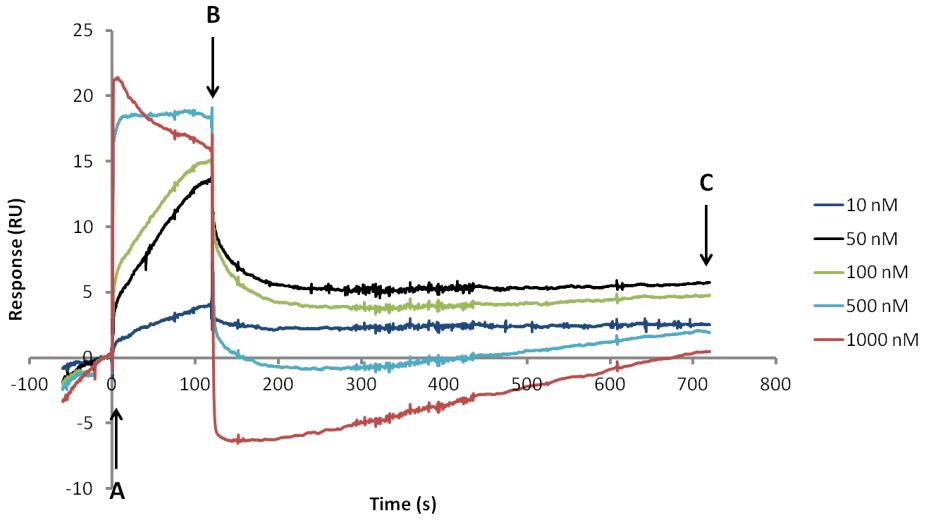

Figure 4.5: bCheA-P1P2:CheY blank subtracted sensograms. The bCheA-P1P2 domains are immobilised on chip surface (ligand), CheY (analyte) flowed over surface at different concentrations (see legend for details). A: Analyte injection and capture, B: Analyte injection stop and dissociation and C: Regeneration of sensor surface.

*b*CheA-P2:CheY Binding

Figure 4.6 shows blank subtracted sensograms for bCheA-P2:CheY. Fast association followed by equilibrium binding is exhibited by both 10nM and 1000nM of CheY when applied to bCheA-P2. Concentrations of 50-500nM display a fast association phase upon CheY injection at A, followed by slow association over the remainder of the CheY pulse. At the end of the CheY pulse, B in Figure 4.6, fast dissociation can be observed across the range of concentrations, however, it is evident that CheY remains bound to the bCheY-P2 cell and until the regeneration solution clears the sensor surface slow dissociation can be discerned. bCheA-P2 was immobilised to 250 RU, generating a calculated Rmax of 215 RU. The experimentally derived Rmax is 130 RU at 1000nM of CheY, which indicates that 60.5% of the ligand was active.

Despite the varied kinetic characteristics of the bCheA-P2:CheY sensograms, they were best fit to a steady state 1:1 binding model, generating a K_d of 333.7 $\pm$25.6 nM from three independent experiments (Figure 4.7). The reported K_d values for CheA-P2:CheY range from 90nM to 1.7μM (85) (83). The results from this study fall in this range. Based on these preliminary results, the bCheA-P2 construct was chosen for further experiments with the wild-type and chimeric RRs.

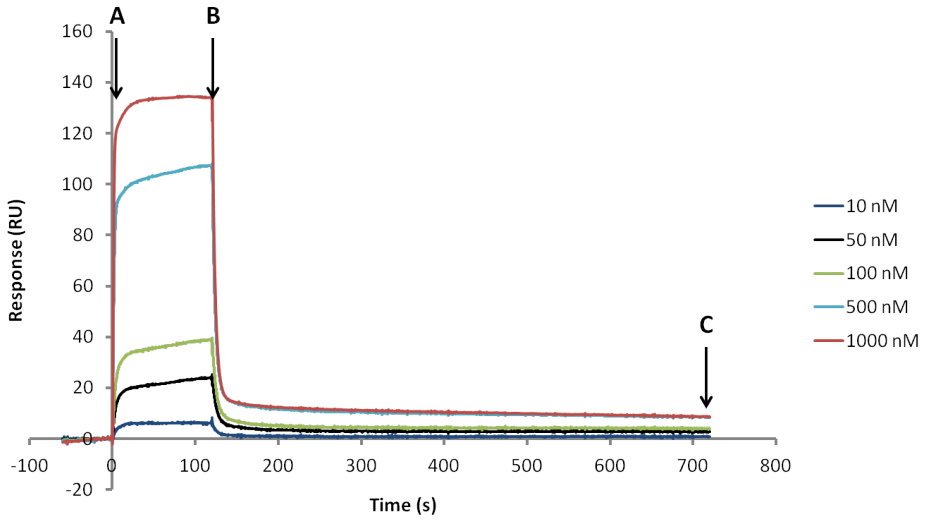

Figure 4.6: bCheA-P2:CheY blank subtracted sensograms. CheA-P2 domain immobilised on chip surface (ligand), CheY (analyte) flowed over surface at different concentrations (see legend for details). A: Analyte injection and capture, B: Analyte injection stop and dissociation and C: Regeneration of sensor surface.

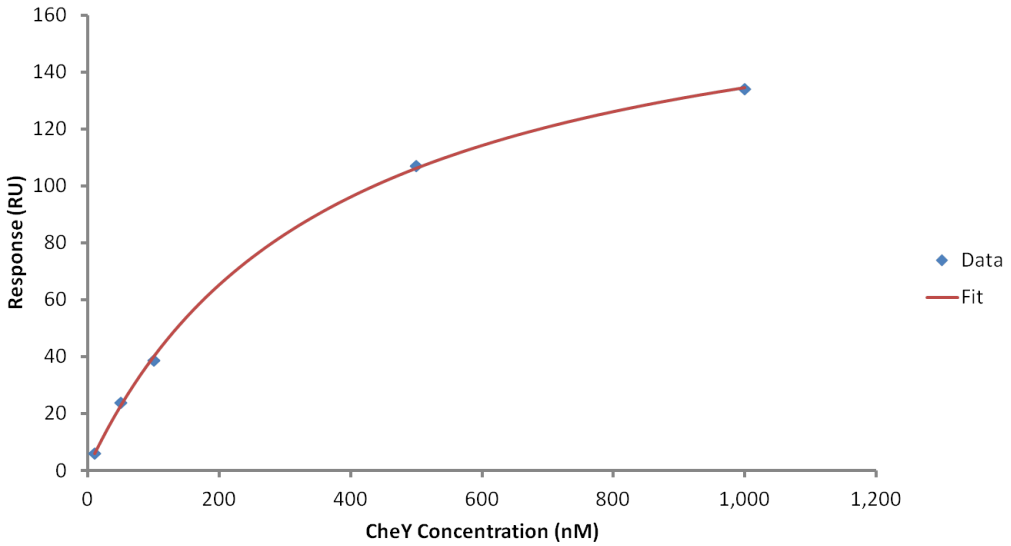

Figure 4.7: Steady state affinity model fit of the bCheA-P2:CheY sensogram data. Curve represents a fit of CheY binding to the bCheA-P2 domain at steady state; default settings for the fit were used, as such data points for different concentrations are taken 4s before the end of the pulse with a 5s window.

Conclusion

Data from the preliminary experiments, testing CheY against the binding domains of CheA, show that using bCheA-P1 is not suitable for further testing since stable immobilisation of the ligand could not be obtained. bCheA-P1P2 will not be used for tests involving the chimeric RRs because the sensograms displayed variation between kinetic and steady state binding, as such the data could not be fit to a binding model. The reported values for bCheA-P1P2:CheY affinity range from 170nM up to 2000nM, indicating a detectable affinity between these components (50) (56) (85). bCheA-P2 will be used to assay the affinity of the fusion constructs, the variation shown in wild-type binding is not severe enough to preclude model fitting and the sensograms generated a plausible K_d with reference to the literature.

4.3 Further *bm*EnvZ Experiments

Preliminary experiments established that under the conditions used the bmEnvZ:OmpR interaction generated a K_d in the range of the reported values. Consequently, further experiments were undertaken with CheY and the chimeric RRs, F2-4. Blank subtracted sensograms for the bmEnvZ:CheY, the negative control interaction, are displayed in Figure 4.8. There is no binding interaction between bmEnvZ and CheY. Figure 4.9 shows the results of bmEnvZ:F4 and Figure 4.10 the results of bmEnvZ:F3 experiments. F4 and F3 both contain the entire CheY protein upstream of the OmpR linker and CTD, neither associate with bmEnvZ. The results of the interaction between bmEnvZ and F2 are displayed in Figure 4.11. An interaction between bmEnvZ and F2 can be observed when applying 100nM of the RR; fast association at the start of the RR pulse is followed by slow association over the remainder of the injection. The end of the F2 pulse leads fast dissociation proceeded by slow dissociation until the surface is regenerated. However, no binding occurs at other F2 concentrations. In these experiments, bmEnvZ was immobilised to a level of 175 RU, generating a calculated Rmax of 81 for CheY, 148 for F4, 151 for F3 and 151 for F2. Only F2 produced an experimental Rmax, 18 RU, indicating a ligand activity of 11.9%. However, this analysis should be used with caution with CheY, F4 and F3 since they lack the largest SDR patch of OmpR, as such this analysis cannot be used to determine ligand activity in these cases.

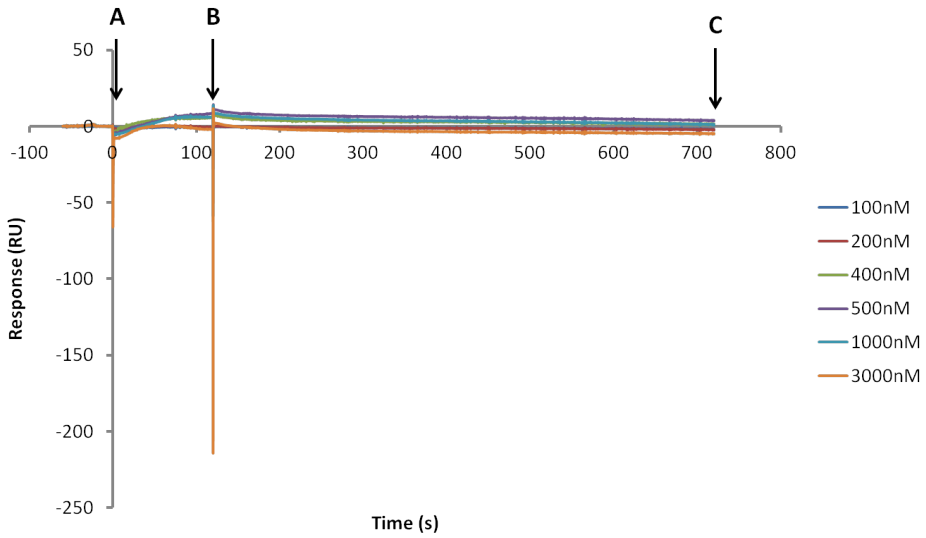

Figure 4.8: bmEnvZ:CheY blank subtracted sensograms. bmEnvZ immobilised on chip surface (ligand), CheY (analyte) flowed over surface at different concentrations (see legend for details). A: Analyte injection and capture, B: Analyte injection stop and dissociation and C: Regeneration of sensor surface.

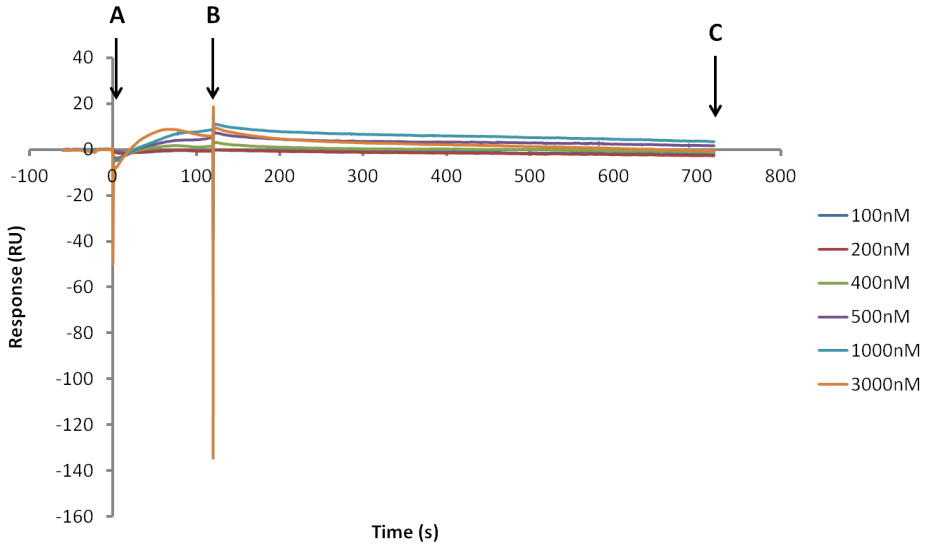

Figure 4.9: EnvZ-F4 blank subtracted sensograms. bmEnvZ immobilised on chip surface (ligand), F4 (analyte) flowed over surface at different concentrations (see legend for details). A: Analyte injection and capture, B: Analyte injection stop and dissociation and C: Regeneration of sensor surface.

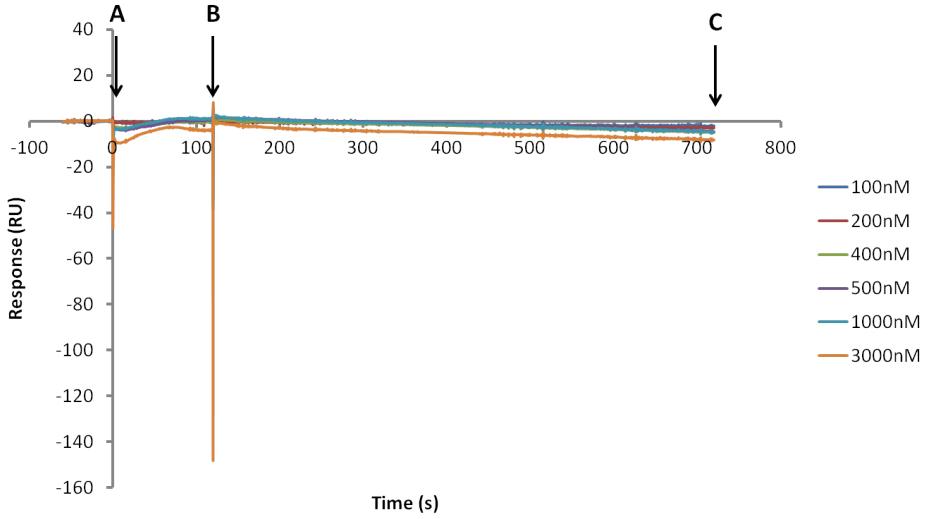

Figure 4.10: bmEnvZ:F3 blank subtracted sensograms. bmEnvZ immobilised on chip surface (ligand), F3 (analyte) flowed over surface at different concentrations (see legend for details). A: Analyte injection and capture, B: Analyte injection stop and dissociation and C: Regeneration of sensor surface.

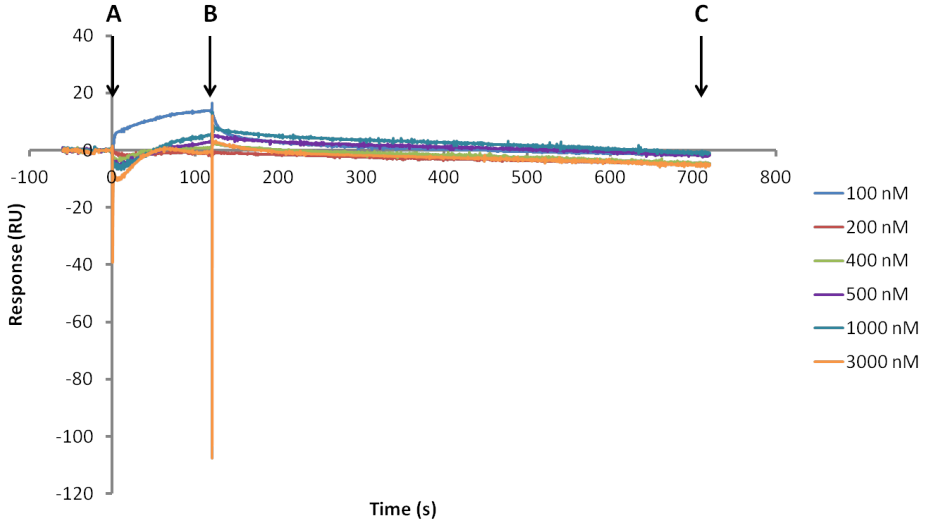

Figure 4.11: bmEnvZ:F2 blank subtracted sensograms. bmEnvZ immobilised on chip surface (ligand), F2 (analyte) flowed over surface at different concentrations (see legend for details). A: Analyte injection and capture, B: Analyte injection stop and dissociation and C: Regeneration of sensor surface.

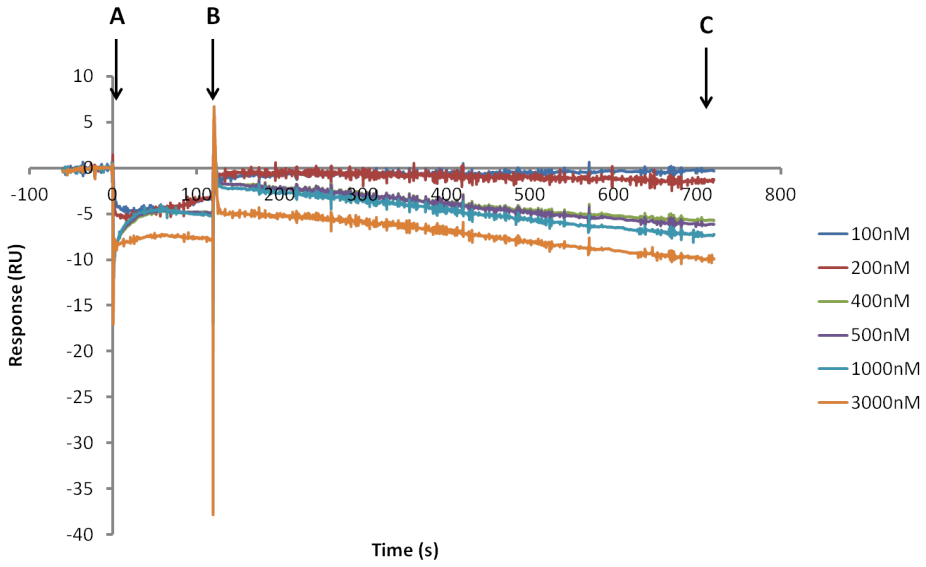

Figure 4.12: bCheA-P2:OmpR blank subtracted sensograms. bCheA-P2 domain immobilised on chip surface (ligand), OmpR (analyte) flowed over surface at different concentrations (see legend for details). A: Analyte injection and capture, B: Analyte injection stop and dissociation and C: Regeneration of sensor surface.

4.4 Further *b*CheA-P2 Experiments

Preliminary binding experiments with the biotinylation tagged CheY binding domains of CheA established that bCheA-P1 and bCheA-P1P2 were not suitable candidates for further testing with the chimeric RRs. However, bCheA-P2:CheY generated a viable K_d with reference to the literature and could be fit to a steady state affinity model. bCheA-P2 was used in further binding experiments with wild-type and chimeric RRs, F2-4.

4.4.1 *b*CheA-P2:OmpR

Figure 4.12 displays the blank subtracted sensograms for the interaction between bCheA-P2 and OmpR, the negative control. These sensograms strongly suggest that there is no binding interaction between bCheA-P2 and OmpR. Further, the negative range of all the sensograms over the duration of the OmpR pulse could indicate that OmpR associates with the blank flow-cell to a greater extent than bCheA-P2.

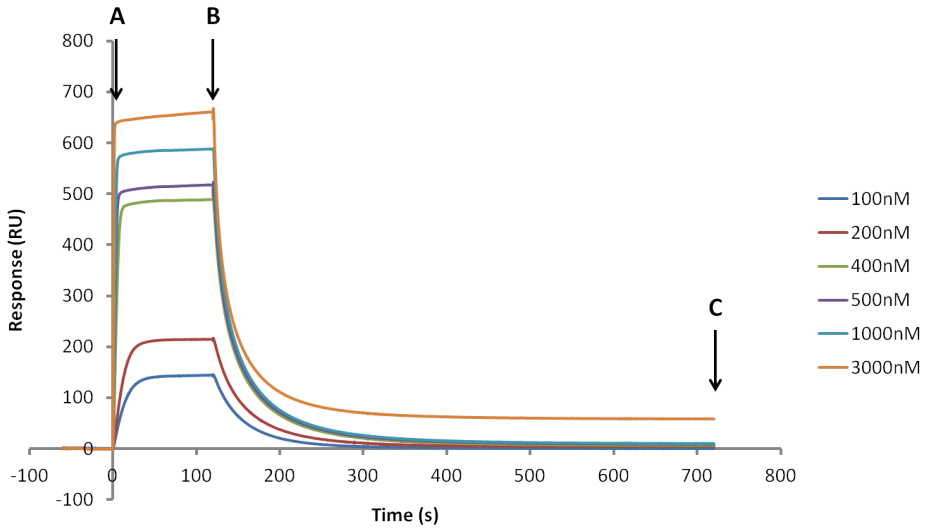

Figure 4.13: bCheA-P2:F4 blank subtracted sensograms. bCheA-P2 domain immobilised on chip surface (ligand), F4 (analyte) flowed over surface at different concentrations (see legend for details). A: Analyte injection and capture, B: Analyte injection stop and dissociation and C: Regeneration of sensor surface.

4.4.2 *b*CheA-P2:Fusions

Figure 4.13 displays the blank subtracted results of the binding interaction between F4 and bCheA-P2. At the start of the F4 pulse, 100 and 200nM of F4 display a slower association phase than 400-3000nM. After the start of the injection of F4, 100 and 200nM exhibit equilibrium binding, while 400-3000nM display a gradual association. At the end of the pulse, all concentrations of F4 slowly dissociate. Unlike the other concentrations, the highest (3000nM) does not dissociate fully over the remainder of the assay. This could indicate an avidity effect, which can act to slow dissociation and have an affect on affinity (70). In this case, F4 could be bound to 2 bCheA-P2 molecules simultaneously; upon dissociation F4 could bind to another bCheA-P2 before fully dissociating from another. When including 3000nM of F4, the average K_d from 3 independent experiments is 144.5nM ±30.6 nM, Figure 4.14. Excluding 3000nM of F4, the average K_d from 3 independent experiments is 200nM ±32.4 nM. An unpaired t-test did not find a significant difference between the two mean K_d values. However, since 3000nM of F4 displays avidity which could skew results, the K_d value excluding 3000nM of F4 will be used in comparison with the K_d of CheY (see later).

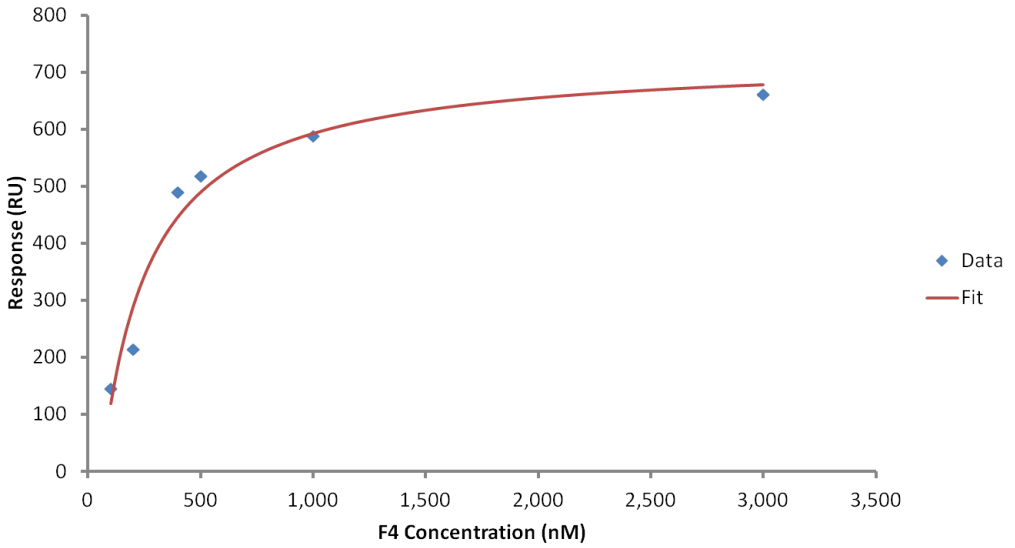

Figure 4.14: Steady state affinity model fit of the bCheA-P2:F4 sensogram data. Curve represents a fit of F4 binding to the bCheA-P2 domain at steady state; default settings for the fit were used, as such data points for different concentrations are taken 4s before the end of the pulse with a 5s window.

Similar results were obtained when using F3 as an analyte with bCheA-P2, Figure 4.15. 100 and 200nM of F3 show a slower association at the beginning of the RR injection when compared to higher concentrations. Over the remainder of the F3 pulse, only 400-1000nM approach equilibrium binding, 100 and 200nM associate slowly and 3000nM exhibits a slower association until the end of the F3 injection. At the end of the pulse, F3 dissociates slowly, although, the effects of avidity can be observed with 3000nM. Including 3000nM, the average K_d from 3 independent experiments is 154.7nM $\pm$30.6 nM, Figure 4.16. Excluding 3000nM, the average K_d of F3 for bCheA-P2 from 3 independent experiments is 201nM $\pm$73.4 nM. An unpaired t-test did not find a significant difference between the two mean K_d values. However, since 3000nM of F3 displays avidity which could skew results, the K_d value excluding 3000nM of F3 will be used in comparison with the K_d of CheY. A comparison of the affinity constants for CheY, F4 and F3 is displayed in Table 4.1. A one-way ANOVA test of the K_d of CheY, F4 and F3, identified a significant effect of RR used on the K_d value at the $p \prec .05$ level [$F(2,6)=7.526, p=0.023$]. Post hoc comparisons using the Holm-Sidak test indicated that F3 (M=201, SD=73.4) and F4 (M=200, SD=32.4) were both significantly different from CheY (M=333.7, SD=25.6). However, F3 and

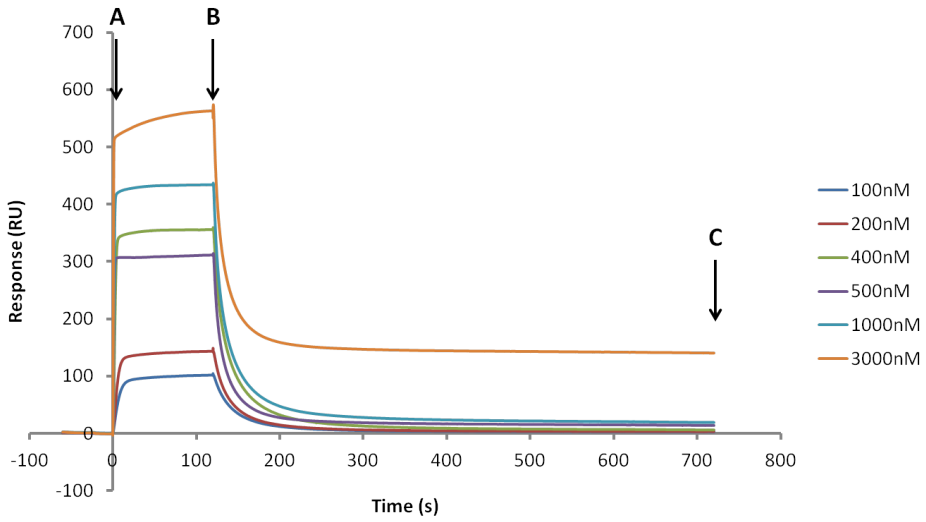

Figure 4.15: bCheA-P2-F3 blank subtracted sensograms. bCheA-P2 domain immobilised on chip surface (ligand), F3 (analyte) flowed over surface at different concentrations (see legend for details). A: Analyte injection and capture, B: Analyte injection stop and dissociation and C: Regeneration of sensor surface.

F4 did not significantly differ from each other.

Figure 4.17 displays the results of F2 binding to immobilised bCheA-P2. These data demonstrate no steady state binding between F2 and bCheA-P2. There is a slow association from the start of the F2 injection, the end of the pulse is followed by slow dissociation, perhaps due to avidity. The sensograms do not show a concentration dependence, 3000nM of F2 produces a response below that of 1000nM and 500nM. There is an interaction between F2 and bCheA-P2, although the sensograms are inconsistent and not amenable to kinetic or affinity model fitting. bCheA-P2 was immobilised to a level of 160 RU, which generates a Rmax of 257. The experimental Rmax for F2 is only 30 RU indicative of the weak binding between the proteins.

4.5 Discussion

The main results of testing the affinity of the chimeric RRs for bmEnvZ and bCheA are that none of of the fusion RRs, F2-4, show any high affinity for bmEnvZ. F4 and F3 display a significantly higher affinity for bCheA-P2 than CheY.

Data indicate that only F2 associates with immobilised bmEnvZ, however, only weak affinity was observed and the association did not show concentration depen-

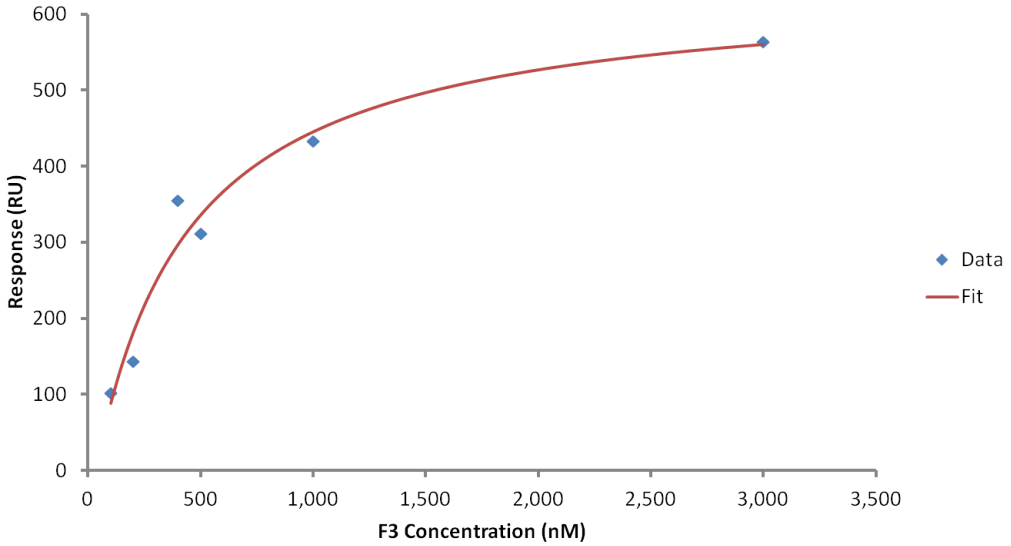

Figure 4.16: Steady state affinity model fit of the CheA-P2-F3 sensogram data. Curve represents a fit of F3 binding to the bCheA-P2 domain at steady state; default settings for the fit were used, as such data points for different concentrations are taken 4s before the end of the pulse with a 5s window.

Response Regulator	**kD1 (nM)**	**kD2 (nM)**	**kD3 (nM)**	**Average kD (nM)**
CheY	329.5	361.1	310.4	333.7 ±25.6
F4*	234	194.8	169.7	200nM ±32.4
F3*	181.6	139.3	282.2	201nM ±73.4

Table 4.1: CheY, F4 and F3 affinity constants, K_d calculated from 3 independent experiments. F4* and F3* represent steady-state affinity fits of the F4 and F3 sensograms excluding 3000nM (T200 Evaluation Software, GE Healthcare).

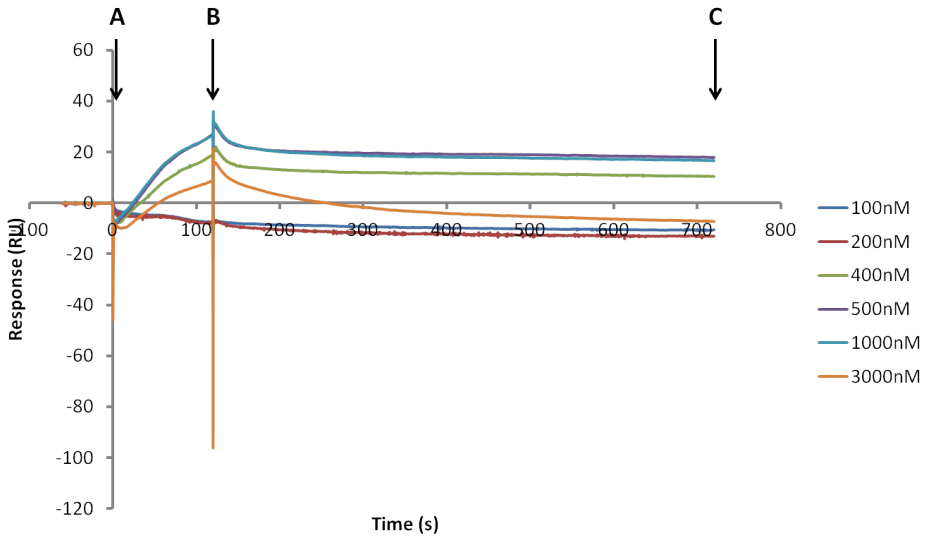

Figure 4.17: bCheA-P2:F2 blank subtracted sensograms. bCheA-P2 domain immobilised on chip surface (ligand), F2 (analyte) flowed over surface at different concentrations (see legend for details). A: Analyte injection and capture, B: Analyte injection stop and dissociation and C: Regeneration of sensor surface.

dence; only 100nM of F2 bound detectably. F2 lacks the largest SDR patch of OmpR, located on helix 1, but retains 75% of the SDRs of loop 5 in addition to OmpR α_5. Due to sequence conservation between CheY and OmpR, F4 and F3 also retain 75% of the SDRs of this region. However, F4 or F3 displayed no affinity for bmEnvZ, ruling out binding mediated solely by loop 5 and by the OmpR loop and CTD, common to each chimera. Consequently, bmEnvZ binding by F2 could be mediated by what remains of loop 5 SDRs perhaps coupled with residues from α_5. The SDRs identified are only those residues that have the greatest affect on specificity, therefore, other binding residues that could be used by OmpR are not included in this analysis (76) (14). These data suggest that α_5 residues could provide additional weak binding sites for bmEnvZ.

The bCheA-P1 construct did not associate properly with sensor surface, sensograms show it was completely removed by the wash step prior to analyte injection. This could be indicative of an inefficient biotinylation process *in vivo*, which itself could be due to weak expression or mutations to the biotinylation tag. ESI-MS results indicated that bCheA-P1 was truncated, SPR results suggest that truncations may have been made to the biotinylation tag which would affect stable association with the sensor surface. The bCheA-P1P2 construct bound efficiently to the chip surface.

However, binding by CheY was highly variable, sensograms displayed steady state or kinetic behaviour. It has been demonstrated that SPR can be used successfully to assay the affinity between the CheA-P1P2 domain and CheY, reporting a K_d of 370nM, well within the detectable range of the instrument used in this study (83). However, CheY was used as the ligand and CheA-P1P2 as the analyte, possibly thus avoiding the problems observed in the current study. A possible explanation of the varied sensograms observed could be that the P1-P2 domains are acting independently, not binding CheY together, arguably due to incorrect assembly on the chip surface.

The chimeric RRs, F3 and F4, showed avidity for bCheA-P2 at the highest concentration used, 3000nM. This effect appears to be only concentration dependent, and acts to slow dissociation resulting in a higher affinity. Although the K_d values of F3 and F4 were not significantly different when excluding 3000nM from the steady state K_d calculation, the K_d values excluding 3000nM were used in statistical tests with CheY so as not to bias any results due to avidity. The chimeric RRs, F3 and F4, exhibited a statistically significantly higher affinity for bCheA-P2 compared to CheY, indicating the addition of the OmpR linker and CTD are not detrimental to bCheA-P2 binding arguably ameliorating the association with this domain.

F2 did not associate in a steady state manner with bCheA-P2 and the sensograms do not show a concentration dependent response level, as a result they could not be fit to an affinity model. F2 contains the 10 α_4-β_5 CheA-P2 binding residues of CheY, lacking the 3 α_5 binding residues. The loss of the α_5 residues is clearly detrimental to the high affinity association with bCheA-P2 observed with CheY and the other chimeras. It is arguable that the addition of OmpR α_5 binding residues could act to further perturb the interaction between the remaining binding residues and CheA-P2.

4.6 Conclusion

The use of chimeric RRs to modulate the input-output of a synthetic TCS, requires a RR to bind to CheA; F2, F3 and F4 all bind to bCheA-P2, albeit with very different affinities. Further chapters will assay the functional behaviour of these synthetic RRs; whether they can be phosphorylated and bind to promoter sites.

Chapter 5

Phosphotransfer

5.1 Overview and Aims

SPR experiments established that F3 and F4 had significantly higher affinity than CheY for bCheA-P2, and that F2 had affinity for this domain of CheA but it could not be fitted to a binding model. The effect of these differences in affinity for bCheA-P2 will be tested functionally in the proceeding experiments, which will assay phosphotransfer from the HPKs, CheA and mEnvZ, to the RRs.

In a synthetic TCS where chemotactic stimuli drive transcription, phosphotransfer from the wild-type HPK, CheA, to the synthetic RR is the first step in the flow of information from wild-type $\rightarrow$ synthetic $\rightarrow$ wild-type components. Binding between a cognate HPK and RR demonstrates an overwhelming kinetic preference and is predicated on the presence of SDRs in both components (13) (76). For binding to lead to phosphotransfer, the RR active site must present an acidic pocket of conserved residues coordinated by a divalent cation (11) (28) (47) (52) (73) (78) (79) (107). Phosphorylation leads to RR activation and modulation of an output, therefore a RR needs to retain the phosphoryl group long enough to maintain an activated state to produce the output. Phosphoryl group stability is ensured by the conserved residues of the active site, competing with this is the rate of auto-dephosphorylation, which appears to be controlled by specific residues, 59 and 89 (CheY numbering), and secondary structure movements initiated by phosphorylation itself (86) (69). It has been demonstrated that auto-dephosphorylation rates are tuned to particular RR outputs, for example protein modulating CheYs generally have faster auto-dephosphorylation rates than promoter binding class II RRs, such as OmpR (86) (69).

In the following experiments the chimeric RR's phosphorylation and dephosphorylation characteristics were determined. Each was mixed with phosphorylated HPK, CheA or mEnvZ, while wild-type RRs, CheY and OmpR, where used as controls. The REC domains of both F3 and F4 contain the wild-type CheY active site and auto-dephosphorylation residues. Consequently, phosphotransfer from CheA is likely to proceed similarly to wild-type but no phosphotransfer from mEnvZ is likely to be observed. The REC domain of F2 also retains the auto-dephosphorylation residues of CheY and, through sequence conservation with OmpR, the conserved active site residues shared by all RRs. Consequently, phosphotransfer from CheA to F2 could proceed similarly to wild-type. However, the presence of OmpR α_5 clearly had an affect on F2 binding to CheA-P2, which could affect phosphotransfer between the proteins. The presence of the OmpR linker and CTD could interfere with phospho-

transfer in any of the chimeric RRs.

In vitro phosphotransfer was used to determine phosphotransfer between HPKs and RRs. HPKs, CheA or mEnvZ, were autophosphorylated for 30 minutes at room temperature in an excess of [γ-^{32}P] ATP, in roughly a 1:100 ratio. Subsequently, an excess of RR was incubated with a phosphorylated HPK, in a 2:1 ratio. Reactions were quenched at different time points allowing phosphorylation and auto-dephosphorylation of the RR to be monitored.

Two phases of phosphotransfer experiments were undertaken; preliminary and final. Initial, exploratory experiments were done to establish whether phosphotransfer could be detected between cognate HPKs and RRs. Further, time points were taken up to 4 minutes to determine the kinetics of phosphotransfer to the RR and auto-dephosphorylation of the RR. Preliminary experiments were completed with F2 and F3. Once the alignment error made in the design of F3 had been discovered and F4 had been designed and purified, final experiments were completed.

5.2 Preliminary Experiments

5.2.1 Phosphotransfer from Wild-type EnvZ

Initial phosphotransfer experiments with wild-type EnvZ and OmpR highlighted that, under the conditions used, the EnvZ phosphatase function dominated its kinase function, Figure 5.1. Phosphotransfer from EnvZ-P to OmpR it complete by 30s; the concentration of EnvZ-P falls close to zero. OmpR-P reaches a maximum at 30s, remaining unchanged over the rest of the time course. These characteristics are in agreement with data from the literature (109) (100). Auto-dephosphorylation of OmpR-P has a $t_{\frac{1}{2}}$ of $\approx$90 min, therefore its contribution to dephosphorylation of OmpR-P over the course of this assay would be minimal (109). This indicates that under these conditions the major influence on the level of OmpR-P is EnvZ phosphatase activity.

To remove the competing phosphatase activity of EnvZ, mEnvZ (EnvZLeu288Pro) was purified. As discussed previously, Leu288 is located in the X-motif, an unstructured carboxyl terminal region on top of the central 4 helix bundle (DHp domain) of EnvZ. OmpR binds to the base of the DHp so the mutation does not act by altering the interaction with OmpR, but is thought to act by changing the relative positions of the DHp and CA domains, since it resides in a turn between the two (109). Ad-

ditionally, since CheA lacks phosphatase activity this mutant allows results with the different HPKs to be more comparable.

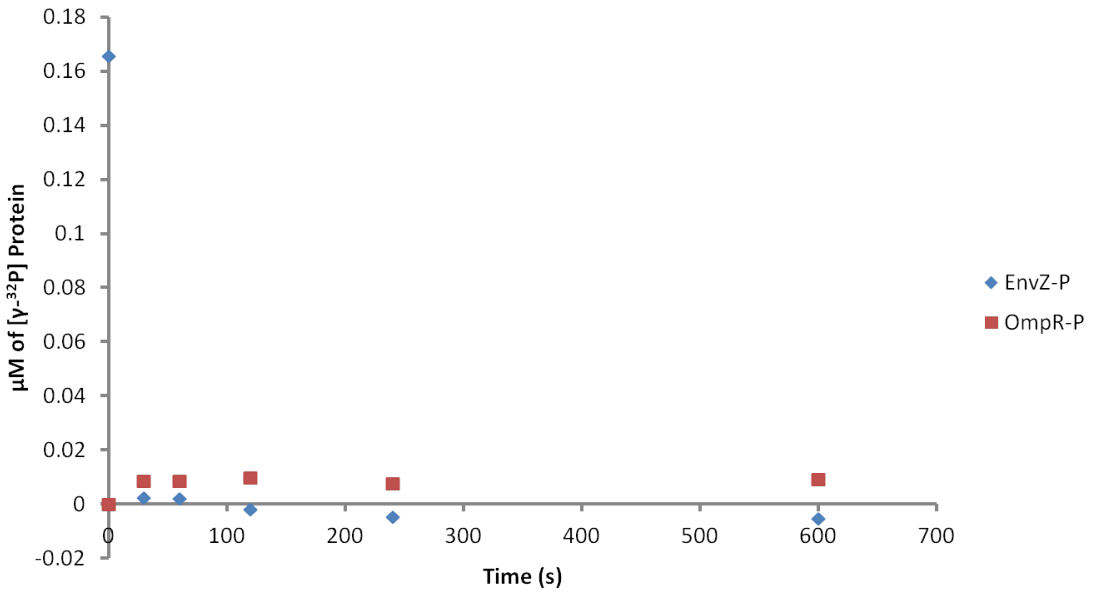

Figure 5.1: Phosphotransfer from EnvZ-P to OmpR. 5μM of HPK-P was incubated with 10μM of RR, final concentrations. Aliquots were removed and quenched at 0, 30, 60, 120, 240 and 600 seconds. Samples were run on a SDS gel and subsequently exposed to x-ray plates. Graph represents the result of a single experiment, quantitative results in μM of radioactive protein based on appropriate calibration curve.

5.2.2 Phosphotransfer from *m*EnvZ

Figure 5.2 shows phosphotransfer between mEnvZ-P:OmpR in A, and mEnvZ-P:CheY in B. mEnvZ-P:OmpR phosphotransfer represents the positive control, while mEnvZ-P:CheY is a negative control. mEnvZ-P is dephosphorylated by OmpR, mEnvZ-P reaches its minimal level at 15 seconds, and mEnvZ-P gradually rephosphorylates over the remainder of the time course. Phosphotransfer to OmpR is essentially complete by 15s, and the level of OmpR-P does not change detectably after this time point. OmpR-P is stable, having a half life of $\approx$ 90 minutes (109). Over the 240 second time course OmpR-P dephosphorylation would therefore be undetectable. The rephosphorylation of mEnvZ from 90s could be explained by postulating that maximal phosphorylation of the OmpR population has been reached, although ultimately this phenomenon is difficult to explain. Panel B shows phosphotransfer from mEnvZ-P

to CheY, a negative control, there is no phosphotransfer detected over 240s.

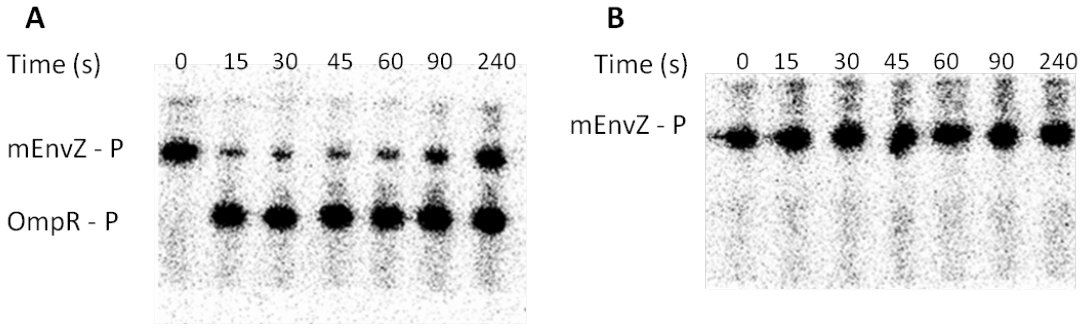

Figure 5.2: Phosphotransfer from mEnvZ-P to OmpR (A) and to CheY (B). Autoradiograph shows a time course over 240 seconds, 5μM of HPK-P was incubated with 10μM of RR, final concentrations. Aliquots were removed and quenched at 0, 15, 30, 45, 60, 90 and 240 seconds. Samples were run on a gel and subsequently exposed to x-ray plates. Labels represent the positions of each species. Time points are indicted above the autoradiograph. Data represent the results of one experiment

Figure 5.3 shows phosphotransfer from mEnvZ-P to F2 (panel A) and F3 (panel B). F4 had yet to be made at this point, so is not included in these exploratory experiments. There is no phosphotransfer from mEnvZ-P to any of the chimeric RRs.

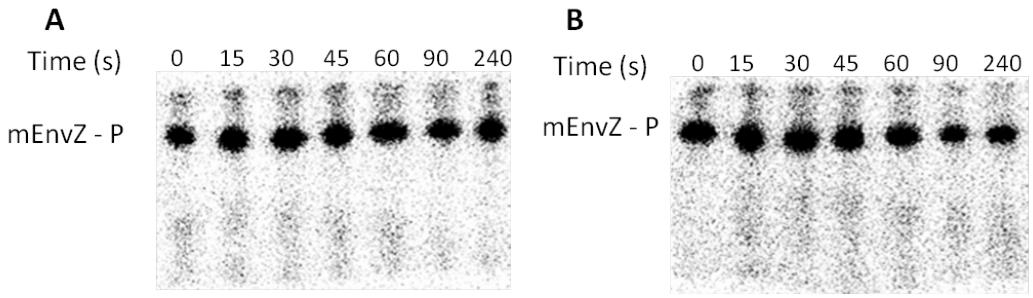

Figure 5.3: Phosphotransfer from mEnvZ-P to F2 (A) and to F3 (B). Autoradiograph shows a time course over 240 seconds, 5μM of HPK-P was incubated with 10μM of RR, final concentrations. Aliquots were removed and quenched at 0, 15, 30, 45, 60, 90 and 240 seconds. Samples were run on a gel and subsequently exposed to x-ray plates. Labels represent the positions of each species. Time points are indicted above the autoradiograph. Data represent the results of one experiment

5.2.3 Phosphotransfer from CheA

Figure 5.4 panel A shows the results of phosphotransfer from CheA-P to CheY, a positive control for phosphotransfer from CheA-P. CheA-P is completely dephosphorylated by 15 seconds and remains so for the rest of the assay. This indicates the rate of phosphotransfer to CheY is faster than the rate of CheA autophosphorylation. CheY-P reaches its maximum level at 15 seconds, dephosphorylating gradually over the rest of the time course. It has been demonstrated that phosphotransfer from CheA-P to CheY is complete by $\approx$ 1s and CheY-P auto-dephosphorylates over $\approx$ 60s (79). These data were determined using rapid reaction equipment and a large molar excess of CheY:CheA, $\geq$5:1, possibly explaining the difference in speed observed compared to the current study. Figure 5.4 panel B shows the results of phosphotransfer from CheA-P to OmpR, a negative control. As expected, there is no phosphotransfer from CheA-P to OmpR.

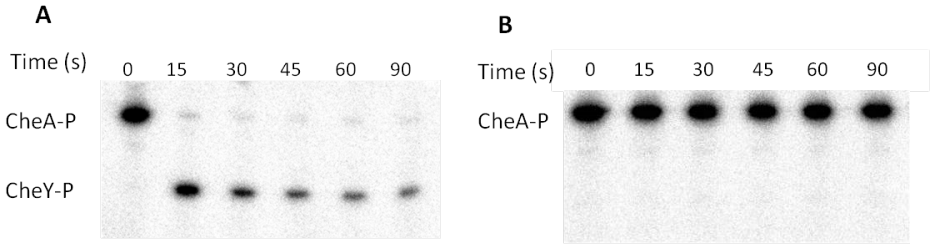

Figure 5.4: Phosphotransfer from CheA-P to CheY (A) and to OmpR (B). Autoradiograph shows a time course over 90 seconds, 5μM of HPK-P was incubated with 10μM of RR, final concentrations. Aliquots were removed and quenched at 0, 15, 30, 45, 60 and 90 seconds. Samples were run on a gel and subsequently exposed to x-ray plates. Labels represent the positions of each species. Time points are indicted above the autoradiograph. Data represent the results of one experiment

Figure 5.5 shows the results of phosphotransfer from CheA-P to F2 in panel A and from CheA-P to F3 in panel B. Phosphotransfer from CheA-P to F2 completely depletes CheA-P of phosphoryl groups by 60s, this is slower than phosphotransfer from CheA-P to CheY, where CheA-P had been completely dephosphorylated by 15s. There is little change in the level of F2-P from 15 to 45 seconds, indicating that F2-P nears its maximal level at 15 seconds. After 45 seconds, F2-P auto-dephosphorylates over the rest of the time course. These data indicate that the rate of CheA autophosphorylation is slower than the rate of phosphotransfer from CheA-P to F2, evident in the zero level of CheA-P after 60 seconds. Compared with phosphotransfer to

CheY, the rate of phosphotransfer from CheA-P to F2 is slower but is still sufficient to keep CheA dephosphorylated. The auto-dephosphorylation rate of F2-P is similar to CheY-P, reaching a comparable level by 90s.

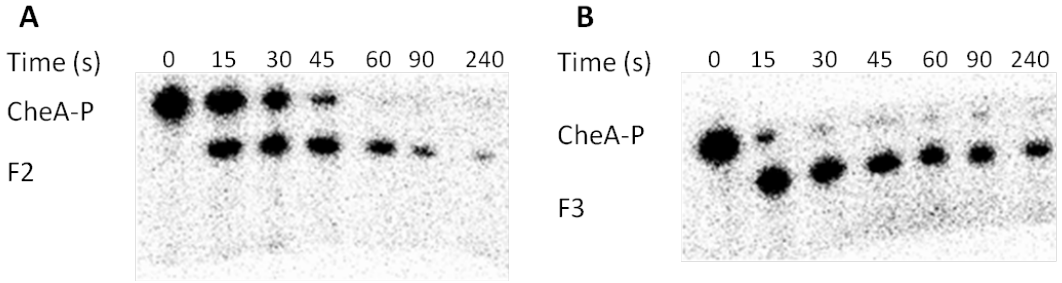

Figure 5.5: Phosphotransfer from CheA-P to F2 (A) and to F3 (B). Autoradiograph shows a time course over 240 seconds, 5μM of HPK-P was incubated with 10μM of RR, final concentrations. Aliquots were removed and quenched at 0, 15, 30, 45, 60, 90 and 240 seconds. Samples were run on a SDS gel and subsequently exposed to x-ray plates. Labels represent the positions of each species. Time points are indicted above the autoradiograph. Data represent the results of one experiment

Panel B of Figure 5.5 shows phosphotransfer from CheA-P to F3. When incubated with F3, CheA-P is depleted of phosphoryl groups by 30s, having undergone an appreciable decrease by 15s. In contrast, phosphotransfer to CheY from CheA-P is complete in 15s, while full phosphotransfer from CheA-P to F2 takes 60s. F3-P auto-dephosphorylates over rest of the assay, however, this reaction is also slowed compared to CheY-P and F2-P.

5.2.4 Conclusion

These initial results established that the wild-type proteins interact and that HPKs and the chimeras are capable of phosphotransfer. Rapid reaction kinetics noted in the literature for CheA-P:CheY demonstrate that manual mixing used in this study cannot properly capture phosphotransfer reaction kinetics. For results in triplicate to quantify the level of radioactive protein *in vitro*, phosphotransfer was taken to 15 seconds only. This time point is the most physiologically relevant, and thus the most relevant for constructing a synthetic TCS.

5.3 Final Experiments

5.3.1 Phosphotransfer from *m*EnvZ

Figure 5.6 shows that phosphotransfer occurs after 15s from mEnvZ-P only to its cognate RR, OmpR. No phosphotransfer is observed to any of the chimeric RRs or CheY, the negative control. Figure 5.6 shows quantified phosphotransfer results, which were derived by including [γ-^{32}P] ATP standards with the autoradiograph. OmpR undergoes phosphotransfer from mEnvZ-P, phosphotransfer to OmpR occurs at a greater rate than mEnvZ can autophosphorylate, evident in the low level of mEnvZ-P compared with the level of OmpR-P. Overall from these experiments, it can be concluded that the chimeric RRs and CheY do not interact successfully with EnvZ-P to produce phosphotransfer after 15 seconds of incubation. This is in line with the preliminary phosphotransfer results discussed above.

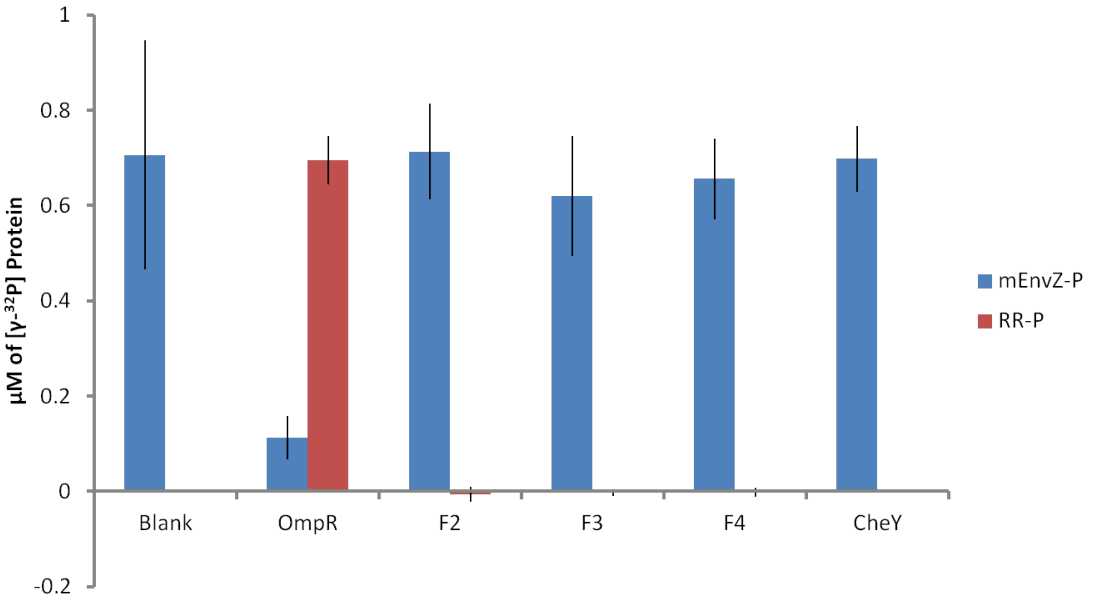

Figure 5.6: Quantified phosphotransfer from mEnvZ-P to wild-type and chimeric RRs after 15s incubation. 5μM of HPK-P was incubated with 10μM of RR, final concentrations. Red bars = μM RR-[γ-^{32}P], blue bars = μM mEnvZ-[γ-^{32}P]. Blank lane contains just mEnvZ-P. Data shown is the average of three separate reactions quenched at 15s. Error bars are calculated as the standard deviation. [γ-^{32}P] ATP standards of 5, 4, 3, 2, 1, 0.5, 0.4, 0.3, 0.2, 0.1 and 0.05 pmol/μl were included to allow quantification.

5.3.2 Phosphotransfer from CheA

Figure 5.7 shows phosphotransfer from CheA-P to the wild type and chimeric RRs after a 15 second incubation. The quantified results demonstrate that F3 and F4 are phosphorylated to a similar level as CheY-P, while F2 is phosphorylated less so after 15 seconds. Phosphotransfer does not occur to OmpR. These results agree with the previously presented preliminary experiments.

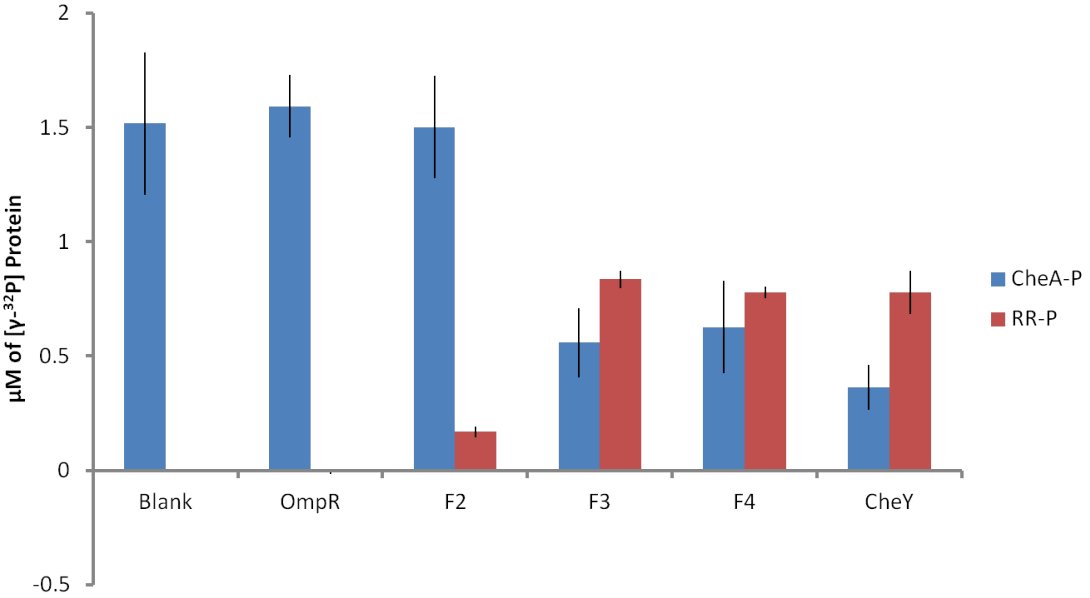

Figure 5.7: Quantified phosphotransfer from CheA-P to wild-type and chimeric RRs after 15s incubation. 5μM of HPK-P was incubated with 10μM of RR, final concentrations. Red bars = μM RR-[γ-^{32}P], blue bars = μM CheA-[γ-^{32}P]. Blank lane contains just phosphorylated CheA-P. Data shown is the average of three separate reactions quenched after 15s of incubation. Error bars are calculated as the standard deviation. [γ-^{32}P] ATP standards of 5, 4, 3, 2, 1, 0.5, 0.4, 0.3, 0.2, 0.1 and 0.05 pmol/μl were included to allow quantification.

5.4 Discussion

The main results from phosphotransfer experiments with HPKs and RRs, are that the fusion RRs do not undergo phosphotransfer from mEnvZ but phosphotransfer from CheA is detected.

Chimeric RRs, F2-4, are not phosphorylated by mEnvZ after 15s incubation, and F2 and F3 are not even phosphorylated by mEnvZ after 240s incubation. F4, F3 and F2 do not contain the largest patch of SDRs of OmpR α_1, however, F3 and F4 retain 75% and F2 100% of the SDRs of loop 5. Additionally, F2 maintains the α_5 helix of OmpR, which could be involved in non-SDR binding to EnvZ. Any binding that does occur in these fusions is not sufficient to lead to phosphotransfer from mEnvZ to the chimeric RRs. No depletion of mEnvZ-P is observed either ruling out phosphotransfer with rapid auto-dephosphorylation of the chimeras.

F2, F3 and F4 are all phosphorylated by CheA-P. F4 and F3 appear to be phosphorylated to wild-type levels after 15s incubation with CheA-P, and both contain wild-type CheY fused to the OmpR linker and CTD. Incubation of F2 with CheA-P for 15s results in level of F2-P that is 21% of the wild-type level, showing that F2 is phosphorylated 5 times slower than CheY, F4 and F3. A one-way ANOVA test of the concentration of RR-P after 15s incubation with CheA-P identified a significant effect of RR used on the RR-P level at the $p<.05$ level [$F(3,8)=98.978$, $p<0.001$]. Post hoc comparisons using the Holm-Sidak test indicated that CheY (M=0.78, SD=0.096), F4 (M=0.78, SD=0.025) and F3 (M=0.83, SD=0.038) are not significantly different. However, CheY, F4 and F3 are all significantly different from F2 (M=0.17, SD=0.027). These data indicate that F4 and F3 exhibit wild-type levels of phosphotransfer after 15s, demonstrating that the addition of the OmpR linker and CTD are not detrimental to CheY's phosphotransfer ability. F2 contains OmpR's α_5 helix and 1 loop 5 residue unique to OmpR in addition to the OmpR linker and CTD; the conserved active site residues are contributed by CheY. In the light of these results, it can be surmised that the addition of OmpR's α_5 helix could be detrimental to phosphotransfer from CheA-P. Data from preliminary experiments indicate that over 240s F2 is phosphorylated more slowly than CheY, but F2-P auto-dephosphorylates at approximately the same rate as CheY-P. These preliminary data, although not taken in triplicate, indicate that the stability of F2-P is similar to CheY-P, indicating that the low level of phosphotransfer observed at 15s in the final experiments is due to slower phosphotransfer of F2 by CheA-P.

5.5 Conclusion

The design of the synthetic TCS requires that a synthetic RR binds and is subsequently phosphorylated by CheA-P, and the results from phosphotransfer experiments show that F2, F3 and F4 fulfil this criteria. The final function of the synthetic RR is to modulate an output of transcription, which will be assayed by promoter binding in the following chapter.

Chapter 6

DNA Binding

6.1 Overview and Aims

SPR and phosphotransfer experiments established that the chimeric RRs could bind CheA and be phosphorylated by CheA-P. To test whether phosphorylation leads to activation of the chimeric RRs' OmpR DNA binding domain, fluorescent anisotropy was used to test promoter binding *in vitro*.

To transduce chemotactic stimuli into an output of gene transcription, the synthetic RRs need to successfully bind promoter DNA. SDRs control the binding preferences of cognate HPKs and RRs, while phosphotransfer to RRs depends on the conserved residues of the active site (13) (76) (11) (28) (47) (52) (73) (78) (79) (107). In wild-type RRs, phosphorylation leads to activation, which results in an output because the auto-dephosphorylation rate matches the time scale on which the specific RR acts (86). It can be deduced that the difference in the half-life of CheY-P and OmpR-P, $\approx$ 20s and 90min, is due to the different time scales at which their outputs are effective (28) (106) (107) (52) (109). CheY is responsible for changing motor direction via protein interactions, which requires rapid activation/inactivation of CheY for the bacterium to effectively navigate its changing environment. OmpR is responsible for gene transcription upon ingestion by a host, OmpR-P's stability allows long-term adaptation to the host environment.

RR activation leads to conserved changes in the α_4-β_5-α_5 region, such as Y-T coupling and movement of loop 4 and helix 4 to accommodate the phosphoryl group (47). In the OmpR/PhoB family of RRs activation leads to homodimerisation via the entire α_4-β_5-α_5 region; these RRs can bind DNA and activate transcription only as dimers (89) (90) (60) (2) (26) (29). It has been postulated that activation of OmpR/PhoB family members utilises the conserved mechanism of RR activation; upon phosphorylation, movements of the α_4-β_5-α_5 region break any NTD-linker contacts and facilitates homodimerisation, which occurs via binding of α_4 of one RR-P with α_5 of a second RR-P. Subsequently, the CTD is freed from any inhibitory interactions with the NTD and linker allowing promoter binding to occur. Consequently, in wild-type RRs activation and output modulation is integrated with and controlled by phosphorylation. F4 and F3 lack any of OmpR's α_4-β_5-α_5 region, which is implicated as central to DNA binding, consequently the presence of the OmpR linker and CTD are unlikely to result in promoter binding. F2 contains α_5 of OmpR in addition to the linker and CTD, the presence of α_5 in the F2 REC domain could lead to DNA binding upon activation.

In the following experiments the promoter binding ability of the chimeric RRs was tested with fluorescent anisotropy, in the presence and absence of the HPKs CheA-P and mEnvZ-P. Fluorescent anisotropy is a solution technique, in this study promoter DNA is fluorescently tagged with fluorescein (Fl-DNA) and different concentrations of phosphorylated and unphosphorylated chimeric and wild-type RR are added. In solution the Fl-DNA has a characteristic rotation rate. Since Fl-DNA is small any RR binding, therefore any increase in mass, will act to slow this rotation. The relative speed of rotation is detected due to changes in the relative amount of polarised light emitted by the fluorescent species when excited. If immobile over the course of the excitation life time, the fluorochrome will emit light with the same extent of polarisation as the excitation light. As such, a complex with a higher mass, for example when all promoter sites are bound, will emit more polarised light, than a lower mass complex, where there is no or only partial binding. Consequently, a binding curve can be generated for different concentrations of RR. *In vivo*, OmpR binds to two promoter regions; *pompF*, consisting of 3 main activation sites, F1-F2-F3, and a distal F4 site involved in repression, and *pompc*, comprised of C1-C2-C3 (32) (104). In this study the composite sites F1-F2-F3 and C1-C2-C3, tagged with fluorescein (Fl-F123 and Fl-C123) were used to assay RR promoter affinity.

Two stages of experiments were undertaken; preliminary experiments established a reproducible binding curve for OmpR and OmpR-P for C123 DNA and optimised the technique, final experiments were conducted with all the chimeric RRs and CheA.

6.1.1 Preliminary Anisotropy Experiments

OmpR:F*l*-C123 Anisotropy Trials

Initial experiments aimed to determine wild-type levels of Fl-C123 binding by OmpR and OmpR-P. To increase accuracy at low protein concentrations Biotix lo-bind tips were used for all stages of the phosphorylated and unphosphorylated assay.

Unphosphorylated OmpR was diluted to stock concentrations of 1000nM and 100nM then diluted to reaction concentrations and aliquotted in to a 96 well plate to a final volume of 100μl per well, using 3 wells per concentration. Phosphorylated OmpR was obtained by incubation with a phosphorylated mEnvZ; 5μM of mEnvZ was autophosphorylated at room temperature for 30 minutes in the presence of 5mM ATP. OmpR was diluted to stock concentrations of 1000nM and 100nM in a 1:2 ratio

with mEnvZ-P (RR:HPK-P). Reactions were incubated for at least 10 minutes to ensure the phosphotransfer reaction had reached its end-point. Stock concentrations were diluted to the reaction concentrations and aliquotted in to a 96 well plate to a final volume of 100μl per well, using 3 wells per concentration. The result of this approach can be seen in Figure 6.1.

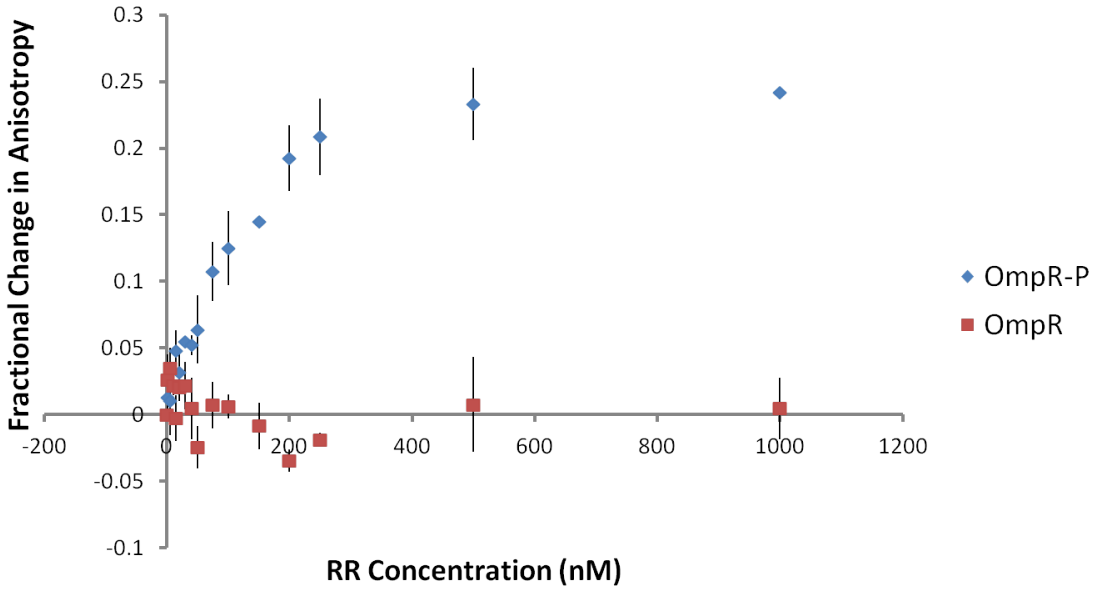

Figure 6.1: OmpR and mEnvZ-P:OmpR Fl-C123 promoter binding. Red: 1-1000nM of OmpR incubated with 5nM Fl-C123 DNA, final concentrations. Blue: 1-1000nM of OmpR incubated with mEnvZ-P in a 1:2 ratio (RR:HPK-P) subsequently mixed with 5nM Fl-C123 DNA, final concentrations. Data represent the average fractional change in anisotropy for three independent experiments. Error bars represent the standard deviation.

Data indicate that only OmpR-P condition can bind DNA. These data could be fit to a model where K_d represents the concentration of RR at the half-maximal fractional change in anistropy. This was done in SigmaPlot, fitting with a non-linear least squares single rectangular hyperbola with y replicates, of the form;

$$f = a \times x \div (b + x) \tag{6.1}$$

Where a represents Vmax, the maximal fractional change in anisotropy, x is the RR concentration and b is the apparent dissociation constant, K_d. This particular model was chosen because it describes a classical binding curve, a rectangular hyper-

bola, which shows saturation at high enough concentrations. The calculated K_d for these data was 131 ±15 nM, it has been demonstrated that the K_d of OmpR-P for Fl-C123 is 31.4 ±8 nM (32). However, the reported K_d value used highly purified OmpR-P and a higher concentration of fluorescein tagged DNA, 10nM (32). Further preliminary experiments sought to emulate these results and used 10nM of Fl-C123 DNA and RR:HPK in a 2:1 ratio, Figure 6.2. These conditions yielded a K_d of 34.41 ±7.18 nM, matching the reported results.

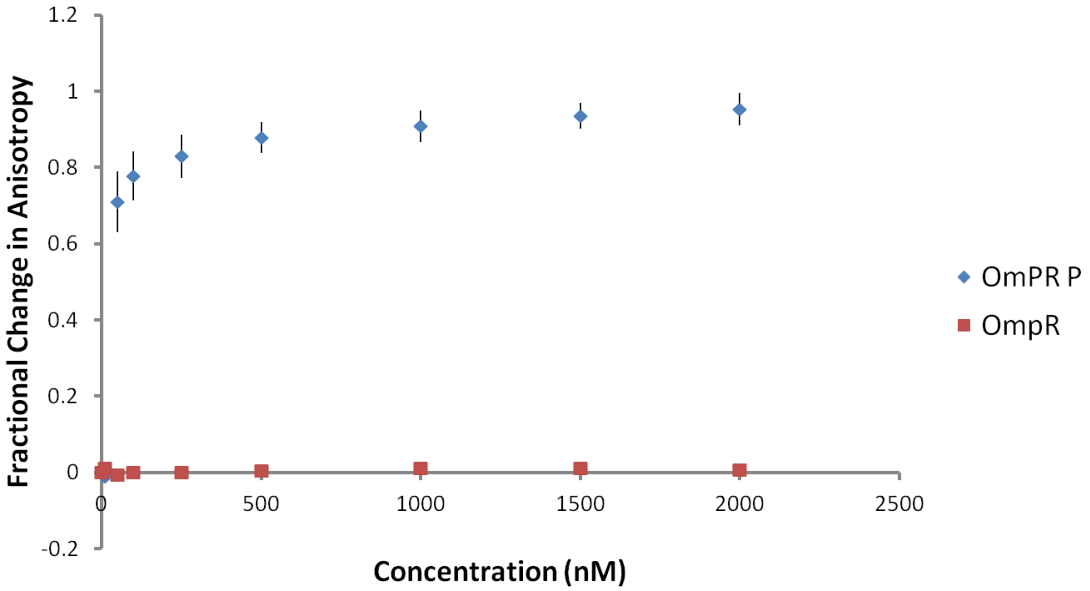

Figure 6.2: mEnvZ:OmpR and mEnvZ-P:OmpR binding to 10nM of Fl-C123. Exploratory experiment with 10nM Fl-C123 DNA to emulated reported K_d values in the literature (32). Red: 10-2000nM of OmpR was incubated in a 2:1 ratio with mEnvZ and mixed with 10nM Fl-C123 DNA, final concentrations. Blue: 10-2000nM of OmpR incubated with mEnvZ-P in a 2:1 ratio (RR:HPK-P) subsequently mixed with 10nM Fl-C123 DNA, final concentrations. Data represent the average fractional change in anisotropy for three independent experiments. Error bars represent the standard deviation.

To conserve promoter material a lower concentration of promoter DNA was used in this study, 5nM. Further preliminary experiments assayed the Fl-C123 binding activity of mEnvZ, mEnvZ-P, CheA and CheA-P, none of these conditions resulted in promoter binding (data not shown). The contribution of the buffer, fluorescein tagged DNA, and ATP and HPK/HPK-P to the anisotropy signal was controlled for by subtracting their signals from the OmpR dependent anisotropy.

These optimised conditions were applied with 5nM F1-F2-F3 and C1-C2-C3 Fl-DNA, which were tested with active and inactive OmpR, F2, F3, F4 and CheY, the results of which will be described below.

6.1.2 Final Anisotropy Experiments

F*l*-F123 Anisotropy

Figure 6.3 shows a comparison of 5nM Fl-F123 DNA incubated with phosphorylated and unphosphorylated OmpR and F2. OmpR-P and OmpR represents wild type Fl-F123 binding, acting as controls. OmpR shows no binding to Fl-F123 promoter DNA, while OmpR-P binds with the promoter DNA. The phosphorylated and unphosphorylated chimeric RR, F2 and F2-P demonstrate similar levels of Fl-F123 promoter binding. This indicates that in this mutant, DNA binding is most probably decoupled from the activated state. It has been established that F2-P has a similar auto-dephosphorylation rate as CheY-P (Chapter 5.1.2.3), therefore their $t_{\frac{1}{2}}$ are likely to be very similar; the $t_{\frac{1}{2}}$ of CheY-P is $\approx$ 20s (28) (106) (107) (52). To ensure that ATP was not exhausted between assay preparation and assay measurement a ratio of HPK:ATP of 1:1000 was chosen. A $t_{\frac{1}{2}}$ of $\approx$ 20s, would equate to 90-135 half lives over the 30-45 minutes required to complete the assay. Taking the multiple dilution steps into account for making stocks and experimental samples, results in a final ratio of HPK:ATP of 1:700. Consequently, ATP should not be exhausted over the course of the anisotropy experiment with F2-P thus ensuring that F2 is indeed phosphorylated in the presence of CheA-P when measurements are taken. F2-P, and CheY-P, have the fastest rates of auto-dephosphorylation of the RRs used, in comparison OmpR-P has a $t_{\frac{1}{2}}$ of $\approx$ 90min, thus would not exhaust ATP either.

The fractional change in anisotropy elicited by OmpR-P is greater than either F2 or F2-P. Taking the end-point value of the assay at 1000nM and normalising to the OmpR-P response, F2 and F2-P are $\approx$26% of the OmpR-P response. These anisotropy data were fit to the model described above, where K_d represents the concentration of RR at the half-maximal fractional change in anisotropy.

Both OmpR-P and F2-P could be fit to the model, the results of the fitting procedure are presented in Table 6.1, and Figures 6.4 and 6.5. The fitted data indicate that OmpR-P has a higher affinity for Fl-F123 than F2-P (Table 6.1). F2-P and OmpR-P have similar Rsqr values, 0.9761 for OmpR-P and 0.9231 for F2-P.

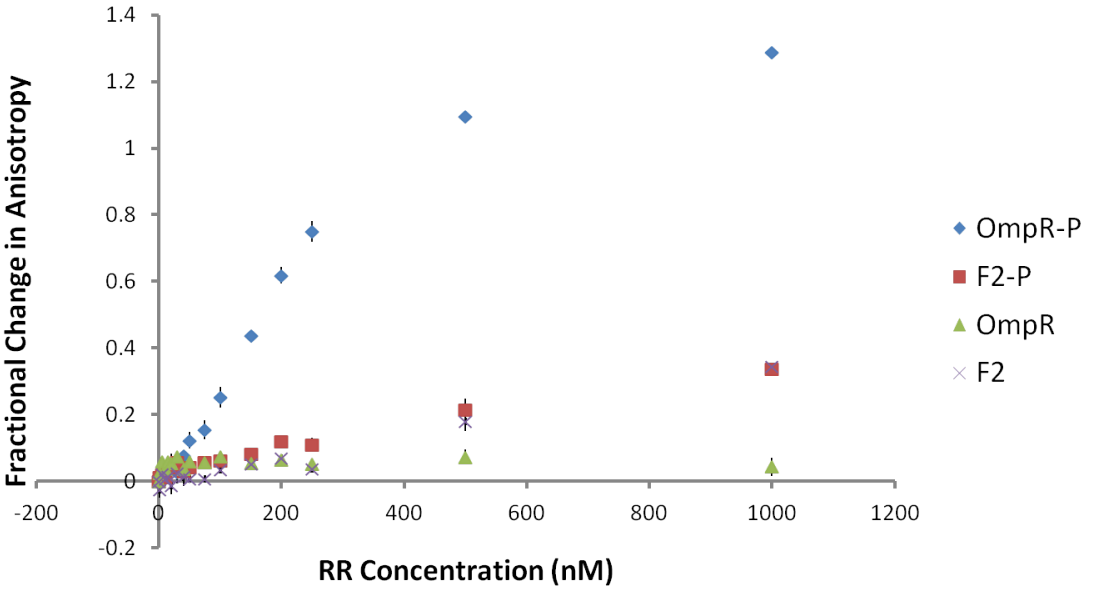

Figure 6.3: OmpR, mEnvZ-P:OmpR, F2 and CheA-P:F2 binding to 5nM Fl-F123. 1-1000nM of RR incubated with 5nM Fl-F123 DNA, final concentrations. 1-1000nM of RR incubated with HPK-P in a 1:2 ratio (RR:HPK-P) subsequently mixed with 5nM Fl-F123 DNA, final concentrations. Data represent the average fractional change in anisotropy for three independent experiments. Error bars represent the standard deviation.

However, the t statistic of the F2-P fit is less than half that of the OmpR-P fit. This indicates that the standard error in the regression is greater when fitting the F2-P data, hence the error in estimating the K_d for F2-P is higher than OmpR-P. Therefore, there can be less confidence in the dependence of Fl-F123 binding on the concentration of F2-P.

The K_d of F2-P for Fl-F123 is 991 $\pm$218 nM, indicating a lower affinity for promoter DNA than OmpR-P. Interestingly, F2 also demonstrates a similar affinity for the Fl-F123 than F2-P. However, the F2 binding data failed the fitting procedure to the rectangular hyperbola model. This is despite a respectable Rsqr value of 0.9429, however failure was due to a large standard error which produced a very low t statistic (0.0001) leading to a large P value of 0.9999. Lower concentrations of F2, up to 75nM, do not show the same concentration dependence as F2-P, the lack of a concentration dependent binding trend at these concentrations may have caused the failure of the fit.

The other RRs, F3-P, F4-P and CheY-P and their unphosphorylated counterparts

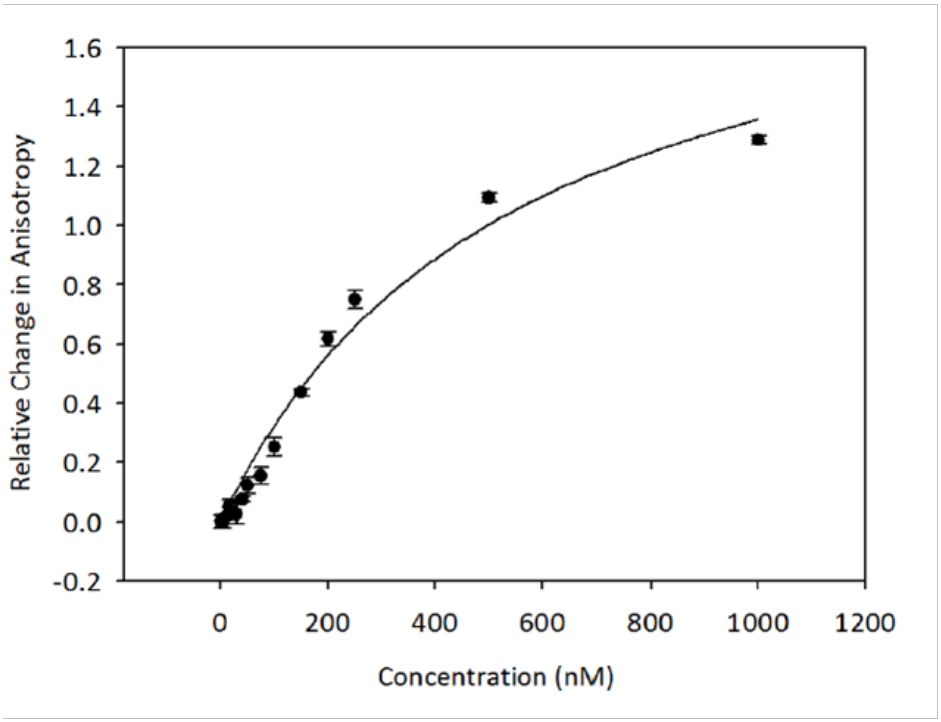

Figure 6.4: SigmaPlot fit of OmpR-P:Fl-F123 binding data. Non-linear least squares single rectangular hyperbola fit, with y replicates, in SigmaPlot. Error bars represent the standard deviation for three independent experiments.

Protein	**Kd ± standard error (nM)**	**Rsqr**	**t statistic**	**P value**
OmpR-P	545 ±56.9	0.9761	9.5870	< 0.0001
F2-P	991 ±218	0.9231	4.5439	< 0.0001

Table 6.1: Fitting statistics for OmpR-P and F2-P incubated with Fl-F123 DNA. Rsqr, measures how well the model describes the data, a value of 1 indicates the model describes the relationship between the dependent and independent variables precisely. The t statistic tests the null hypothesis; that there is no relationship between the RR-P concentration (independent variable) and the fractional change in anisotropy (dependent variable). A larger t statistic indicates that it is less probable that the experimental values are random. The P value is a measure of the probability of falsely rejecting the null hypothesis.

show no Fl-F123 binding, Figure 6.6. CheY-P acted as the negative control in this assay since it has no DNA binding domain. F4-P and F3-P exhibited negative control levels of DNA binding. None of these results could be fit to the model.

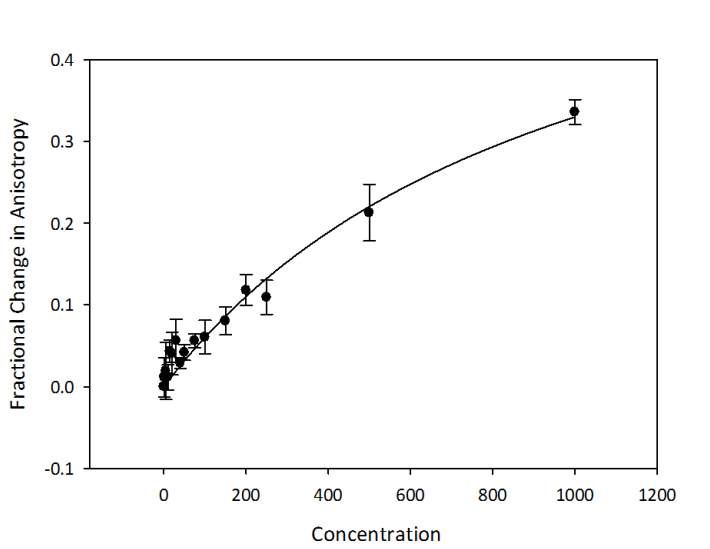

Figure 6.5: SigmaPlot fit of F2-P:Fl-F123 binding data. Non-linear least squares single rectangular hyperbola fit, with y replicates, in SigmaPlot. Error bars represent the standard deviation for three independent experiments.

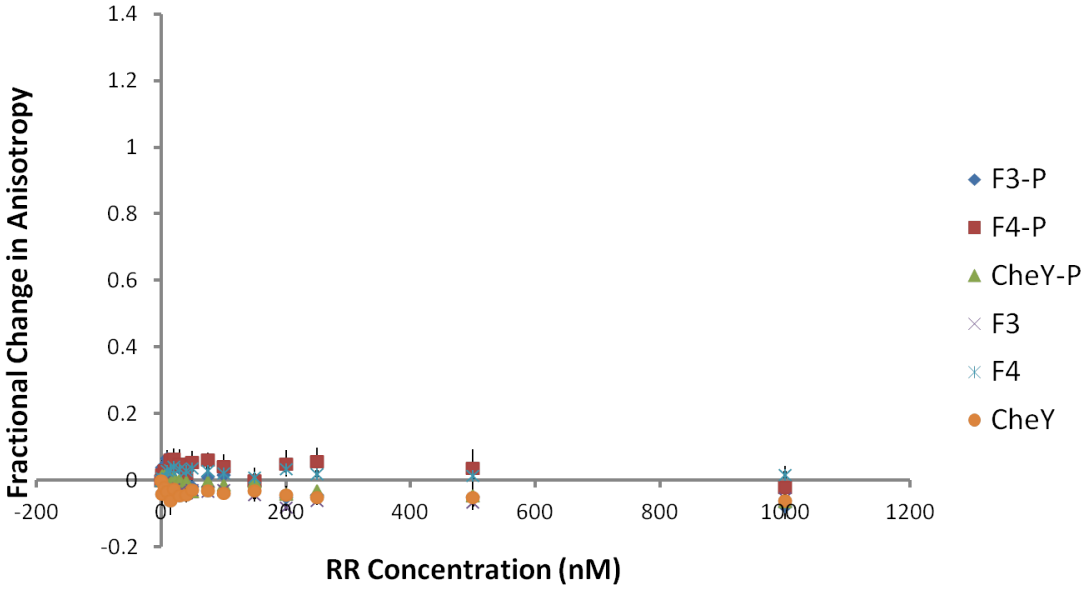

Figure 6.6: F3, CheA-P:F3, F4, CheA-P:F4, CheY and CheA-P:CheY Binding to 5nM Fl-F123. 1-1000nM of RR incubated with 5nM Fl-F123 DNA, final concentrations. 1-1000nM of RR incubated with HPK-P in a 1:2 ratio (RR:HPK-P) subsequently mixed with 5nM Fl-F123 DNA, final concentrations. Data represent the average fractional change in anisotropy for three independent experiments. Error bars represent the standard deviation.

Fl-C123 Anisotropy

Figure 6.7 shows a comparison of Fl-C123 incubated with phosphorylated and unphosphorylated OmpR and F2. OmpR-P and OmpR represent wild type DNA binding, acting as controls. OmpR shows no binding to Fl-C123 promoter DNA, while OmpR-P binds with a higher affinity. The phosphorylated and unphosphorylated chimeric RR, F2 and F2-P both show affinity for the Fl-C123 promoter. Taking the end-point value of the assay at 1000nM and normalising to the OmpR-P response, F2 provides the next highest response, ≈85% of OmpR-P, F2-P is ≈68% of OmpR-P induced anisotropy. These anisotropy data were fit to the model described above, where K_d represents the concentration of RR at the half-maximal fractional change in anisotropy, Table 6.2 and Figures 6.8, 6.9 and 6.10.

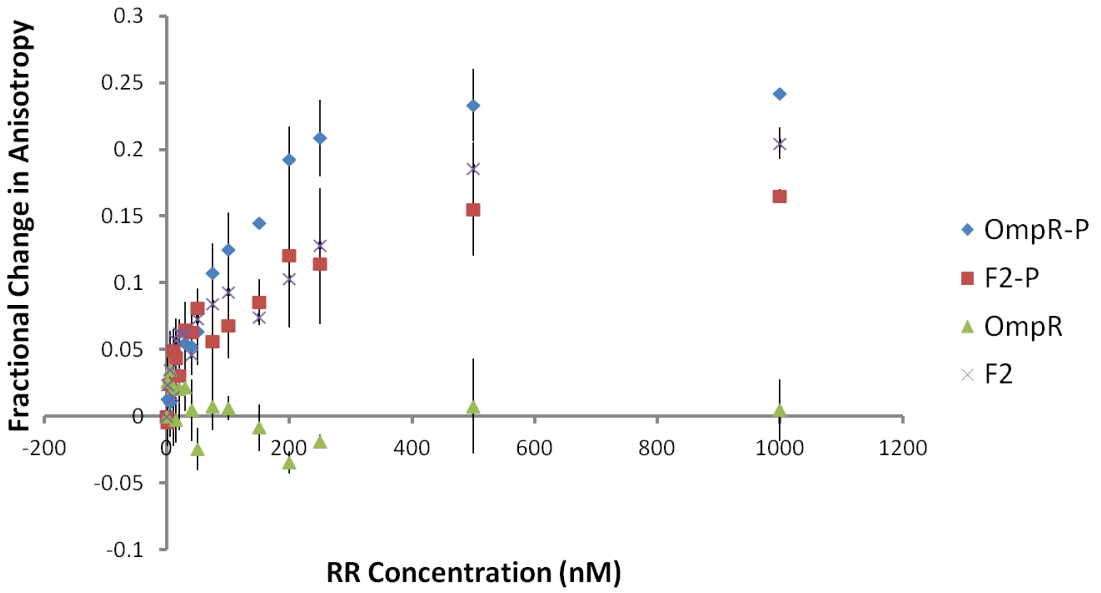

Figure 6.7: OmpR, mEnvZ-P:OmpR, F2 and CheA-P:F2 binding to 5nM Fl-C123. 1-1000nM of RR incubated with 5nM Fl-C123 DNA, final concentrations. 1-1000nM of RR incubated with HPK-P in a 1:2 ratio (RR:HPK-P) subsequently mixed with 5nM Fl-C123 DNA, final concentrations. Data represent the average fractional change in anisotropy for three independent experiments. Error bars represent the standard deviation.

OmpR-P, F2-P and F2 could be fit to the model to varying degrees. The highest Rsqr value and t statistic were obtained with OmpR-P, which generated a K_d of 131 ±15 nM with a $p<0.0001$. It can be observed in Figure 6.7 that F2 has a higher

end-point interaction with Fl-C123 than F2-P. However, an unpaired t-test indicates that the raw data for F2 and F2-P binding Fl-C123 are not significantly different, generating a p value of 0.0810, and a t statistic of 2.32 (GraphPad Software, Inc.). This result suggests that the binding affinity of F2 to Fl-C123 is not dependent on phosphorylation.

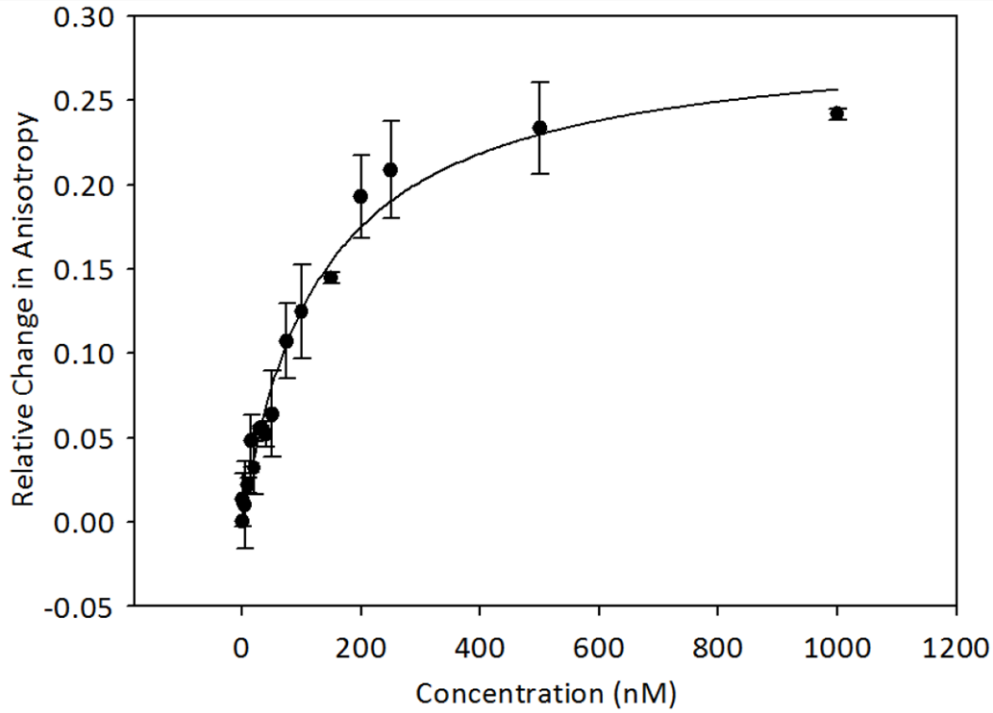

Figure 6.8: SigmaPlot fit of OmpR-P:Fl-C123 binding data. Non-linear least squares single rectangular hyperbola fit, with y replicates, in SigmaPlot. Error bars represent the standard deviation for three independent experiments. Fit statistics are displayed in Table 6.2

The other RRs, F3-P, F4-P and CheY-P and their inactive counterparts show no concentration dependent interaction with Fl-C123 DNA, Figure 6.11. CheY-P acted as the negative control in this assay since it has no DNA binding domain. F4-P and F3-P exhibited negative control levels of DNA binding. None of these results could be fit with the model.

Protein	Kd ± standard error (M)	Rsqr	t statistic	P value
OmpR-P	131 ±15	0.9477	8.8811	< 0.0001
F2-P	79 ±21	0.7061	3.7632	<0.0005
F2	127 ±29	0.7637	4.4080	<0.0001

Table 6.2: Fitting statistics for OmpR-P, F2-P and F2 binding data for Fl-C123 DNA. Rsqr, measures how well the model describes the data, a value of 1 indicates the model describes the relationship between the dependent and independent variables precisely. The t statistic tests the null hypothesis; that there is no relationship between the RR-P concentration (independent variable) and the fractional change in anisotropy (dependent variable). A larger t statistic indicates that it is less probable that the experimental values are random. The P value is a measure of the probability of falsely rejecting the null hypothesis.

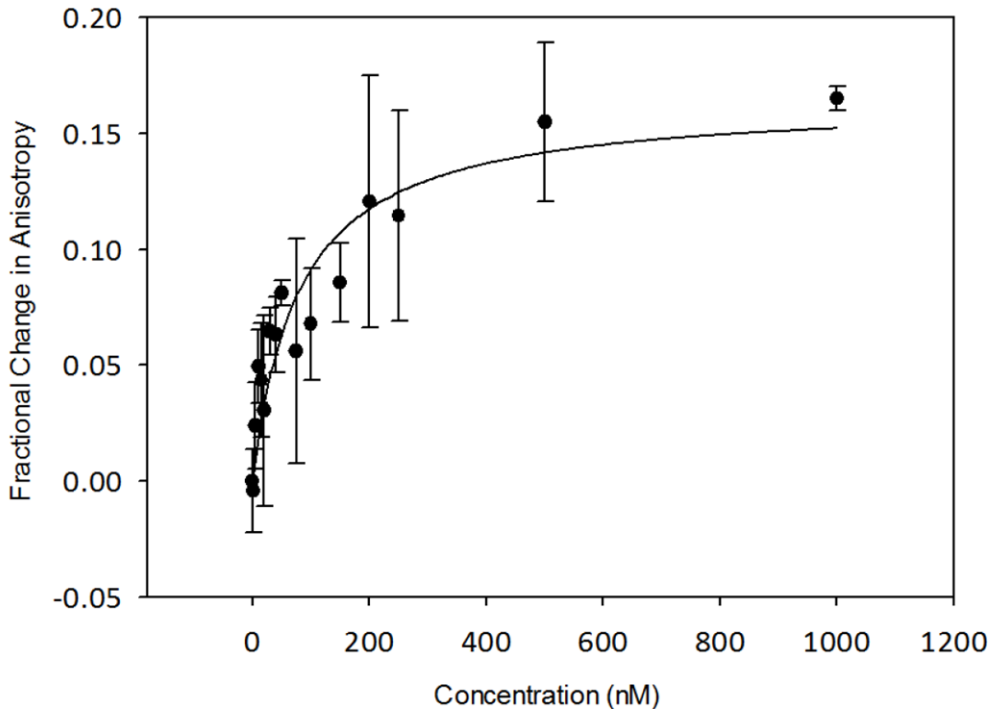

Figure 6.9: SigmaPlot fit of F2-P:Fl-C123 binding data. Non-linear least squares single rectangular hyperbola fit, with y replicates, in SigmaPlot. Error bars represent the standard deviation for three independent experiments. Fit statistics are displayed in Table 6.2

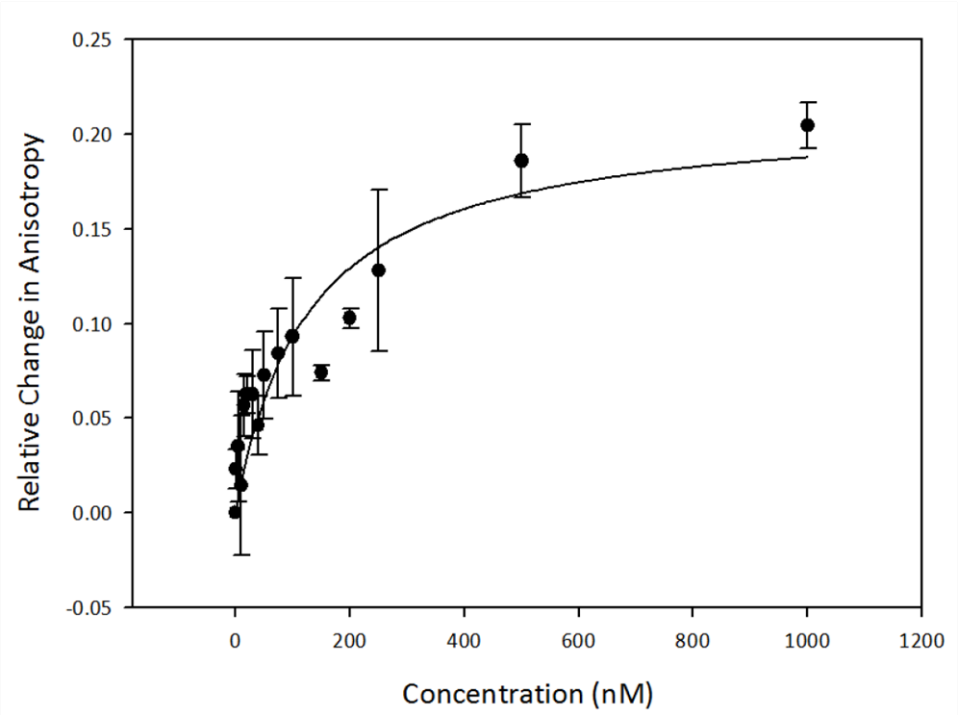

Figure 6.10: SigmaPlot fit of F2:Fl-C123 binding data. Non-linear least squares single rectangular hyperbola fit, with y replicates, in SigmaPlot. Error bars represent the standard deviation.

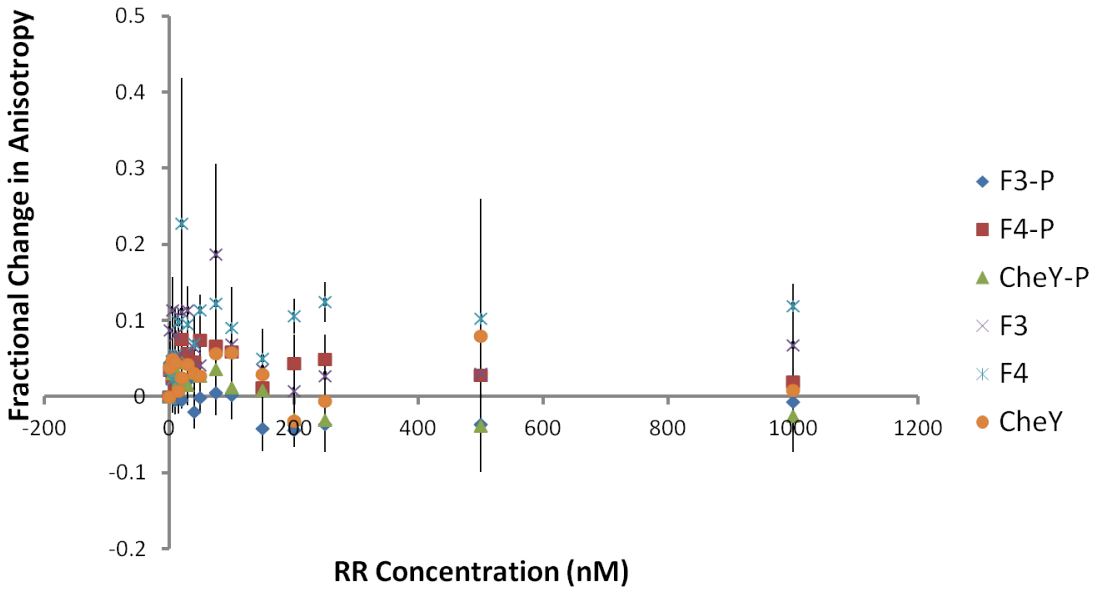

Figure 6.11: F3, CheA-P:F3, F4, CheA-P:F4, CheY and CheA-P:CheY Binding to 5nM Fl-C123. 1-1000nM of RR incubated with 5nM Fl-C123 DNA, final concentrations. 1-1000nM of RR incubated with HPK-P in a 1:2 ratio (RR:HPK-P) subsequently mixed with 5nM Fl-C123 DNA, final concentrations. Data represent the average fractional change in anisotropy for three independent experiments. Error bars represent the standard deviation.

6.2 Discussion

The main result of testing the promoter binding affinity of the chimeric RRs is that only F2 can bind promoter DNA, regardless of phosphorylation state. The other chimeric RRs, F3 and F4, do not demonstrate any promoter DNA binding ability.

Data indicate that OmpR-P binds both Fl-C123 and Fl-F123, however, OmpR does not bind either promoter. This contrasts with the reported binding data, in which both OmpR-P and OmpR bind Fl-C123 and Fl-F123 (32). It has been demonstrated that OmpR bound Fl-C123 with a K_d of 86.7 $\pm$32.5 nM and Fl-F123 with a K_d of 496.5 $\pm$60.9 nM (32). These affinities are within the sensitivity of the instrument used in this study. Although, there are differences in the buffer and experimental set-up used in this study, the K_d of OmpR-P for Fl-C123 reported in the literature could be emulated by matching the concentration of Fl-DNA used. However, using a higher Fl-DNA concentration still did not result in OmpR binding to Fl-DNA. Furthermore, the elution profile of unphosphorylated OmpR indicates that very little dimerisation takes place in solution, see Figure 3.4. It can be deduced that there is a fundamental difference between the experiments and proteins used that is causing a consistent lack of OmpR Fl-DNA binding in this study. It should be noted that the sequences for the Fl-DNA were taken directly from the literature, removing differences in promoter sequences as a potential variable (32). Ultimately, a full explanation is difficult to determine. Underlining these differences further, the K_d values reported in the literature demonstrate that OmpR-P binds with a lower affinity to Fl-C123 compared with Fl-F123 (32), whilst in this study the reverse is observed. Furthermore, the magnitude of the difference between the K_d values is different; the affinity of OmpR-P for Fl-C123 is 131 $\pm$15 nM and 545 $\pm$56.9 nM for Fl-F123 in this study, whilst in the literature OmpR-P binds Fl-C123 with an affinity of 31.4 $\pm$8 nM and Fl-F123 with an affinity of 15.4 $\pm$3.5 nM (32).

It has been demonstrated that activation of OmpR/PhoB family members produces dimerisation, which is essential to bind DNA (89) (90) (60) (2) (26) (29). Further, the $\Delta\Delta G_{dimerisation}$ of OmpR-P is greater than the $\Delta\Delta G_{binding}$ of OmpR-P to DNA, it has been postulated that the difference in the free energy of these processes could provide the driving force for stable DNA binding (4). This $\Delta\Delta G$ difference could help explain the observed DNA binding affinities of OmpR and OmpR-P, a decrease in the $\Delta\Delta G_{dimerisation}$ from OmpR-P to OmpR monomers could affect the free energy available to drive and stabilise Fl-DNA binding. The complete lack of

Fl-DNA binding by OmpR observed in this study indicates that OmpR monomers are not dimerising under the conditions used, providing little free energy to drive stable Fl-DNA binding.

Data indicate that F2 and F2-P associate with Fl-C123 and Fl-F123, and are not significantly different. The affinity of F2 and F2-P for promoter DNA is less than that of OmpR-P. F2 contains the α_5 helix of OmpR in addition to the linker and CTD. It is evident that the presence of the CTD is not sufficient for Fl-DNA binding, since no promoter binding is observed with either F4 or F3. Consequently, the presence of OmpR's α_5 helix appears to affect the Fl-DNA binding propensity of F2. OmpR's α_5 helix takes part in the dimer interface formed by interactions across the α_4-β_5-α_5 region of two OmpR monomers. The α_5 helix of one monomer packs against the α_4 helix of another monomer via an extensive array of salt bridges and to a lesser extent hydrophobic interactions (89) (90) (60) (2) (26) (29). The α_4 helix of F2 is composed entirely from CheY, as such it lacks the normal binding surface which is complementary to OmpR's α_5 helix. However, helix 4 of F2 does contain charged residues which may be sufficient to form the salt bridges for F2 dimerisation leading to Fl-DNA binding.

An alternative hypothesis is that F2 could bind DNA as a monomer, such behaviour would be dependent on helix 5 since no DNA binding is observed in either F4 or F3 experiments. It has been demonstrated with NMR titrations that an isolated OmpR CTD can bind to the C1b half-site with a $K_d >> 1.5\mu$M (71). However, full-length OmpR cannot bind to DNA half-sites (4). The low affinity of the the isolated CTD for the high affinity C1b half-site contrasts with the calculated K_d of F2 and F2-P for Fl-C123 of 79 and 127nM. Furthermore, the K_d of dimeric OmpR-P for Fl-C123 is 131nM. It has been demonstrated that the addition of C2 and C3 to the C1 binding site leads to decreased DNA affinity for OmpR-P (32). Assuming DNA binding by the chimeric RR is governed by the same phenomenon, these data do not suggest low affinity Fl-C123 binding by monomeric F2 or F2-P.

F2 binds Fl-DNA regardless of phosphorylation state. The decoupling of DNA binding from the phosphorylation state of F2 could indicate that the activation of the REC domain in this mutant is not successfully propagated through the REC domain to the all of the α_4-β_5-α_5 region. This could mean that helix 5 is independent of the rest of the REC domain in the F2 chimera and is able to access an activated state constitutively. Furthermore, the elution profile of unphosphorylated F2 demonstrates

that the chimeric RR is capable of dimerisation in solution, and it forms a greater proportion of the total F2 population when compared to wild-type OmpR, see Figure 3.5.

6.3 Conclusions

A synthetic TCS designed to function around a chimeric RR requires that the RR's output can be modulated by the input to the system. Fluorescence anisotropy experiments established that chimeric RRs F4 and F3 do not bind Fl-DNA and although F2 can bind promoter DNA it is independent of its phosphorylation state and therefore would not be modulated by input to the TCS.

Chapter 7

General Discussion, Future Work and Conclusion

7.1 General Discussion and Future Work

The aim of this study was to determine whether it is possible to create a synthetic TCS from both class I and class II components. A system was devised where chemotactic stimuli drive transcription via a chimeric RR composed of regions of CheY and OmpR. The different functions of the REC domains of CheY and OmpR dictated the design of the chimeras. The rationale for the chimeric RRs composed of CheY and OmpR was that they would retain the ability to bind to and undergo phosphotransfer from CheA. Phosphorylation would be transduced into a conformational change transmitted to the α_4-β_5-α_5 region of the chimeric REC domain, where the OmpR component would dimerise and mediate the output of DNA binding to *pOmpC* or *pOmpF*.

The aims of this study were;

- To determine the optimum fusion sites between CheY and OmpR, a number of fusion sites across the α_4-β_5-α_5 region were created and the chimeric proteins characterised by circular dichroism and ESI-MS.
- To determine the HPK binding affinity of the fusion constructs, assayed by surface plasmon resonance.
- To determine the phosphotransfer capabilities of the fusion constructs, assayed by *in vitro* phosphotransfer from CheA-P and mEnvZ-P.
- To determine the *pompC* and *pompF* binding capabilities of the constructs, assayed by fluorescence anisotropy.

Expression of the F2 and F1 chimeric RRs proved challenging, upon further investigation with ESI-MS and CD only fusions F2-4 were folded at room temperature. Evidently, replacing all of the α_4-β_5-α_5 region of CheY with OmpR, as done with F1, has catastrophic effects on RR stability.

Surface plasmon resonance experiments determined that F4 and F3 had the highest affinity for bCheA-P2, 200 $\pm$32.4 nM and 201 $\pm$73.4 nM, both of which are significantly higher than the wild-type affinity of CheY, 333.7nM $\pm$25.6 nM. This could indicate that the presence of the OmpR linker and CTD are helping to increase the affinity of the chimeras. Interestingly, sensograms for F3 and F4 display avidity at high concentrations, which can act to slow dissociation and increase the calculated affinity because a single analyte binds to 2 or more ligand molecules. However, no

such effects were observed at the concentrations used to calculate the K_d values which were used in the statistical tests, ruling out avidity as an explanation for the lower K_d values. The OmpR linker and CTD could have a universal affect on chimera affinity, F2 binds bCheA-P2 but does not contain the fifth helix of the α_4-β_5-α_5 binding region. F2 does bind bCheA-P2 but the data could not be fit to a binding model. To clarify the effect of the CTD on bCheA-P2 binding, further experiments could use the isolated OmpR CTD as an analyte for bCheA-P2, and the isolated REC domain of F2, and extensions into the linker and CTD to isolate the influence of the REC, linker and CTD to bCheA-P2 binding. Further surface plasmon resonance experiments could also look at the dissociation behaviour of phosphorylated chimeras by using full-length HPKs and introducing a pulse of ATP. This could help elucidate whether the linker and CTD additions affect dissociation from the HPK when compared with CheY-P.

The increase in affinity observed with F4 and F3 does not lead to a significant change in phosphotransfer from CheA-P at 15s when compared with CheY. This most likely indicates that the rate of phosphotransfer from CheA-P to CheY is highly optimised, such that no further increases in the rate of phosphotransfer are possible by increasing the affinity between the HPK-P and RR. F2 was phosphorylated to a significantly lesser extent than CheY, F4 and F3 by CheA-P at 15s. This result most likely stems from the lower affinity for bCheA-P2 observed with the F2 chimera. Interestingly, when extending the time course to 240s, F2 was capable of maintaining CheA in a dephosphorylated state from 60s onwards and has a similar auto-dephosphorylation rate as CheY-P. Indicating that F2's impaired affinity for bCheA-P2 is not severe enough to prevent phosphorylation by CheA-P, and the replacement of helix 5 with that of OmpR does not significantly affect the auto-dephosphorylation rate when compared with CheY-P. The rates of phosphotransfer to CheY and auto-dephosphorylation of CheY-P have been investigated with rapid reaction experiments (79) (56), and similar experiments could be used to determine the fine detail in the phosphotransfer and auto-dephosphorylation rates of the chimeric RRs. These data could indicate whether the OmpR linker and CTD have affects on the rate constants.

Fluorescence anisotropy experiments determined the DNA binding ability of the chimeric RRs. F4 and F3 do not bind with Fl-F123 or Fl-C123, regardless of phosphorylation state. This indicates that activation of the REC domains of F4 and F3

is not not transmitted to the OmpR linker or CTD. The lack of DNA binding by F3 and F4 could indicate that inhibitory interactions with the OmpR REC domain are not required for inhibition of DNA binding. Alternatively, this could suggest that the DNA binding domain of OmpR is held in an inhibited conformation when fused to CheY and that this inhibition is not released by phosphorylation of the CheY REC domain.

F2 does bind Fl-F123 and Fl-C123 but not in a phosphorylation dependent manner. The activation of the F2 REC domain is either not transmitted to the linker and CTD, or if it is, has no affect on DNA binding ability. However, these data indicate that the CTD of F2 is constitutively active to some extent. The difference between F2 and F3/F4 is the presence of OmpR's fifth helix. In F2, α_5 appears to allow the linker and CTD to access an active state, suggesting that α_5 is normally restrained by the rest of the REC domain in wild-type OmpR; a strong inactivating interaction between the NTD and CTD of OmpR is evident in the lack of DNA binding observed for OmpR. These data could indicate that α_5 itself is also constitutively active in F2. Based on these results, a previously unknown role for α_5 emerges as the activator of DNA binding in OmpR. To further delineate the role of α_5 in wild-type OmpR, helix 5 could be replaced by helix 5 of CheY. If wild-type OmpR α_5 does activate DNA binding, this mutant should knock-out this function. Truncations of OmpR's fifth helix could serve a similar purpose.

7.2 Conclusion

This study has established that the design of chimeric RRs which retain the functionality of both CheY and OmpR can not be accomplished using a simple fusion approach. Based on these data there is no optimum fusion site between CheY and OmpR for the creation of a fully functional chimeric RR. However, this study has established that various chimeric RRs are structurally viable and retain some of the characteristics of a wild-type RR; HPK binding, phosphorylation, activation, output modulation and dephosphorylation. It should be noted that there are a few natural examples in which a chemotaxis-like pathway is linked to a transcriptional output, for example the Che3 pathway in *Myoxocoxxus xanthus* (42). Consequently, fine tuning of the design of the synthetic RRs, perhaps with point mutations or based on the *M. xanthus* system, could yet yield a functional RR for synthetic biology with a defined

chemical input and controllable transcriptional output.

Chapter 8

Media Recipes and Reagents

8.1 Recipes

8.1.1 Luria-Bertani Broth

- Tryptone $10g^{-1}$
- Yeast Extract $5g^{-1}$
- NaCl $5g^{-1}$
- pH 7.0

8.1.2 2xTY

- Tryptone $16g^{-1}$
- Yeast extract $10g^{-1}$
- NaCl $5g^{-1}$
- pH 7.0

8.1.3 LB Agar

- Tryptone $10g^{-1}$
- Yeast Extract $5g^{-1}$
- NaCl $5g^{-1}$
- Agar $16g^{-1}$
- pH 7.0

8.1.4 10 x TBE

- Tris base 108 g
- Boric acid 55 g
- EDTA 7.4 g
- dissolved in 1L distilled water

8.1.5 5 x DNA Loading Dye

- Glycerol 70%
- Bromophenol Blue 0.25%
- Xylene Cyanol 0.25%
- 1 x TE 30%

8.1.6 DNA Ladder

- 1Kb ladder (Invitrogen) 37.5μl
- 1 x TE 362.5μl
- Loading dye 100μl

8.1.7 TFBI Buffer

- Potassium Acetate 30mM
- Rubidium Chloride 100mM
- $CaCl_2 2\,H_2O$ 10mM
- $MnCl_2 4\,H_2O$ 50mM
- pH 5.8

8.1.8 TFBII Buffer

- PIPES 10mM
- $CaCl_2 2\,H_2O$ 75mM
- Rubidium Chloride 10mM
- Glycerol 15%
- pH 6.8

8.1.9 His-Tagged Protein Lysis Buffer

- Tris-HCl pH 8.0 50mM
- NaCl 150mM
- DTT 1mM
- Imidazole 10mM
- EDTA-free Protease Inhibitor Cocktail Tablets (1/50ml buffer)
- pH 8

8.1.10 His-Tagged Protein Wash Buffer I

- Tris-HCl pH 8.0 50mM
- NaCl 150mM
- DTT 1mM
- Imidazole 20mM
- EDTA-free Protease Inhibitor Cocktail Tablets (1/50ml buffer)
- pH 8

8.1.11 His-Tagged Protein Wash Buffer II

- Tris-HCl pH 8.0 50mM
- NaCl 150mM
- Glycerol 10%
- DTT 1mM
- Imidazole 20mM
- EDTA-free Protease Inhibitor Cocktail Tablets (1/50ml buffer)
- pH 8

8.1.12 His-Tagged Protein Elution Buffer

- Tris-HCl pH 8.0 50mM
- NaCl 150mM
- Glycerol 10%
- DTT 1mM
- Imidazole 250mM
- pH 8

8.1.13 GST-Tagged Protein Binding Buffer

- Phosphate Buffered Saline pH 7.3

8.1.14 GST-Tagged Protein Elution Buffer

- Tris-HCl pH 8.0 50mM
- Reduced Glutathione 10mM
- DTT 1mM

8.1.15 Gel Filtration Buffer

- Tris-HCl pH 8.0 50mM
- Glycerol 10%
- NaCl 150mM
- TCEP 0.5mM

8.1.16 20 x Reducing Buffer for SDS-PAGE

- MOPS 0.6M
- Tris 1.2M

- SDS 2%
- Sodium Bisulfite 50mM
- pH between 8.2 and 8.3

8.1.17 5 x SDS-PAGE Loading Dye

- Glycerol 50%
- Tris-HCl pH 6.8 0.5M
- β-mercaptoethanol 5%
- SDS 5% (w/v)
- Bromophenol Blue

8.1.18 20 x Native Running Buffer

- Tricine 0.8M
- Tris 1.2M
- pH 8.3

Native Gel Loading buffer

- Bromophenol Blue 0.25%
- Xylene Cyanol FF 0.25%
- Ficoll Type 400 in H_2O 15%

8.1.19 Circular Dichroism Buffer

- Phosphate Buffered Saline 10mM
- NaCl 20mM

8.1.20 Histidine Kinase Autophosphorylation Buffer

- Tris-HCl pH 8.0 50mM
- Glycerol 10%
- NaCl 150mM
- KCl 50mM
- $MgCl_2$ 5mM
- TCEP 0.5mM
- Histidine Kinase 5μM
- ATP 0.67mM

8.1.21 1 x Phosphotransfer Assay Buffer

- Tris-HCl pH 8.0 50mM
- Glycerol 10%
- NaCl 150mM
- TCEP 0.5mM

8.1.22 Phosphotransfer Loading Dye

- Tris-HCl pH 6.8 37.5mM
- Glycerol 37.5%
- β-mercaptoethanol 3%
- EDTA 90mM
- SDS 7.5%

8.1.23 Phosphotransfer 15% Gel

- 30% Acrylamide 200ml
- 1.5M Tris-HCl pH 8.8 100ml
- 10% SDS 4ml
- 10% APS 4ml
- TEMED 0.16ml
- Water 92ml

8.1.24 Phosphotransfer Stacking Gel

- 30% Acrylamide 17ml
- 1M Tris-HCl pH 6.8 25ml
- 10% SDS 1ml
- 10% APS 1ml
- TEMED 0.1ml
- Water 55.5ml

8.1.25 Anisotropy Buffer

- Tris-HCl pH 8.0 50mM
- Glycerol 10%
- NaCl 150mM
- KCl 50mM
- $MgCl_2$ 5mM
- TCEP 0.5mM
- 5nM Flc-tagged promoter DNA

8.1.26 Oligo Annealing Buffer

- Tris-HCL pH 8.0
- NaCl 50mM
- EDTA 1mM

8.1.27 Surface Plasmon Resonance Buffer

- 10mM HEPES pH 7.4
- 150mM NaCl
- Tween 20 0.05%(v/v)

8.1.28 Biotin CAPture Reagent - 50μg/ml

- HEPES pH 7.4 0.01M
- NaCl 0.15M
- EDTA 3mM
- Surfactant P20 0.005%

8.1.29 Surface Plasmon Resonance Regeneration Buffer

- Regeneration Stock 1 (Guanidine-HCl 8M) 3 parts
- Regeneration Stock 2 (NaOH 1M) 1 part

Chapter 9

PCR Primers and Programmes

9.1 PCR Primers

9.1.1 Primers to Create Fusion Constructs

For the creation of the fusion products;
F1-3 Table 9.1:

1. 1st rounds of PCR use primers of the type CheYOE_XY(Z) as reverse primers with CheY FW EcoRI with wild-type CheY as a template, primers of the type OmpROE_XY(Z) are used as forward primers with OmpR RV BamHI with wild-type OmpR as a template.

2. 2nd round overlap extension PCR use primers CheY FW NcoI and OmpR RV BamHI with any CheY-FX and OmpR-FX, where X denotes the same number

F4 Table 9.2:

1. 1st round of PCR use primer OmpR Oe0 prop as a forward primer with OmpR RV BamHI with wild-type OmpR as a template.

2. 2nd round overlap extension PCR, for use primers CheY FW EcoRI and OmpR RV BamHI with the CheY-F4 and OmpR-F4.

Primer Name	**Sequence**	**Product**
CheY FW EcoRI	CACTAG<u>GAATTC</u>ATGGCGGATAAAGAACTTAAATTTTTGG	
OmpR RV BamHI	CACTGT<u>GGATCC</u>TGCTTTAGAGCCGTCCGGTAC	
CheYOE_264	**CACTTCTTCCCCTTTT**GCAGTCACCATTAAC	CheY-F1
OmpROE_253	TTAATGGTGACTGCA**AAAGGGGAAGAAGTGG**	OmpR-F1
CheYOE_333	**GCAGTTCACGCGGGTT**AAATGGCTTCACCAC	CheY-F2
OmpROE_322	GTGGTGAAGCCATTT**AACCCGCGTGAACTGC**	OmpR-F2
CheYOE_FL	**CGCCTGGCAGTTC**CATGCCCAGTTTCTC	CheY-F3
OmpROE_376	GAGAAACTGGGCATG**GAACTGCCAGGCG**	OmpR-F3

Table 9.1: Primers to make fusion proteins of CheY and OmpR. All primers are displayed 5' to 3'. Underline text marks a restriction site. Bold text marks an overlap extension site between primers.

Primer Name	Sequence	Product
CheY FW EcoRI	CACTAGGAATTCATGGCGGATAAAGAACTTAAATTTTTGG	
GB CheY OE4	**GTGCGCCTGGCAGTTCGTTCGCCTG**CATGCCCAGTTTCTCAAAGATTTTG	CheY-F4
OmpR RV BamHI	CACTGTGGATCCTGCTTTAGAGCCGTCCGGTAC	
GB OmpR OE4 short	**CAGGCGAACGAACTGCCAGGCGCAC**C	OmpR-F4

Table 9.2: Primers to make F4. All primers are displayed 5' to 3'. Underline text marks a restriction site. Bold text marks an overlap extension site between primers.

9.1.2 Primers to Create Biotinylation Tagged Constructs

Primer Name	Sequence	Product
bCheA-P1 BamHI FW	CACTAGGGATCCATGGTGAGCATGGATATAAGCG	CheA-P1
bCheA-P1 HindIII RV	CACTAGAAGCTTTCA*TTCATGCCATTCAATTTTTTGAGCTTCAAAAAT*-	
	-*ATCATTAAGACC*GCCGCCCGGTTCACTTTTGGCAACC	biotinylation tagged CheA-P1
bCheA-P2 BamHI	CACTAGGGATCCCGTCAACTGGCATTAGAAGC	CheA-P2
bCheA-P2 HindIII RV	CACTAGAAGCTTTCA*TTCATGCCATTCAATTTTTTGAGCTTCAAAAATAT*-	
	-*CATTAAGACC*GCCGCCGCGCGTCGTTTTTTCCCGC	biotinylation tagged CheA-P2
mEnvZ BamHI FW	CACTAGGGATCCATTCGTATCCAGAACCGACCG	mEnvZ
bmEnvZ HindIII RV	CACTAGAAGCTTTCA*TTCATGCCATTCAATTTTTTGAGCTTCAAAAATATCATT*-	
	-*AAGACC*GCCGCCCCCTTCTTTTGTCGTGCCCTGC	biotinylation tagged mEnvZ

Table 9.3: Primers to make biotinylated SPR constructs. All primers are displayed 5' to 3'. Underline text marks a restriction site. Italic text marks the biotinylation sequence.

9.1.3 Primers to Create Wild-type and Site Directed Mutagenesis Constructs

Primer Name	Sequence
EnvZHAMP BamHI FW	GACTGAGGATCCATCCAGAACCGACC
EnvZHAMP EcoRI RV	ACGTAGGAATTCTTACCCTTCTTTTGTC
EnvZ L288P FW	ATTGAGCAGTTTATCGACTACccgCGCACCGGGCAGGAG
EnvZ L288P RV	TCCTGCCCGGTGCGcggGTAGTCGATAAACTGCTCAATG

Table 9.4: Primers to make EnvZ and mEnvZ. All primers are displayed 5' to 3'. Underline text marks a restriction site. Lower-case text marks mutation site.

Primer Name	Sequence
CheY FW EcoRI	CACTAGGAATTCATGGCGGATAAAGAACTTAAATTTTTGG
CheY RV BamHI	CACTAGGGATCCCATGCCCAGTTTCTCAAAGATTTTG
OmpR FW EcoRI	CACTAGGAATTCATGCAAGAGAACTACAAGATTCTGG
OmpR RV BamHI	CACTGTGGATCCTGCTTTAGAGCCGTCCGGTAC

Table 9.5: Primers to make CheY and OmpR. All primers are displayed 5' to 3'. Underline text marks a restriction site.

9.1.4 Primers to Create Fluorescein Tagged Promoter DNA

Primer Name	Sequence
F1-F2-F3 Flc	[Flc]ATTTTACTTTTGGTTACATATTTTTTCTTTTTGAAACCAAA-
	-TCTTTATCTTTGTAGCACTTTCACGG
F1-F2-F3 comp	CCGTGAAAGTGCTACAAAGATAAAGATTTGGTTTCAAAAAGAA-
	-AAAATATGTAACCAAAAGTAAAAT
C1-C2-C3 Flc	[Flc]CCTTGCATTTACATTTTGAAACATCTATAGCGATAAATGAAA-
	-CATCTTAAAAGTTTTAGTATCATATTCG
C1-C2-C3 comp	CGAATATGATACTAAAACTTTTAAGATGTTTCATTTATCGCTA-
	-TAGATGTTTCAAAATGTAAATGCAAGG

Table 9.6: Primers to make fluorescein tagged double stranded promomter DNA. All primers are displayed 5' to 3'. [Flc] denotes the fluorescein tag added by Sigma during synthesis.

9.2 PCR Programmes

9.2.1 Gradient PCR

Time	Temperature
2 minutes	98°C
2 minutes	60°C $\delta 20°C$
500bps per minute + 2 minutes	72°C

Table 9.7: Programme for gradient PCR. Programme was carried out for 29 cycles, with a gradient over 20°C using 60°C as the median temperature.

9.2.2 PCR

Time	Temperature
2 minutes	98°C
2 minutes	appropriate temperature based on gradient
500bps per minute + 2 minutes	72°C

Table 9.8: Programme for PCR. Programme was carried out for 29 cycles.

9.2.3 Site Directed Mutagenesis PCR

Time	Temperature
30 seconds	95°C
1 minute	55°C
500bps per minute + 2 minutes	72°C

Table 9.9: Programme for Site Directed Mutagenesis PCR. Programme was carried out for 16 cycles.

9.2.4 Annealing PCR

Time	Temperature
2 minutes	92°C
5 minutes	25°C
5 minutes	4°C

Table 9.10: Programme for Annealing PCR. Programme was carried out for 1 cycle. The rate of change between step one and two was set to the slowest available, 0.1°C.

Bibliography

[1] Anand, G. S., Goudreau, P. N., and Stock, A. M. Activation of Methylesterase CheB: Evidence of a Dual Role for the Regulatory Domain. *Biochemistry 37*, 40 (1998), 14038–14047.

[2] Bachhawat, P., Swapna, G., Montelione, G. T., and Stock, A. M. Mechanism of Activation for Transcription Factor PhoB Suggested by Different Modes of Dimerization in the Inactive and Active States. *Structure 13* (2005), 1353–1363.

[3] Barak, R., Prasad, K., Shainskaya, A., Wolfe, A. J., and Eisenbach, M. Acetylation of the Chemotaxis Response Regulator CheY by Acetyl-CoA Synthetase Purified from Escherichia coli. *Journal of Molecular Biology 342*, 2 (2004), 383 – 401.

[4] Barbieri, C. M., Wu, T., and Stock, A. M. Comprehensive Analysis of OmpR Phosphorylation, Dimerization, and {DNA} Binding Supports a Canonical Model for Activation. *Journal of Molecular Biology 425*, 10 (2013), 1612 – 1626.

[5] Batchelor, E., and Goulian, M. Robustness and the cycle of phosphorylation and dephosphorylation in a two-component regulatory system. *Proceedings of the National Academy of Sciences 100*, 2 (2003), 691–696.

[6] Batchelor, E., and Goulian, M. Imaging OmpR localization in Escherichia coli. *Molecular Microbiology 59*, 6 (2006), 1767–1778.

[7] Beckett, D., Kovaleva, E., and Schatz, P. J. A minimal peptide substrate in biotin holoenzyme synthetase-catalyzed biotinylation. *Protein Science 8*, 4 (1999), 921–929.

[8] Bell, C. H., Porter, S. L., Strawson, A., Stuart, D. I., and Armitage, J. P. Using Structural Information to Change the Phosphotransfer Specificity of a Two-Component Chemotaxis Signalling Complex. *PLoS Biol 8*, 2 (02 2010), e1000306.

[9] Benenson, Y., Gil, B., Ben-Dor, U., Adar, R., and Shapiro, E. An autonomous molecular computer for logical control of gene expression. *Nature 429* (2004), 423–429.

[10] Bilwes, A. M., Alex, L. A., Crane, B. R., and Simon, M. I. Structure of CheA, a Signal-Transducing Histidine Kinase . *Cell 96*, 1 (1999), 131 – 141.

[11] Bourret, R. B., Drake, S. K., Chervitz, S. A., Simon, M. I., and Falke, J. J. Activation of the phosphosignaling protein CheY. II. Analysis of activated mutants by 19F NMR and protein engineering. *Journal of Biological Chemistry 268*, 18 (1993), 13089–13096.

[12] Cai, S. J., and Inouye, M. EnvZ-OmpR Interaction and Osmoregulation in Escherichia coli. *Journal of Biological Chemistry 277*, 27 (2002), 24155–24161.

[13] Capra, E., Perchuk, B., Skerker, J., and Laub, M. Adaptive Mutations that Prevent Crosstalk Enable the Expansion of Paralogous Signaling Protein Families. *Cell 150*, 1 (2012), 222 – 232.

[14] Capra, E. J., Perchuk, B. S., Lubin, E. A., Ashenberg, O., Skerker, J. M., and Laub, M. T. Systematic Dissection and Trajectory-Scanning Mutagenesis of the Molecular Interface That Ensures Specificity of Two-Component Signaling Pathways. *PLoS Genet 6*, 11 (11 2010), e1001220.

[15] Casino, P., Rubio, V., and Marina, A. Structural Insight into Partner Specificity and Phosphoryl Transfer in Two-Component Signal Transduction. *Cell 139*, 2 (2009), 325 – 336.

[16] Chang, Y.-C., Armitage, J. P., Papachristodoulou, A., and Wadhams, G. H. A single phosphatase can convert a robust step response into a graded, tunable or adaptive response. *Microbiology 159*, Pt 7 (2013), 1276–1285.

[17] Cho, H. S., Lee, S.-Y., Yan, D., Pan, X., Parkinson, J. S., Kustu, S., Wemmer, D. E., and Pelton, J. G. NMR structure of activated CheY. *Journal of Molecular Biology 297*, 3 (2000), 543 – 551.

[18] Creighton, T. *Proteins: Structure and Molecular Properties*. W. H. Freeman, 1992.

[19] Danino, T., Mondragon-Palomino, O., Tsimring, L., and Hasty, J. A synchronized quorum of genetic clocks. *Nature 463* (2010), 326–330.

[20] Dutta, R., Qin, L., and Inouye, M. Histidine kinases: diversity of domain organization. *Molecular Microbiology 34*, 4 (1999), 633–640.

[21] Dutta, R., Yoshida, T., and Inouye, M. The Critical Role of the Conserved Thr247 Residue in the Functioning of the Osmosensor EnvZ, a Histidine Kinase/Phosphatase, in Escherichia coli. *Journal of Biological Chemistry 275*, 49 (2000), 38645–38653.

[22] Elowitz, M. B., and Leibler, S. A synthetic oscillatory network of transcriptional regulators. *Nature 403* (2000), 335–338.

[23] Elowitz, M. B., Levine, A. J., Siggia, E. D., and Swain, P. S. Stochastic Gene Expression in a Single Cell. *Science 297*, 5584 (2002), 1183–1186.

[24] Filimonov, V. V., Prieto, J., Martinez, J. C., Bruix, M., Mateo, P. L., and Serrano, L. Thermodynamic analysis of the chemotactic protein from Escherichia coli, CheY. *Biochemistry 32*, 47 (1993), 12906–12921.

[25] Fisher, S. L., Kim, S.-K., Wanner, B. L., and Walsh, C. T. Kinetic Comparison of the Specificity of the Vancomycin Resistance Kinase VanS for Two Response Regulators, VanR and PhoB. *Biochemistry 35*, 15 (1996), 4732–4740.

[26] Friedland, N., Mack, T. R., Yu, M., Hung, L.-W., Terwilliger, T. C., Waldo, G. S., and Stock, A. M. Domain Orientation in the Inactive Response Regulator Mycobacterium tuberculosis MtrA Provides a Barrier to Activation. *Biochemistry 46*, 23 (2007), 6733–6743. PMID: 17511470.

[27] Galperin, M. Y. Structural Classification of Bacterial Response Regulators: Diversity of Output Domains and Domain Combinations. *Journal of Bacteriology 188*, 12 (2006), 4169–4182.

[28] Ganguli, S., Wang, H., Matsumura, P., and Volz, K. Uncoupled Phosphorylation and Activation in Bacterial Chemotaxis: The 2.1-A structure of a threonine to isoleucine mutant at position 87 of CheY. *Journal of Biological Chemistry 270*, 29 (1995), 17386–17393.

[29] Gao, R., Tao, Y., and Stock, A. M. System-level mapping of Escherichia coli response regulator dimerization with FRET hybrids. *Molecular Microbiology 69*, 6 (2008), 1358–1372.

[30] Gardner, T. S., Cantor, C. R., and Collins, J. J. Construction of a genetic toggle switch in Escherichia coli. *Nature 403* (2000), 339–342.

[31] Gouet, P., Chinardet, N., Welch, M., Guillet, V., Cabantous, S., Birck, C., Mourey, L., and Samama, J.-P. Further insights into the mechanism of function of the response regulator CheY from crystallographic studies of the CheY–CheA124-257 complex. *Acta Crystallographica Section D 57*, 1 (Jan 2001), 44–51.

[32] Head, C. G., Tardy, A., and Kenney, L. J. Relative binding affinities of OmpR and OmpR-phosphate at the ompF and ompC regulatory sites . *Journal of Molecular Biology 281*, 5 (1998), 857 – 870.

[33] Hess, J. F., Oosawa, K., Kaplan, N., and Simon, M. I. Phosphorylation of three proteins in the signaling pathway of bacterial chemotaxis. *Cell 53* (1988), 79–87.

[34] Hsing, W., and Silhavy, T. J. Function of conserved histidine-243 in phosphatase activity of EnvZ, the sensor for porin osmoregulation in Escherichia coli. *Journal of Bacteriology 179*, 11 (1997), 3729–35.

[35] Huang, K. J., Lan, C. Y., and Igo, M. M. Phosphorylation stimulates the cooperative DNA-binding properties of the transcription factorOmpR. *Proceedings of the National Academy of Sciences 94*, 7 (1997), 2828–2832.

[36] Igo, M. M., Ninfa, A. J., Stock, J. B., and Silhavy, T. J. Phosphorylation and dephosphorylation of a bacterial transcriptional activator by a transmembrane receptor. *Genes & Development 3*, 11 (1989), 1725–1734.

[37] Jensen, H. M., Albers, A. E., Malley, K. R., Londer, Y. Y., Cohen, B. E., Helms, B. A., Weigele, P., Groves, J. T., and Ajo-Franklin, C. M. Engineering of a synthetic electron conduit in living cells. *Proceedings of the National Academy of Sciences 107*, 45 (2010), 19213–19218.

[38] Jiang, M., Tzeng, Y.-L., Feher, V. A., Perego, M., and Hoch, J. A. Alanine mutants of the Spo0F response regulator modifying specificity for sensor kinases in sporulation initiation. *Molecular Microbiology 33*, 2 (1999), 389–395.

[39] Josenhans, C., and Suerbaum, S. The role of motility as a virulence factor in bacteria. *International Journal of Medical Microbiology 291*, 8 (2002), 605 – 614.

[40] Kenney, L. J., Bauer, M. D., and Silhavy, T. J. Phosphorylation-dependent conformational changes in OmpR, an osmoregulatory DNA-binding protein of Escherichia coli. *Proceedings of the National Academy of Sciences 92*, 19 (1995), 8866–8870.

[41] King, S., and Kenney, L. Application of Fluorescence Resonance Energy Transfer to Examine EnvZ/OmpR Interactions. *Methods in Enzymology 422* (2007), 352–360.

[42] Kirby, J. R., and Zusman, D. R. Chemosensory regulation of developmental gene expression in Myxococcus xanthus. *Proceedings of the National Academy of Sciences 100*, 4 (2003), 2008–2013.

[43] Kofoid, E. C., and Parkinson, J. S. Transmitter and receiver modules in bacterial signaling proteins. *Proceedings of the National Academy of Sciences 85*, 14 (1988), 4981–4985.

[44] Kondo, H., Nakagawa, A., Nishihira, Y., Mizuno, T., and Tanaka, I. Escherichia col positive regulator OmpR has a large loop structure at the putative RNA polymerase interaction site. *Nature Structural & Molecular Biology 4* (1997), 28–31.

[45] Lan, C. Y., and Igo, M. M. Differential Expression of the OmpF and OmpC Porin Proteins in Escherichia coli K-12 Depends upon the Level of Active OmpR. *Journal of Bacteriology 180*, 1 (1998), 171–174.

[46] Larkin, M., Blackshields, G., Brown, N., Chenna, R., McGettigan, P., McWilliam, H., Valentin, F., Wallace, I., Wilm, A., Lopez, R., Thompson, J., Gibson, T., and Higgins, D. Clustal W and Clustal X version 2.0. *Bioinformatics 23*, 21 (2007), 2947–2948.

[47] Lee, S. Y., Cho, H. S., Pelton, J. G., Yan, D., Berry, E. A., and Wemmer, D. E. Crystal Structure of Activated CheY: Comparison with other activated receiver domains. *Journal of Biological Chemistry 276*, 19 (2001), 16425–16431.

[48] Lee, S. Y., Cho, H. S., Pelton, J. G., Yan, D., Henderson, R. K., King, D. S., Huang, L. s., Kustu, S., Berry, E. A., and Wemmer, D. E. Crystal structure of an activated response regulator bound to its target. *Nat Struct Mol Biol 9* (2001), 52–56.

[49] Levskaya, A., Chevalier, A. A., Tabor, J. J., Simpson, Z. B., Lavery, L. A., Levy, M., Davidson, E. A., Scouras, A., Ellington, A. D., Marcotte, E. M., and Voigt, C. A. Synthetic biology: Engineering Escherichia coli to see light. *Nature 438* (2005), 441–442.

[50] Li, J., Swanson, R. V., Simon, M. I., and Weis, R. M. Response Regulators CheB and CheY Exhibit Competitive Binding to the Kinase CheA. *Biochemistry 34*, 45 (1995), 14626–14636.

[51] Libby, E. A., Ekici, S., and Goulian, M. Imaging OmpR Binding to Native Chromosomal Loci in Escherichia coli. *Journal of Bacteriology 192*, 15 (2010), 4045–4053.

[52] Lukat, G. S., Lee, B. H., Mottonen, J. M., Stock, A. M., and Stock, J. B. Roles of the highly conserved aspartate and lysine residues in the response regulator of bacterial chemotaxis. *Journal of Biological Chemistry 266*, 13 (1991), 8348–8354.

[53] Lukat, G. S., Stock, A. M., and Stock, J. B. Divalent metal ion binding to the CheY protein and its significance to phosphotransfer in bacterial chemotaxis. *Biochemistry 29*, 23 (1990), 5436–5442.

[54] Martinez-Hackert, E., and Stock, A. M. The DNA-binding domain of OmpR: crystal structures of a winged helix transcription factor. *Structure 5*, 1 (1997), 109 – 124.

[55] Mattison, K., Oropeza, R., and Kenney, L. J. The Linker Region Plays an Important Role in the Interdomain Communication of the Response Regulator OmpR. *Journal of Biological Chemistry 277*, 36 (2002), 32714–32721.

[56] Mayover, T. L., Halkides, C. J., and Stewart, R. C. Kinetic Characterization of CheY Phosphorylation Reactions: Comparison of P-CheA and Small-Molecule Phosphodonors. *Biochemistry 38*, 8 (1999), 2259–2271.

[57] McEvoy, M. M., Bren, A., Eisenbach, M., and Dahlquist, F. W. Identification of the binding interfaces on CheY for two of its targets the phosphatase CheZ and the flagellar switch protein FliM. *Journal of Molecular Biology 289*, 5 (1999), 1423 – 1433.

[58] McEvoy, M. M., Hausrath, A. C., Randolph, G. B., Remington, S. J., and Dahlquist, F. W. Two binding modes reveal flexibility in kinase/response regulator interactions in the bacterial chemotaxis pathway. *Proceedings of the National Academy of Sciences 95*, 13 (1998), 7333–7338.

[59] McEvoy, M. M., Muhandiram, D. R., Kay, L. E., and Dahlquist, F. W. Structure and Dynamics of a CheY-Binding Domain of the Chemotaxis Kinase CheA Determined by Nuclear Magnetic Resonance Spectroscopy. *Biochemistry 35*, 18 (1996), 5633–5640.

[60] Menon, S., and Wang, S. Structure of the Response Regulator PhoP from Mycobacterium tuberculosis Reveals a Dimer through the Receiver Domain. *Biochemistry 50*, 26 (2011), 5948–5957.

[61] Mizuno, T. Compilation of All Genes Encoding Two-component Phosphotransfer Signal Transducers in the Genome of Escherichia coli. *DNA Research 4*, 2 (1997), 161–168.

[62] Mo, G., Zhou, H., Kawamura, T., and Dahlquist, F. W. Solution Structure of a Complex of the Histidine Autokinase CheA with Its Substrate CheY. *Biochemistry 51*, 18 (2012), 3786–3798.

[63] Mourey, L., Da Re, S., Pdelacq, J.-D., Tolstykh, T., Faurie, C., Guillet, V., Stock, J. B., and Samama, J.-P. Crystal Structure of the CheA Histidine Phosphotransfer Domain that Mediates Response Regulator Phosphorylation in Bacterial Chemotaxis. *Journal of Biological Chemistry 276*, 33 (2001), 31074–31082.

[64] Nikaido, H., and Rosenberg, E. Y. Porin channels in Escherichia coli: studies with liposomes reconstituted from purified proteins. *Journal of Bacteriology 153*, 1 (1983), 241–252.

[65] Oshima, T., Aiba, H., Masuda, Y., Kanaya, S., Sugiura, M., Wanner, B. L., Mori, H., and Mizuno, T. Transcriptome analysis of all two-component regulatory system mutants of Escherichia coli K-12. *Molecular Microbiology 46*, 1 (2002), 281–291.

[66] Ottemann, K. M., and Lowenthal, A. C. Helicobacter pylori Uses Motility for Initial Colonization and To Attain Robust Infection. *Infection and Immunity 70*, 4 (2002), 1984–1990.

[67] Park, H., Saha, S. K., and Inouye, M. Two-domain reconstitution of a functional protein histidine kinase. *Proceedings of the National Academy of Sciences 95*, 12 (1998), 6728–6732.

[68] Parkinson, J. S., and Kofoid, E. C. Communication Modules in Bacterial Signaling Proteins. *Annual Review of Genetics 26*, 1 (1992), 71–112. PMID: 1482126.

[69] Pazy, Y., Wollish, A. C., Thomas, S. A., Miller, P. J., Collins, E. J., Bourret, R. B., and Silversmith, R. E. Matching Biochemical Reaction Kinetics to the Timescales of Life: Structural Determinants That Influence the Autodephosphorylation Rate of Response Regulator Proteins. *Journal of Molecular Biology 392*, 5 (2009), 1205 – 1220.

[70] Radnai, L., Rapali, P., Hdi, Z., Sveges, D., Molnr, T., Kiss, B., Bcsi, B., Erddi, F., Buday, L., Kardos, J., Kovcs, M., and Nyitray,

L. Affinity, Avidity, and Kinetics of Target Sequence Binding to LC8 Dynein Light Chain Isoforms. *Journal of Biological Chemistry 285*, 49 (2010), 38649–38657.

[71] Rhee, J. E., Sheng, W., Morgan, L. K., Nolet, R., Liao, X., and Kenney, L. J. Amino Acids Important for DNA Recognition by the Response Regulator OmpR. *Journal of Biological Chemistry 283*, 13 (2008), 8664–8677.

[72] Roberts, D. L., Bennett, D. W., and Forst, S. A. Identification of the site of phosphorylation on the osmosensor, EnvZ, of Escherichia coli. *Journal of Biological Chemistry 269*, 12 (1994), 8728–8733.

[73] Sanders, D. A., Gillece-Castro, B. L., Stock, A. M., Burlingame, A. L., and Koshland, D. E. Identification of the site of phosphorylation of the chemotaxis response regulator protein, CheY. *Journal of Biological Chemistry 264*, 36 (1989), 21770–21778.

[74] Santoro, J., Bruix, M., Pascual, J., Lpez, E., Serrano, L., and Rico, M. Three-dimensional structure of chemotactic che Y protein in aqueous solution by nuclear magnetic resonance methods. *Journal of Molecular Biology 247*, 4 (1995), 717 – 725.

[75] Schuster, S. C., Swanson, R. V., Alex, L. A., Bourret, R. B., and Simon, M. I. Assembly and function of a quaternary signal transduction complex monitored by surface plasmon resonance. *Nature 365* (1993), 343 –347.

[76] Skerker, J. M., Perchuk, B. S., Siryaporn, A., Lubin, E. A., Ashenberg, O., Goulian, M., and Laub, M. T. Rewiring the Specificity of Two-Component Signal Transduction Systems . *Cell 133*, 6 (2008), 1043 – 1054.

[77] Slauch, J. M., and Silhavy, T. J. Cis-acting ompF mutations that result in OmpR-dependent constitutive expression. *Journal of Bacteriology 173*, 13 (1991), 4039–4048.

[78] Sola, M., Lopez-Hernandez, E., Cronet, P., Lacroix, E., Serrano, L., Coll, M., and Parraga, A. Towards understanding a molecular switch

mechanism: thermodynamic and crystallographic studies of the signal transduction protein CheY. *Journal of Molecular Biology 303*, 2 (2000), 213 – 225.

[79] Stewart, R. C. Kinetic Characterization of Phosphotransfer between CheA and CheY in the Bacterial Chemotaxis Signal Transduction Pathway. *Biochemistry 36*, 8 (1997), 2030–2040.

[80] Stock, A. M., Mottonen, J. M., Stock, J. B., and Schutt, C. E. Three-dimensional structure of CheY, the response regulator of bacterial chemotaxis. *Nature 337* (1989), 745–749.

[81] Stock, J. B., Ninfa, A. J., and Stock, A. M. Protein phosphorylation and regulation of adaptive responses in bacteria. *Microbiological Reviews 53*, 4 (1989), 450–490.

[82] Stock, J. B., Stock, A. M., and Mottonen, J. M. Signal transduction in bacteria. *Nature 344*, 6265 (Mar. 1990), 395–400.

[83] Swanson, R. V., Schuster, S. C., and Simon, M. I. Expression of CheA fragments which define domains encoding kinase, phosphotransfer, and CheY binding activities. *Biochemistry 32*, 30 (1993), 7623–7629.

[84] Tanaka, T., Saha, S. K., Tomomori, C., Ishima, R., Liu, D., Tong, K. I., Park, H., Dutta, R., Qin, L., Swindells, M. B., Yamazaki, T., Ono, A. M., Kainosho, M., Inouye, M., and Ikura, M. NMR structure of the histidine kinase domain of the E. coli osmosensor EnvZ. *Nature 396* (1998), 88– 92.

[85] Thakor, H., Nicholas, S., Porter, I. M., Hand, N., and Stewart, R. C. Identification of an Anchor Residue for CheA-CheY Interactions in the Chemotaxis System of Escherichia coli. *Journal of Bacteriology 193*, 15 (2011), 3894–3903.

[86] Thomas, S. A., Brewster, J. A., and Bourret, R. B. Two variable active site residues modulate response regulator phosphoryl group stability. *Molecular Microbiology 69*, 2 (2008), 453–465.

[87] Toker, A. S., and Macnab, R. M. Distinct regions of bacterial flagellar switch protein FliM interact with FliG, FliN and CheY. *Journal of Molecular Biology 273*, 3 (1997), 623 – 634.

[88] Tokishita, S., Kojima, A., Aiba, H., and Mizuno, T. Transmembrane signal transduction and osmoregulation in Escherichia coli. Functional importance of the periplasmic domain of the membrane-located protein kinase, EnvZ. *Journal of Biological Chemistry 266*, 11 (1991), 6780–5.

[89] Toro-Roman, A., Mack, T. R., and Stock, A. M. Structural Analysis and Solution Studies of the Activated Regulatory Domain of the Response Regulator ArcA: A Symmetric Dimer Mediated by the 4-5-5 Face. *Journal of Molecular Biology 349*, 1 (2005), 11 – 26.

[90] Toro-Roman, A., Wu, T., and Stock, A. M. A common dimerization interface in bacterial response regulators KdpE and TorR. *Protein Science 14*, 12 (2005), 3077–3088.

[91] Ulrich, L. E., Koonin, E. V., and Zhulin, I. B. One-component systems dominate signal transduction in prokaryotes. *Trends in Microbiology 13*, 2 (2005), 52 – 56.

[92] Ulrich, L. E., and Zhulin, I. B. The MiST2 database: a comprehensive genomics resource on microbial signal transduction. *Nucleic Acids Research 38*, suppl 1 (2010), D401–D407.

[93] Varughese, K. I., Tsigelny, I., and Zhao, H. The Crystal Structure of Beryllofluoride Spo0F in Complex with the Phosphotransferase Spo0B Represents a Phosphotransfer Pretransition State. *Journal of Bacteriology 188*, 13 (2006), 4970–4977.

[94] Volz, K. Structural conservation in the CheY superfamily. *Biochemistry 32*, 44 (1993), 11741–11753.

[95] Volz, K., and Matsumura, P. Crystal structure of Escherichia coli CheY refined at 1.7-A resolution. *Journal of Biological Chemistry 266*, 23 (1991), 15511–15519.

[96] Wadhams, G., and Armitage, J. Making sense of it all: bacterial chemotaxis. *Nat Rev Mol Cell Biol 5* (2004), 1024–1037.

[97] Welch, M., Chinardet, N., Mourey, L., Birck, C., and Samama, J.-P. Structure of the CheY-binding domain of histidine kinase CheA in complex with CheY. *Nat Struct Mol Biol 5* (1998), 25–29.

[98] Welch, M., Oosawa, K., Aizawa, S.-I., and Eisenbach, M. Effects of Phosphorylation, Mg2+, and Conformation of the Chemotaxis Protein CheY on Its Binding to the Flagellar Switch Protein FliM. *Biochemistry 33*, 34 (1994), 10470–10476.

[99] Yagi, K. Applications of whole-cell bacterial sensors in biotechnology and environmental science. *Applied Microbiology and Biotechnology 73*, 6 (2007), 1251–1258.

[100] Yamamoto, K., Hirao, K., Oshima, T., Aiba, H., Utsumi, R., and Ishihama, A. Functional Characterization in Vitro of All Two-component Signal Transduction Systems from Escherichia coli. *Journal of Biological Chemistry 280*, 2 (2005), 1448–1456.

[101] Yan, J., Barak, R., Liarzi, O., Shainskaya, A., and Eisenbach, M. In Vivo Acetylation of CheY, a Response Regulator in Chemotaxis of Escherichia coli. *Journal of Molecular Biology 376*, 5 (2008), 1260 – 1271.

[102] Yoshida, T., Cai, S. j., and Inouye, M. Interaction of EnvZ, a sensory histidine kinase, with phosphorylated OmpR, the cognate response regulator. *Molecular Microbiology 46*, 5 (2002), 1283–1294.

[103] Yoshida, T., Phadtare, S., and Inouye, M. The Design and Development of Tar-EnvZ Chimeric Receptors. In *TwoComponent Signaling Systems, Part B*, B. R. C. Melvin I. Simon and A. Crane, Eds., vol. 423 of *Methods in Enzymology*. Academic Press, 2007, pp. 166 – 183.

[104] Yoshida, T., Qin, L., Egger, L. A., and Inouye, M. Transcription Regulation of ompF and ompC by a Single Transcription Factor, OmpR. *Journal of Biological Chemistry 281*, 25 (2006), 17114–17123.

[105] Zhao, R., Collins, E. J., Bourret, R. B., and Silversmith, R. E. Structure and catalytic mechanism of the E. coli chemotaxis phosphatase CheZ. *Nat Struct Mol Biol 9* (2002), 570–575.

[106] Zhu, X., Amsler, C. D., Volz, K., and Matsumura, P. Tyrosine 106 of CheY plays an important role in chemotaxis signal transduction in Escherichia coli. *Journal of Bacteriology 178*, 14 (1996), 4208–15.

[107] Zhu, X., Rebello, J., Matsumura, P., and Volz, K. Crystal Structures of CheY Mutants Y106W and T87I/Y106W: CheY activation correlates with movement of residue 106. *Journal of Biological Chemistry 272*, 8 (1997), 5000–5006.

[108] Zhu, Y., and Inouye, M. The role of the G2 box, a conserved motif in the histidine kinase superfamily, in modulating the function of EnvZ. *Molecular Microbiology 45*, 3 (2002), 653–663.

[109] Zhu, Y., Qin, L., Yoshida, T., and Inouye, M. Phosphatase activity of histidine kinase EnvZ without kinase catalytic domain. *Proceedings of the National Academy of Sciences 97*, 14 (2000), 7808–7813.